THE USE OF HERPES SIMPLEX VIRUS-1 VECTORS IN NOCICEPTIVE BIOLOGY

by

Rahul Srinivasan

M.B; B.S, University of Mumbai, 2000

Submitted to the Graduate Faculty of

The Graduate School of Public Health in partial fulfillment

of the requirements for the degree of

Doctor of Philosophy

University of Pittsburgh

2006

UNIVERSITY OF PITTSBURGH

GRADUATE SCHOOL OF PUBLIC HEALTH

This dissertation was presented

by

Rahul Srinivasan

It was defended on

July 19, 2006

and approved by

Robert E. Ferrell, Ph.D, Professor,
Department of Human Genetics,
Graduate School of Public Health,
University of Pittsburgh.

Donald DeFranco, Ph.D, Professor,
Department of Pharmacology,
School of Medicine,
University of Pittsburgh.

Saleem Khan, Ph.D, Professor,
Department of Molecular Genetics and Biochemistry,
School of Medicine,
University of Pittsburgh.

Dissertation Advisor: Joseph C.Glorioso, Ph.D, Professor and Chair,
Department of Molecular Genetics and Biochemistry,
School of Medicine,
University of Pittsburgh.

THE USE OF HERPES SIMPLEX VIRUS-1 VECTORS IN NOCICEPTIVE BIOLOGY

Rahul Srinivasan, PhD

University of Pittsburgh, 2006

ABSTRACT

Public Health Relevance: The United States has 80 million employees with chronic pain resulting in annual losses of 61.2 billion dollars due to pain-related productive time lost. In addition, pain-related depression and inactivity reduce the quality of life. The development of effective analgesics is therefore important from a public health perspective. In this dissertation, the natural properties of herpes simplex virus (HSV-1) vectors are exploited to (i) develop an HSV-1 vector-based selection system that can potentially identify natural or chemical inhibitors of chronic pain and (ii) to test HSV-1 vector-expressed dominant negative PKCε (DNP) as a strategy to treat chronic pain.

The vanilloid/capsaicin receptor (TRPV1) is a pro-nociceptive calcium ion channel that is upregulated in chronic pain. This occurs partly due to protein kinase C epsilon (PKCε)–mediated receptor phosphorylation. An HSV-1 vector expressing TRPV1 (vTT) was engineered and vTT-expressed TRPV1 functionality was confirmed.

Treatment of vTT-infected cells with capsaicin or resiniferatoxin caused concentration-dependent Ca^{+2} influx, leading to cell-death and a dramatic reduction in infectious particle yield. TRPV1 antagonists, ruthenium red and SB-366791 reversed agonist-induced cell-death and rescued vTT growth, providing a basis for selection. Selection for antagonists was modeled using a mixed infection of vTT and vHG (capsaicin resistant control vector) and virus passage in the presence capsaicin. These experiments demonstrated that a single control vector particle was readily isolated from a population of 10^5 vTT particles. This approach can be used to identify antagonists from chemical or gene libraries and offers advantages of (i) a platform assay applicable to other ion channels and (ii) adaptability to high throughput formats.

Dominant negative PKCε (DNP) was engineered into HSV-1 to create the vector, vHDNP. Following functional confirmation of vHDNP in U2OS, Vero cells and neurons, cobalt uptake showed a reduction of capsaicin sensitive vHDNP-transduced neurons. Electrophysiology confirmed this and also demonstrated a knockdown of TRPV1-PKCε coupling in nociceptive neurons. *In-vivo* studies of noxious heat-induced nocisponsive behavior in vHDNP-inoculated rats showed a subtle inhibition of withdrawal responses when compared with controls. In conclusion, HSV-1 expressed dominant negative PKCε is a viable strategy to specifically inhibit TRPV1 function in order to treat chronic pain.

TABLE OF CONTENTS

LIST OF TABLES

LIST OF FIGURES

PREFACE

Although words will not do justice to the role that these people played during my graduate studies, I will attempt to put them down on paper.

I would like to thank my advisor Dr. Joseph Glorioso for his extremely valuable guidance throughout and specifically for his encouragement to make me think as an independent researcher. I would also like to thank my committee members, Dr. Robert Ferrell, Dr. Donald DeFranco and Dr. Saleem Khan for their useful discussions and inputs. My sincerest thanks to Dr. Darren Wolfe for teaching me the basic principles of scientific experimentation and laboratory techniques. A special thanks to Dr. William deGroat and Dr. Adrian Sculptoreanu who shared their vast experiences with me and helped me develop an interest in the field of neuroscience. Last but nor the least, a big thanks to everyone in the lab: Dr. David krisky, Dr. Shahua Huang, Dr. William Goins, Dr. James Wechuck, Dr. Ali Ozuer, Dr. Han Li, Ying, Canping, April, Kyle, Marianna, Anna and everyone who made the lab a fun place.

I dedicate this thesis to my family, without whom I would not have made it this far.

1.0 BACKGROUND AND RATIONALE

1.1 THE BIOLOGY OF PAIN AND NOCICEPTION

1.1.1 Definition of pain and nociception.

The philosopher and scientist, René Descrates first described pain in his treatise, Tractatus de Homine or the Treatise of Man published in 1664 as "the small rapidly moving particle of fire moves the skin of the affected spot causing a thin thread to be pulled. This opens a small valve in the brain and through it animal spirits are sent down to the muscles which withdraw the foot. Just as by pulling at one end of a rope one makes to strike at the same instant a bell which hangs at the other end."

Over 300 years since this first descriptive attempt, pain is currently viewed as a complex, evolutionarily conserved biological process, defined as "an unpleasant sensory and emotional experience associated with actual or potential tissue damage, or described in terms of such damage" [1]. While the sensation of pain encompasses emotion, the term nociception is used to describe the sensory component of pain. In order to apply an objective model for the study of pain, this dissertation, like most pain research is focused on nociception.

1.1.2 The nociceptive pathway.

Painful mechanical, inflammatory and heat stimuli directly activate distinct receptors expressed on the afferent terminals of specific dorsal root ganglion (DRG) neurons called nociceptors which are present in the epidermal and dermal layers of the skin. Following their activation, receptor-mediated nociceptive signaling cascades initiate generator potentials that in turn cause action potentials to propagate along the DRG axon. The consequent release of glutamate at central DRG afferent terminals in the superficial dorsal horn (SDH) of the spinal cord results in a progression of nociceptive currents along the second order axon to the thalamus. Nociceptive currents carried by second order neurons finally propagate to the cortex following a synapse with third order neurons in the thalamic nuclei. This results in the perception of pain at the level of the sensory cortex (Fig. 1).

Pain is subjected to extensive modulation at three levels that effectively form a complex regulatory matrix along the entire neuroanatomical axis of the nociceptive pathway [2]. Fig. 1 illustrates the nociceptive pathway and the levels of nociception, which are described below.

1.1.3 Levels of nociception.

The quality of pain that is experienced results from complex and largely unknown interactions among cellular and anatomical components at three distinct levels of the nociceptive neuraxis. The following section describes these levels of regulation in some detail:

i) At the peripheral level, nociceptive currents are triggered by ion channels and G-protein coupled receptors expressed within terminals of thinly myelinated Aδ and unmyelinated C

afferent fibers. These receptors directly sense inflammation and are regulated by complex intracellular signaling cascades.

ii) The spinal level consists of SDH neurons that are subject to tonic inhibition by interneurons and descending cortical pathways. A quantitative balance between tonic inhibitory and excitatory currents thus decides whether or not nociceptive currents will successfully progress to the cortex. This is described as the gate control theory [3].

iii) The supraspinal level integrates the emotional component of pain and consists of newly discovered, potentially regulatory pathways extending to the dorsolateral frontal lobes of the cortex or to the hypothalamus and amygdala. These cortical pathways may be responsible for the affective or emotional component of pain [4].

Although relatively much is known about nociceptive regulation at the level of the SDH, regulatory mechanisms at peripheral and cortical levels are remain unknown. Recent research has led to the discovery of several new receptors and ion channels at the peripheral level of the nociceptive pathway [5]. Activation mechanisms of many of these ion channels have been uncovered, however, gene products and signaling pathways that negatively regulate or modulate ion channel function are poorly understood. One reason for the lack of progress in this area arises from a dearth of tools to identify novel gene products and consequently, the signaling pathways that negatively modulate ion channel function. Chapter three of this dissertation focuses on the development of a novel method that can be adapted to screen chemical or cDNA libraries in order to identify novel inhibitors or modulatory gene products of these ion channels.

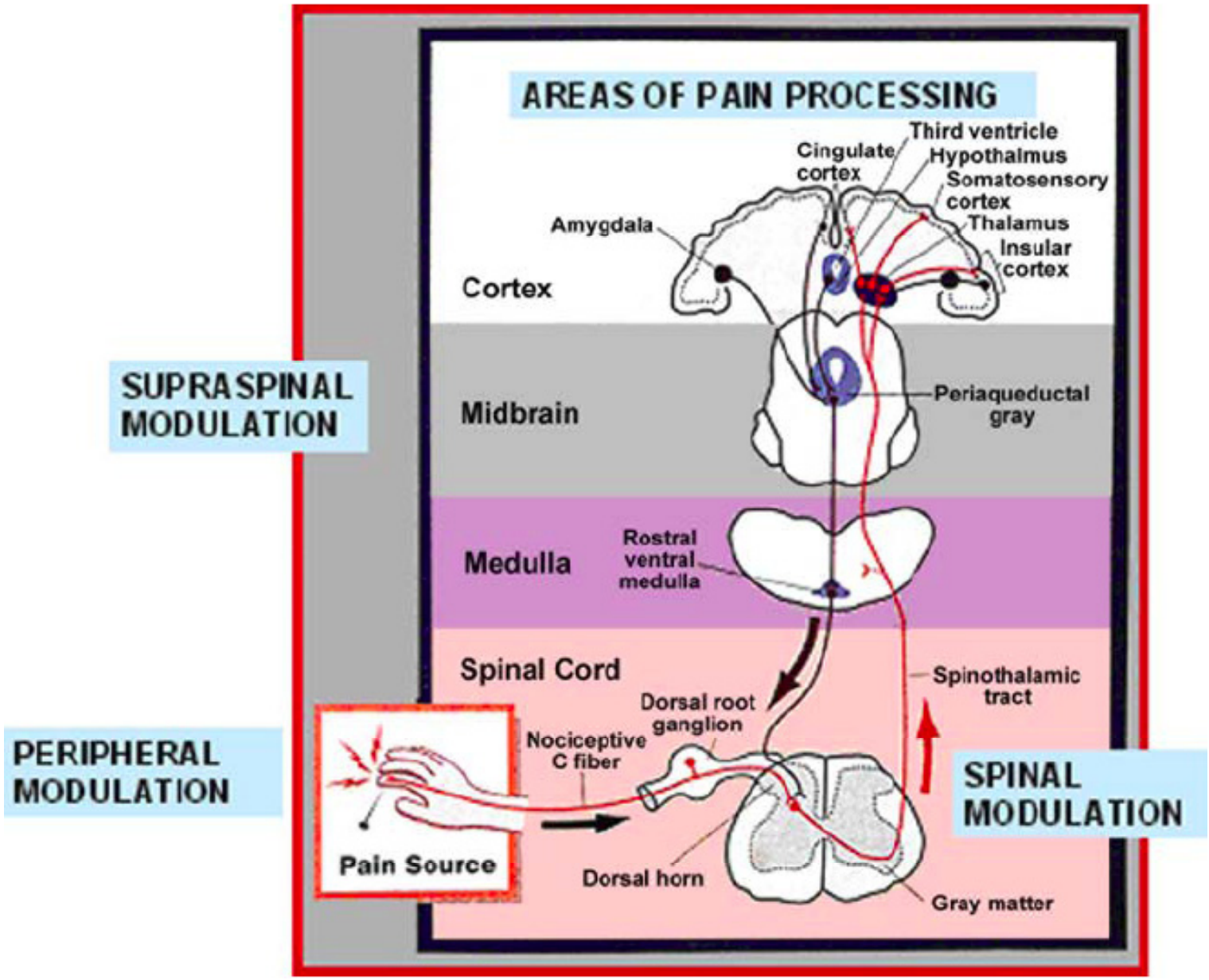

Figure 1. The nociceptive pathway and levels of nociception.

The nociceptive impulse travels from a peripheral pain source to the dorsal horn where, following a synapse, the current propagates along a second order neuron through midbrain structures and onto the thalamus. Third order neurons from the thalamus relay the nociceptive impulse to the somatosensory cortex. Additional modulatory inputs from the hypothalamus to the amygdala exist in the supraspinal region of the nociceptive pathway. Nociception is subject to modulation at peripheral, spinal and supraspinal levels of the nociceptive pathway. (Figure from DeLeo, Journal of bone and Joint Surgery, Vol 88-A, Suppl. 2, 2006)

1.1.4 Acute and chronic pain.

The pain response can be physiologically classified into acute and chronic phases. The pinprick is a typical example of the pain response displaying both these phases. Here, the pricking sensation or "acute first pain" is transmitted by thinly myelinated Aδ-fibers while the burning "chronic second pain" following the prick is transmitted by unmyelinated C-fibers of nociceptive DRG neurons [6]. Fig. 2 shows a compound action potential recording in a peripheral nerve where conduction velocities for thickly myelinated Aβ and thinly myelinated Aδ-fibers are faster when compared with unmylelinated C-fibers. The acute pain response carried by Aδ-fibers is adaptive and necessary for withdrawal from painful stimuli, while chronic pain responses carried by unmyelinated C-fibers are maladaptive and therefore dispensable. The next sections will describe the pathophysiology of chronic pain and its consequent implications from a therapeutic standpoint.

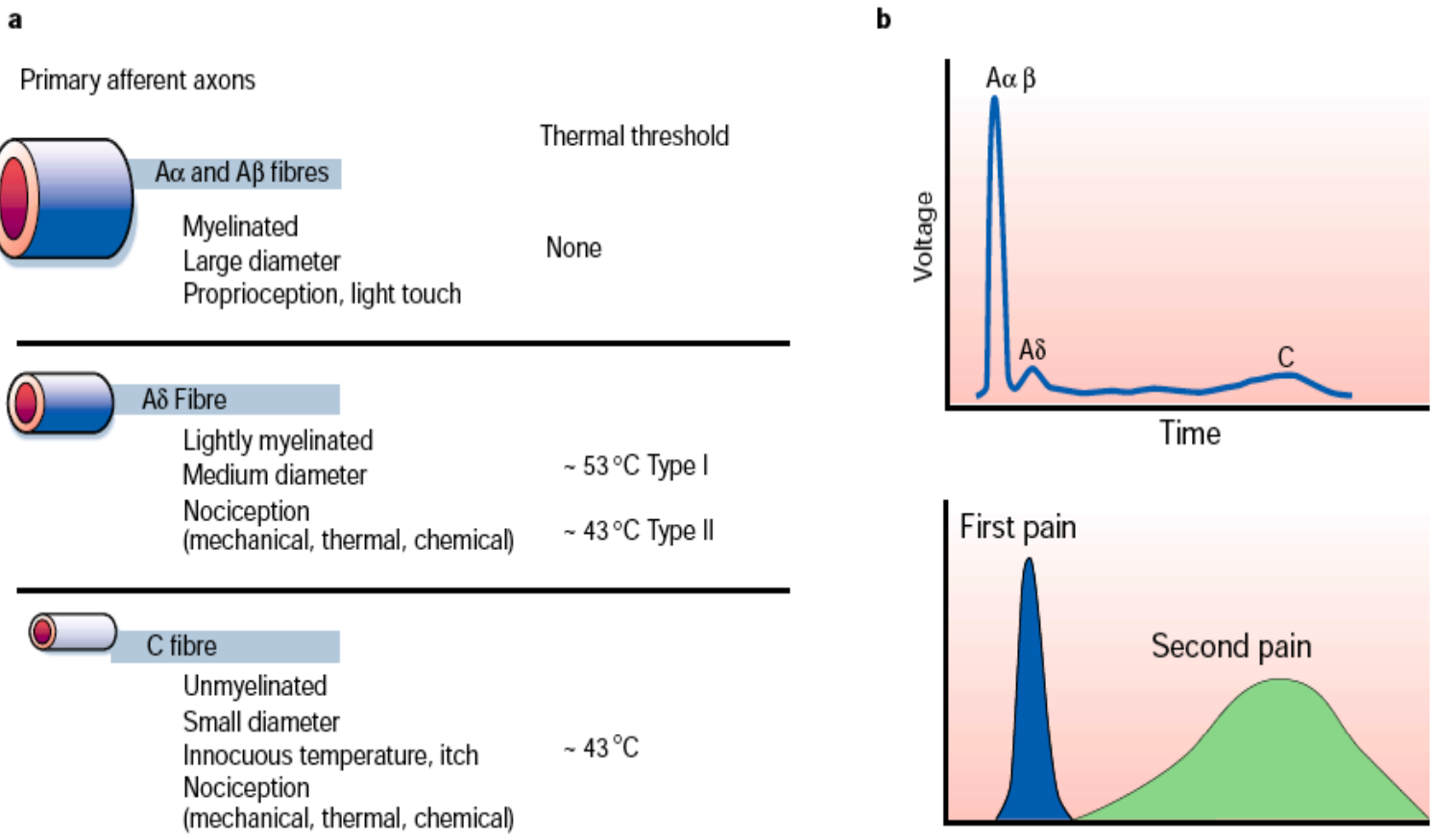

Figure 2. **The physiology of acute and chronic pain responses.**

Panel a depicts the different peripheral afferent nerve fibers along with their respective sensory functions. Thickly myelinated Aα and Aβ fibers carry impulses coding for light touch and proprioception, while thinly myelinated Aδ and unmyelinated C-fibers code for acute and chronic pain impulses respectively. Panel b is a recording of a compound action potential from a nerve fiber. As shown, the Aα and Aβ fibers do not code for pain, but cause a large, rapid depolarization when activated. The first, acute pain impulse is carried by Aδ-fibers and is shorter in duration, while the second or chronic pain impulse is carried by the C fiber and is longer in duration. (From Julius and Basbaum, Nature 413, 203-213, Sept. 2001)

1.2 CHRONIC PAIN

1.2.1 The pathophysiology of chronic pain.

In the clinical setting, pain is chronologically graded as a spectrum of states ranging from acute pain that lasts from a few hours to 3 months, subacute pain lasting from 3 to 6 months and finally, chronic pain that lasts for greater than 6 months [7]. Based on the eitiology, chronic pain is classified as inflammatory or neuropathic. Inflammatory pain in conditions such as arthritis and cancer occurs as a result of tissue damage, while neuropathic pain occurs as a result of neuronal damage and is associated with conditions like diabetes, spinal cord injury and stroke [8]. Unlike acute pain, chronic pain often persists following a resolution of the underlying pathology and becomes associated with a separate set of psychosomatic symptoms that include immobility, depression, insomnia, reduced appetite and drug dependence to name a few (David Niv and Marshall Devor, Pain Practice, Vol. 4 Issue 3, 2004).

Concomitant with a distinct symptomatology, chronic pain causes changes in the expression profiles of several ion channels, receptors and cell signaling molecules at central and peripheral afferent terminals of nociceptive neurons [9]. The resulting phenomena of peripheral and central sensitization occur due to complex morphological changes and phenotypic switches of neurons at different levels of the nociceptive pathway [10]. Sensitization acts as a positive feedback loop for further development of the chronic pain state. This causes an enhancement of nociceptive function characterized by hyperalgesia in which less painful stimuli cause increased pain and allodynia defined as pain due to innocuous stimuli. Chronic pain can thus be regarded as a self-perpetuating disease entity characterized by distinct psychosomatic and molecular phenomena. Indeed, a recent declaration of the European federation of IASP chapters has called

chronic pain "a disease in its own right" (David Niv and Marshall Devor, Pain Practice, Vol. 4 Issue 3, 2004).

1.2.2 Chronic pain from a public health perspective.

According to the Pain and Absenteeism in the Workplace Survey conducted by Louis Harris and associates in 1996, the United States currently has over 80 million full time employees that suffer from chronic pain. As a result of the reduced activity associated with chronic pain, there is an annual loss of 61.2 billion dollars in pain-related loss of productive time[11] and 15 billion dollars are spent annually on pain medications. In addition to the economic costs, chronic pain significantly reduces the quality of life and is a major cause of depression [12]. The treatment of chronic pain is therefore of prime importance from a public health as well as an economic perspective.

1.2.3 Current treatments for chronic pain.

Chronic pain therapy includes a variety of approaches such as physiotherapy, acupuncture and pharmacological management. Several pharmacological agents summarized in table 1 are used to treat pain. Non-steroidal anti-inflammatory drugs (NSAIDs) act at the periphery of the nociceptive pathway while opiates such as morphine and anesthetics like lidocaine primarily exert their effects on receptors at the spinal level. Newer medications include anti-depressants such as amitryptyline that act at the supraspinal level.

Table 1. Analgesics in current use.

Analgesics are classified based on level of action. Side effects for each drug class are given.

CLASS	NAME OF DRUG	LEVEL OF ACTION	SIDE EFFECTS
Non-steroidal anti-inflammatory drugs (NSAIDs)	Acetaminophen, Methyl salicylate, Magnesium salicylate, Choline salicylate , Choline magnesium trisalicylate, Ibuprofen, Ketoprofen, Naproxen, Naproxen sodium, Carprofen, Diflunisal, Fenoprofen calcium, Etodolac, Ketorolac tromethamine, Mefenamic acid, Rofecoxib, Celecoxib.	Peripheral	Nausea, vomiting diarrhea, gastric ulcers, colitis
Corticosteroids	Dexamethasone, Prednisone	Peripheral	Weight gain, gastic ulcers, cardiac problems
Anesthetics	Mexiletine, Lidocaine, Ketamine	Peripheral and spinal	Constipation, nausea, vomiting, arrythmias
Opioids	Morphine, Codeine, Fentanyl, Hydrocodone, Hydromorphone, Levorphanol, Methadone, Oxycodone, Oxymorphone.	Spinal	Dependence, tolerence
Antidepressants	Amitriptyline, Desipramine, Maprotiline, Duloxetine, Nortiptyline, Venlafaxine.	Supraspinal	Nausea, anxiety, weight gain, insomnia, constipation
Anticonvulsants	Carbamazepine, Valproate, Gabapentin, Clonazepam, Lamotrigine, Pregabalin.	Supraspinal	Excessive sleep, polyuria, polyphagia, ataxia

1.2.4 Problems with current analgesics and strategies to improve analgesic efficacy.

Despite the availability of a large range of analgesics, chronic pain remains a difficult condition to treat. Most pain medications target molecules and receptors involved in biological systems other than nociception. The resultant side effects such as gastric ulcers associated with non-steroidal anti-inflammatory drugs (NSAID) and the drug dependence or tolerance associated with opiates [13] make the long-term use of current pain medications detrimental (see Table 1 for side effects of other medications). Indeed, according to the 1999 National Survey for chronic pain, 13.5 million people developed gastrointestinal problems and ulcers following the use of NSAIDs. It follows that the development of analgesics specifically targeting gene products upregulated in chronic pain may help reduce side effects, thus allowing a better management this malady.

One approach to achieve this goal is to recognize chronic pain as a distinct disease entity and identify the phenotypic cellular changes specific to chronic pain states. The vanilloid receptor (TRPV1, formerly known as VR1) has emerged as a classic example of an ion channel that is specifically upregulated in chronic pain. In addition to TRPV1, protein kinase C epsilon (PKCε) is thought to be an important pro-nociceptive kinase at the periphery of the nociceptive pathway. PKCε directly phosphorylates and enhances TRPV1 activity such that the receptor can be activated by lower doses of agonists [14, 15]. TRPV1 hyperactivity is reflected as hyperalgesia and is a hallmark of the development of chronic pain states.

A second approach for the development of more effective analgesics with reduced side effects is the targeted delivery of chronic pain-specific inhibitory gene products to DRG neurons, which are effectively the primary sensors of painful stimuli. The herpes simplex virus 1 (HSV-1) is an attractive delivery vehicle for this purpose. HSV-1 is a large, neurotropic DNA virus that is

retrogradely transported along DRG afferent neurons following a peripheral infection in the skin. Following retrograde transport through afferent nerve axons, HSV-1 loses the ability to replicate and attains a latent state in the neurons of the DRG for the lifetime of the host, but can retain the ability to express transgene products in these neurons when under the transcriptional control of immediate early promoters like the human cytomegalovirus (HCMV) promoter. This property makes HSV-1 a nearly ideal vector for the targeted expression of gene products to inhibit pain-specific signaling molecules in nociceptive neurons. In this dissertation, the natural properties of HSV-1 as a vector delivery system have been exploited to develop tools and methods to identify chemical or natural inhibitors of TRPV1 (chapter 3) and to indirectly attenuate TRPV1 function by the inhibition of PKCε (chapter 4).

The following sections will describe the role of TRPV1 and PKCε in nociception. In addition, the use of HSV-1 as a gene delivery vehicle to treat pain will be discussed in some detail.

1.2.5 The vanilloid receptor and its role in nociception.

The vanilloid receptor or the transient receptor potential vanilloid 1 (TRPV1, formerly known as VR1) has recently emerged as an important receptor, the function of which is specifically upregulated in chronic pain states. TRPV1 is a peripheral pro-nociceptive Ca^{+2} ion channel belonging to the transient receptor potential (TRP) superfamily [16]. TRP ion channels are cellular physiological sensors involved in a variety of important biological functions ranging from hearing to brain development [17, 18]. A growing subfamily of TRP ion channels directly activated by a variety of specific chemical agonists and temperatures ranging from noxious cold to noxious heat have recently been uncovered (Fig. 3) [19, 20]. Of these, TRPV1 is the direct

peripheral sensor of noxious stimuli that include heat (43°C) [21], endovanilloids (anandamide) [22, 23], low pH (protons), capsaicin and resiniferatoxin [24-26]. A network of G-protein coupled receptors including those responsive to bradykinin (BK), nerve growth factor (NGF) and ATP cause the phosphorylation and consequent potentiation of TRPV1 function such that sub-maximal doses of direct stimuli become capable of activating the receptor [27-30]. The TRPV1 hyperactivity that occurs through this complex array of mechanisms results in the development of voltage gated sodium channel (VGSC)-induced neuronal hyperexcitability seen in chronic pain [31]. Being an important pro-nociceptive molecule, TRPV1 is subject to stringent regulatory mechanisms like calcineurin mediated receptor dephosphorylation [32] and tonic TRPV1 inhibition by phosphoinositol diphosphate (PIP2) [33]. Additionally, neurotrophin three (NT-3) causes long-term down-regulation of TRPV1 [34]. TRPV1 knockout mice exhibit reduced responses to noxious thermal stimuli and acidic pH in the setting of inflammation [35], which underscores the contribution of TRPV1 to the pain signaling pathway. These vital roles of TRPV1 in peripheral pain signaling suggest that a further understanding of the regulatory circuits that control TRPV1 function may provide insights into novel means of controlling receptor expression or function and may thereby provide new targets for the treatment of chronic pain.

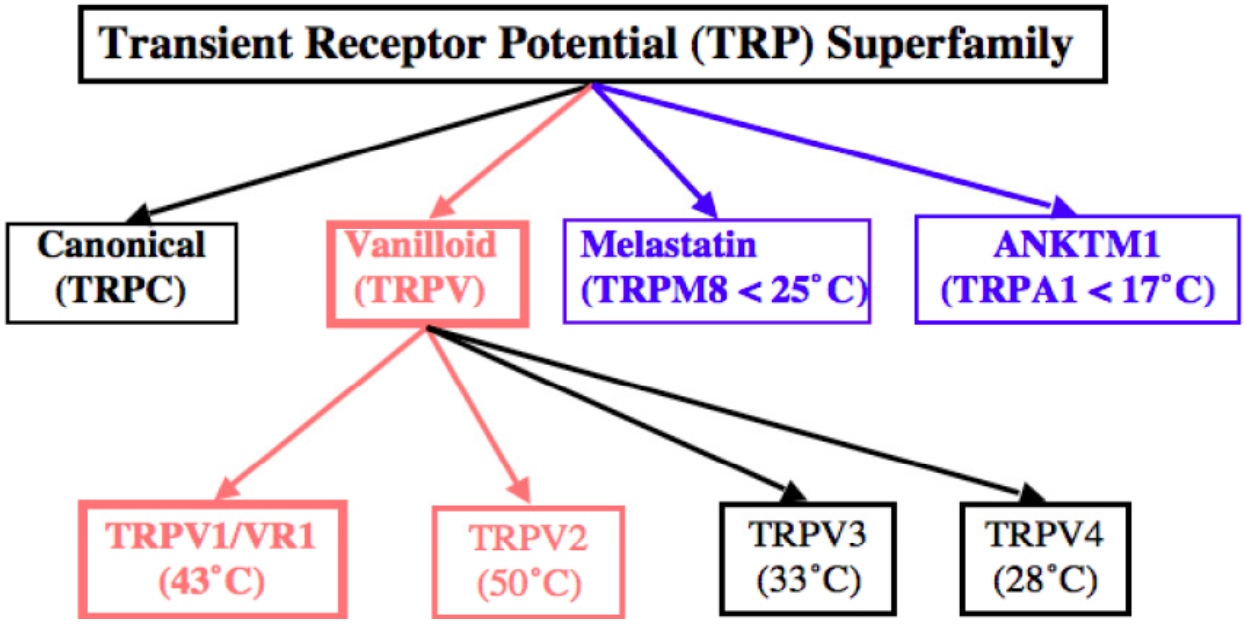

Figure 3. **The transient receptor potential family of ion channels.**

The figure depicts recently discovered members of the transient receptor potential (TRP) family of ion channels involved in sensing a variety of temperatures. The canonical TRP (TRPC) is a classical TRP ion channel, while the vanilloid subfamily (TRPV) can be broken down into four members TRPV1 to 4 that detect the temperatures shown for each channel. The melastatin (TRPM8) and the Ankyrin (ANKTM1 / TRPA1) TRPs detect cold temperatures below 25˚C and 17˚C respectively.

1.2.6 The role of protein kinase C epsilon (PKCε) in nociception.

The evolutionarily conserved protein kinase C (PKC) family of enzymes are involved in a myriad of functions ranging from development to pain perception. These kinases are divided into three subtypes based on their co-factor requirements. The conventional isoforms (cPKCs – PKCα, PKCβ and PKCγ) depend on diacylglycerol (DAG) and Ca^{+2} for their activation, while the novel isoforms (nPKCs - PKCδ, PKCε, PKCη and PKCθ) are activated by DAG in a Ca^{+2} independent manner. Atypical isoforms (aPKCs - PKCζ and PKCλ) are a third subtype, activated independent of DAG and/or Ca^{+2} [36].

Among these kinases, the novel protein kinase PKCε plays a crucial role in oncogenesis, ethanol sensitivity, neurite outgrowth, cardiac reperfusion following ischemia and cytoskeletal re-organization [37]. In addition to these functions, PKCε is a pro-nociceptive signaling molecule in nociceptive neurons [38]. Thus, the functions of this kinase vary depending upon the type of tissue or cell in which it is expressed. Recent studies in PKCε and TRPV1 knockout mice demonstrate reduced painful behaviours in response to thermal stimuli and the PKC activator, phorbol myristate acetate (PMA) respectively [38, 39]. These results indicate that PKCε may exert its pro-nociceptive function by exclusively acting through the TRPV1 receptor. Indeed, PKCε has recently been shown to directly phosphorylate TRPV1 at the Ser502 and Ser800 residues *in-vitro* and *in-vivo* [15, 30]. TRPV1 phosphorylation results in enhanced receptor function such that the receptor is now activated by lower doses of chemical agonists and physiological pH and temperature (37˚C). This phenomenon, called receptor sensitization is critical to the development of chronic pain states [40]. In nociceptors, PKCε is activated downstream of several G-protein coupled receptors including the bradykinin receptor 2 and the purigenic P2Y2 receptor resulting in TRPV1 sensitization [27, 41]. Since inflammatory mediators such as bradykinin and ATP directly activate these receptors, PKCε activation in nociceptors is physiologically relevant in the context of inflammation and the development of a chronic pain state.

Given the importance of PKCε in nociception and chronic pain, the targeted inhibition of this kinase in nociceptive neurons, described in chapter 4, may represent a novel strategy to reduce TRPV1 function and thereby curb the development of a chronic pain state.

1.2.7 Replication defective herpes simplex virus-1 (HSV-1) vectors.

A prerequisite for the safe use of HSV-1 as a gene delivery vector is to attenuate pathogenic attributes of the virus. Viral mutants have been engineered that are non-cytopathic and do not disturb host cell gene expression, yet remain capable of transgene expression in the sensory neurons of animals [42]. During its replicative cycle, HSV-1 undergoes a highly regulated and inter-dependent temporal cascade of viral protein expression (Fig. 4) [43]. The immediate early proteins, infected cell protein (ICP) 0, ICP4, ICP22, ICP27 and ICP47 are expressed within an hour following viral attachment and entry into epithelial cells of the mucosa. These proteins in turn cause the expression of early viral proteins that are involved in viral DNA replication. Early viral proteins trigger the expression of late viral genes that code for structural components of the virus.

The deletion of immediate early viral genes in a variety of combinations results in replication defective HSV-1 viruses that are incapable of reactivation or replication in non-complementing cells. These mutant vectors are consequently suited for the *in-vivo* delivery of therapeutic transgenes. Virus replication and propagation can only be achieved by the *in-vitro, in-trans* complementation of viral functions using cell lines that express the deleted viral proteins [44, 45].

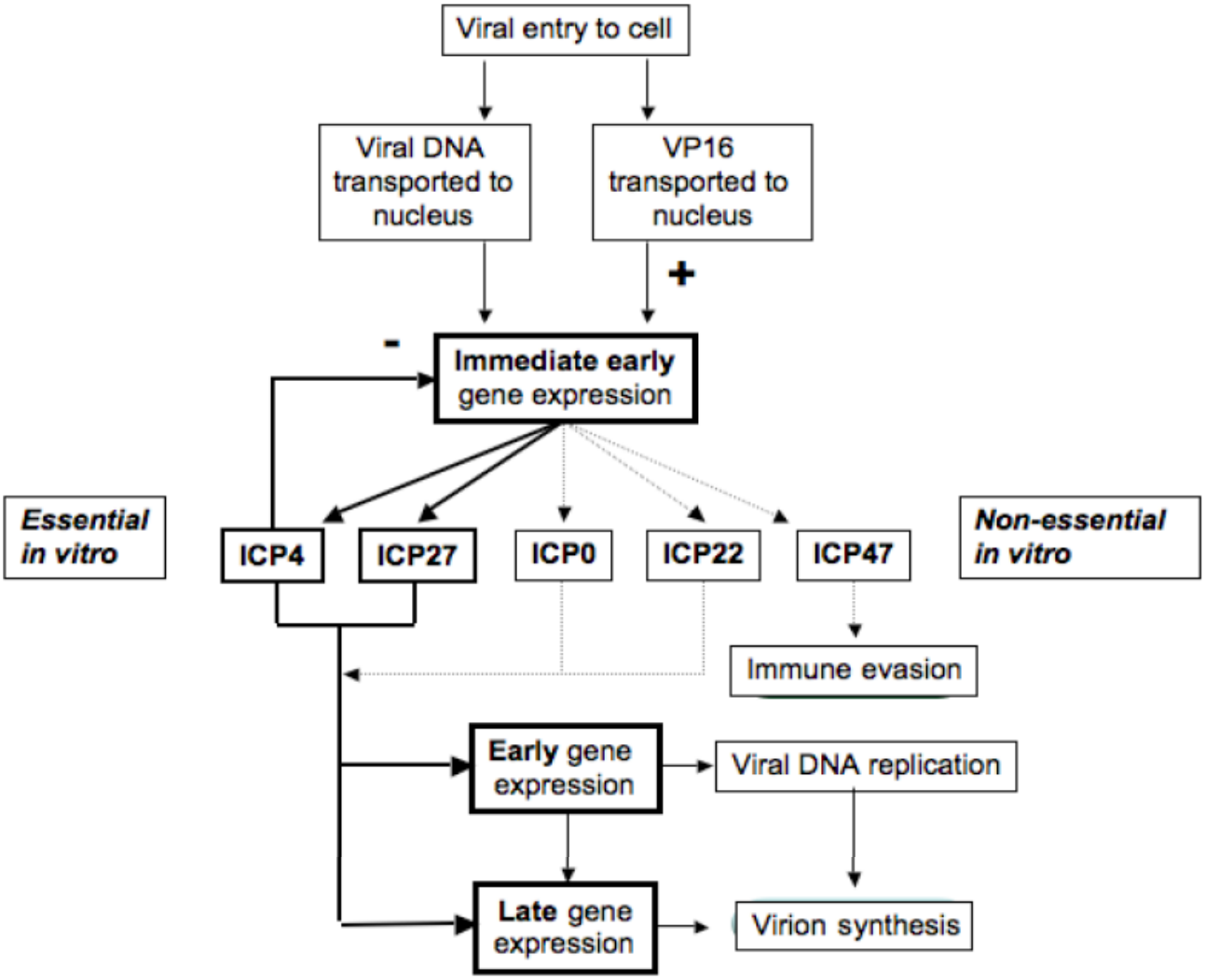

Figure 4. **HSV-1 virus replication cascade.**

The figure depicts the normal, temporally regulated HSV-1 replication cascade. Following viral entry into the cell, the virion component VP16 activates viral promoter sequences of the immediate early genes. This in turn causes the activation of early genes that are involved in viral DNA replication. Early gene products trigger the expression of late genes that code for virion components. Of the immediate early gene products, ICP4 and ICP27 are essential for replication *in-vitro.* Viruses that are deleted for these gene products are therefore replication defective *in-vivo* and in non-complementing cell lines. (Adapted from Burton et al, Stem Cells, 2001 19(5): 358-77)

1.2.8 Herpes Simplex 1 Virus (HSV-1) and the treatment of pain.

HSV-1 has many biological features that make it attractive for gene delivery to the nervous system [46-48]. As mentioned earlier, in natural infection, the virus establishes latency in DRG neurons, a state in which viral genomes may persist for the life of the host as intranuclear episomal elements. Several reports reveal the potential efficacy of HSV-1 to treat neuropathic, inflammatory and bone cancer pain. Salient findings from these reports are described below.

Replication-competent HSV-based vectors expressing proenkephalin (PE) display an anti-hyperalgesic effect following subcutaneous footpad injection in mice. This was demonstrated by an increased latency to foot withdrawal from noxious heat after sensitization of C-fibers by application of capsaicin, or sensitization of Aδ-fibers by application of dimethyl sulfoxide [49]. Another replication-competent HSV-based vector expressing proenkephalin reduced pain in a rodent model of arthritis [50]. Effects of replication-defective vectors expressing PE from the HCMV IE promoter (SHPE) in the formalin model of inflammatory pain have also been examined. Rats injected with SHPE one week prior to formalin testing showed a significant reduction in nocisponsive behaviors [51]. The behavioral response of SHPE-inoculated animals to inflammatory pain waned over a period of weeks as did PE expression from the vector. However, vector re-inoculation re-established the anti-nociceptive effect, suggesting that the loss of effect was not a result of tolerance to vector-mediated opioid expression. This demonstrated that prior inoculation with a non-replicating vector does not prevent the re-application of therapeutic gene transfer with the HSV-1 vector. Similar anti-nociceptive effects have been observed in the spinal nerve ligation (SNL) model of neuropathic pain, where vector re-inoculation could re-establish the analgesic effect [52]. Potential therapeutic effects of HSV-mediated PE expression have also been evaluated in a mouse osteosarcoma model of pain due to

metastatic bone cancer. Animals injected with SHPE demonstrated a significant reduction in spontaneous pain behavior 2 and 3 weeks after tumor implantation [53].

Recent publications show that the expression of glial-derived neurotrophic factor (GDNF) effectively suppresses allodynia caused by the neuropathic spinal nerve ligation model [54]. A replication defective vector expressing GAD67 (glutamic acid decarboxylase) that results in the conversion of glutamic acid to GABA (gamma-amino butyric acid), a potent inhibitory neurotransmitter produced GABA and in a model of below level spinal cord injury (SCI), effectively reversing mechanical allodynia and thermal hyperalgesia. These results suggest that HSV-mediated gene transfer to DRG could be used to treat below-level central neuropathic pain after incomplete SCI. This GAD67 expressing vector is effective at treatment of neuropathic pain in animals models when delivered by peripheral inoculation [55].

Taken together, these results clearly demonstrate the usefulness of replication defective HSV-1 vectors as a gene delivery vehicle to treat chronic pain. In addition to the use of HSV-1 as a gene therapy vector, properties like neurotropism, the ability to simultaneously express multiple transgenes and a large transgene capacity make replication defective HSV-1 vectors an attractive expression system for the *in-vitro* applications described in this dissertation.

1.3 SPECIFIC AIMS

The first part of my thesis focuses on the design and development of a selection system using replication defective HSV-1 vectors as a tool to identify novel inhibitors of ion channels involved in nociception. Given the established role of TRPV1 in nociception, this receptor has been used as a target gene to develop the selection system.

In the second part of my thesis, I have tested the hypothesis that the HSV-1 vector-mediated targeted functional inhibition of a known pro-nociceptive molecule, PKCε in DRG neurons at the periphery of the nociceptive pathway is a means to attenuate TRPV1 activity *in-vitro* and *in-vivo*. The following sections describe these specific aims in some detail.

1.3.1 Specific aim 1.

Several ion channels such as purigenic receptors, voltage gated calcium channels and specific subtypes of sodium channels are upregulated in chronic pain states [5, 56]. Specific aim 1 focuses on the development and characterization of an HSV-1 vector-based selection system to identify inhibitors of these nociceptive ion channels. The TRPV1 receptor is a prototypical example of an ion channel that is upregulated in chronic pain states. Using TRPV1 as a model receptor and exploiting the natural properties of replication defective HSV-1 vectors as a gene expression tool, a selection system is developed that can be used to identify novel inhibitory cDNA products or chemical antagonists of TRPV1. The system is based on the idea that activation of HSV-1 vector-expressed TRPV1 by TRPV1-specific agonists will result in an influx of cytotoxic levels Ca^{+2} into the cell. This will cause cell death before the virus can complete its replicative cycle. A fall in viral titers is thus an indirect indicator of TRPV1 receptor activation by agonists. Selection is based on the rationale that antagonism of receptor activation will prevent cell death and allow the viral replicative cycle to reach completion. Thus the recovery of viral growth is an indirect indicator of receptor antagonism by chemical or natural antagonists. The design, development and characterization of this HSV-1 vector-based selection system will be described in chapter three. As a platform system, selection can be adapted to identify natural or chemical inhibitors of several other ion channels known to be upregulated in

chronic pain. The identification of novel and specific inhibitors of these ion channels has direct implications for the development of better and more specific analgesics with reduced side effects to treat chronic pain.

1.3.2 Specific aim 2.

Specific aim 2 focuses on the use of HSV-1 vector-expressed dominant negative protein kinase C epsilon (PKCε) as an approach to attenuate TRPV1 receptor function *in-vitro* and *in-vivo*. PKCε is a pro-nociceptive protein kinase that is activated by G-protein coupled mechanisms downstream of the purigenic receptor, P2Y2 and bradykinin receptor 2. Following activation, PKCε directly phosphorylates and potentiates TRPV1 function such that the receptor is maximally activated by lower doses of natural and chemical agonists [14, 15, 57, 58]. A study in TRPV1 knockout mice has demonstrated the absence of nocifensive behaviors following stimulation with the known PKC activator, phorbol myristate acetate (PMA) in knockout mice, while wild-type mice display painful behaviors in response to PMA [39]. This result shows that PKCε acts exclusively through the TRPV1 receptor to cause pain. Thus, PKCε coupled to TRPV1 hyperactivation may be specifically involved in the transition from acute to chronic pain states. The targeted inhibition of PKCε function in nociceptors can therefore be a strategy to specifically attenuate TRPV1 function in nociceptors and thereby prevent the development of a chronic pain state. Although PKCε plays a pro-nociceptive role in DRG neurons, other functions of this molecule include neurite outgrowth, anti-apoptosis and cardiac reperfusion following ischemic injury to cardiomyocytes [37]. In this aim, the neurotropism of HSV-1 has been exploited to achieve the targeted inhibition of endogenous PKCε activity, thereby attenuating TRPV1

function in nociceptors without interfering with other biological systems. Chapter four describes experiments to evaluate the inhibition of PKCε by HSV-1 vector-mediated dominant negative PKCε transgene expression as a means to attenuate TRPV1 function *in-vitro* and *in-vivo*.

2.0 MATERIALS AND METHODS

2.1 HSV-1 VECTOR CONSTRUCTS AND PLASMIDS

The HSV-1 vectors used in this dissertation were derived from the wildtype HSV-1 KOS strain 17. The vectors utilized were QOZ (**Q**uadruple mutant backbone, ICP**O**p:Lac**Z**), vHDNP (**v**ector **H**CMVp:**D**ominant **N**egative **P**KCε), vHG (**v**ector **H**CMVp:E**G**FP) and vTT (**v**ector **T**Kp:**T**RPV1). These vectors are replication defective mutants, deleted for the immediate early essential genes, ICP4 and ICP27. Deletion of immediate early genes impairs the ability of these mutant vectors to replicate in non-complementing cells, making *in-trans* complementation of the ICP4 and ICP27 gene products a requirement in order to replicate *in-vitro*. This is achieved by propagating the vectors in a 7B cell line complementing for deleted viral functions [44, 45]. To construct the recombinant viral vectors, plasmids were recombined into the targeted locus of parent vectors by sequential virus infection and plasmid transfection. Screening for marker gene transfer (e.g. EGFP negative plaques) was used to isolate recombinants [59]. Vector plaques were purified by three rounds of limiting dilution and verified by Southern blot analysis. Confirmed vector stocks were expanded in complementing cells, purified by centrifugation to remove excess proteins, titered on complementing cells, aliquoted and stored at –80˚C. The vectors were chronologically engineered as follows:

2.1.1 Construction of the QOZ and vHDNP vectors.

The QOZHG vector (ICP4-,ICP27-, ßICP22,ßICP47, ICP**0**p:Lac**Z**::UL41, **H**CMVp:E**G**FP::ICP27) [60] which is derived from a cross of mutants TOZ.1 [44, 45] and d106 virus [61] was deleted for the EGFP expression cassette by homologous recombination with plasmid pPXE. pPXE contains a *BamH*I-*Sal*I deletion of the UL54 (ICP27) coding sequence with a *Pme*I linker inserted between the *BamH*I and *Sal*I sites [62]. The resultant vector, QOZ (ICP4-,ICP27-,ßICP22,ßICP47, ICP**0**p:Lac**Z**::UL41), was then similarly recombined to contain a dominant negative PKCε cassette fused to GFP and driven by the HCMV promoter (HCMVp:DNP) at the UL41 locus using the plasmid p41HDNP. The vector resulting from this recombination was called vHDNP. Plasmid p41HDNP contains the HCMVp:DNP cassette flanked by UL41 homology sequences and was constructed as follows:

The dominant negative PKCε construct, HDNP was engineered based on previously published work [63] and is deleted for the entire catalytic region, the C2 and the C1b sub-domains. The construct retains the pseudosubstrate region (PS), the C1a sub-domain and a variable region (V3) of the PKCε regulatory domain. This construct is fused to the enhanced green fluorescent protein (EGFP). In order to engineer, HDNP the PKCε cDNA was isolated by RT-PCR from the total mRNA of SH-SY5Y human neuroblastoma cells, obtained using the RNeasy minikit (Qiagen, Valencia, CA). The PKCε cDNA regulatory domain was then cloned into the *Sal*I to *Bgl*II sites of the pEGFPN1 vector (Clontech laboratories, Inc.) by standard restriction digestion, ligation and sub-cloning techniques. The resultant plasmid contains the HCMV promoter in front of the PKCε regulatory domain fused to EGFP. The above plasmid was PCR amplified using primers that each contained an *Mlu*I site (upper primer is 5'-

GCGACGCGTGCCAAAGTACTGGCCGACCTG-3' and lower primer is 5'-GCGACGCGTGATACCGAACTTGTGGGGCAT-3') such that parts of the cDNA coding for C2 and C1b regulatory sub-domains were deleted following cleavage of the PCR product with *Mlu*I and re-ligation to create a dominant negative PKCε construct fused to GFP and driven by the HCMV promoter (HDNP). The HDNP construct was isolated as a *BamH*1 fragment and cloned into the *BamH*1 site of plasmid p41 to create p41HDNP that contains the dominant negative PKCε construct (HDNP) with homologous flanking sequences for the UL41 locus of HSV-1. The vector, vHDNP was created by replacing the ICPO:LacZ cassette at the UL41 locus of QOZ with HDNP. This was achieved by homologous recombination between p41HDNP and the UL41 locus of the QOZ vector. Recombinants were isolated using GFP as a marker. The UL41DNP locus was PCR amplified from the vHDNP viral DNA and sequenced prior to performing experiments.

2.1.2 Construction of the vHG vector.

QOZ was deleted for the ICP0p:LacZ expression cassette present in the UL41 locus using plasmid p41 to make virus Q (ICP4-,ICP27-,ß22,ß47). An HCMV immediate early (IE) promoter driving EGFP (HCMVp:EGFP) was engineered into the ICP4 loci between the *Afl*III-*Sty*I (HSV bases 126413 to 131879) of the Q vector, to make vHG (ICP4-,ICP27-,ßICP22,ßICP47 **H**CMV:E**G**FP::ICP4) that has an expanded ICP4 deletion and truncated ICP22 and ICP47 promoters compared to parental vectors.

2.1.3 Construction of the vTT vector.

The vTT vector (ICP4-, ICP27-, ßICP22, ßICP47, **T**Kp:**T**RPV1::ICP4) was constructed by replacing the HCMVp:EGFP cassette in the ICP4 locus of vHG with a TRPV1 cDNA driven by the early HSV-1 TK promoter (TKp:TRPV1) using plasmid pTT. pTT was constructed by inserting the *Pvu*II-*Bgl*II fragment of pUX containing the early TK promoter and the *Asp*718-*Not*I fragment containing the rat TRPV1 coding sequence (Kind gift of D Julius) [21] into plasmid pSASB3. Plasmid pSASB3 contains the *Sph*I-*Afl*III and *Sty*I-*EcoR*II fragments flanking the ICP4 coding sequence with a unique *BamH*I linker present between the two fragments.

2.2 CELLS, CELL CULTURE, VIRAL INFECTIONS AND TRANSDUCTION

2.2.1 Complementing and non-complementing Vero and U2OS cell lines.

Several experiments in chapter three make use of a complementing cell line (7B cell line) that expresses the ICP4 and ICP27 viral proteins *in-trans* [44, 45]. This allows the *in-vitro* propagation of ICP4$^-$, ICP27$^-$ replication defective HSV-1 vectors. The non-complementing Vero and U2OS cell lines were used for immunostaining and Western blot experiments in chapters 3 and 4 respectively. 7B, Vero and U2OS cell lines were grown and maintained in Dulbecco's Minimum Essential Medium (DMEM) supplemented with 10% fetal bovine serum, 2 mM L-glutamine and 100 U/ml penicillin/streptomycin (all media components from Life Technologies Inc.). Cells were subcultured in 150 cm^2 vented cap polystyrene tissue culture flasks

(Falcon/Becton Dickinson, San Diego, CA) and incubated at 37°C in a humidified 5% CO_2 incubator.

2.2.2 Primary neuronal cell culture.

The adult rat DRG neurons used for experiments in chapter four were isolated by standard enzymatic techniques as previously described for isolation and culture of rat DRG neurons [64]. Briefly, freshly dissected ganglia were minced and washed in cold, oxygenated DMEM (Sigma). This was followed by 10 min dissociation at 37˚C in DMEM containing 0.5 mg/ml trypsin (Sigma). After a 10 min centrifugation, the media was replaced with DMEM containing 1 mg/ml Collagenase B (Boehringer-Mannheim) and 0.5 mg/ml Trypsin Inhibitor type 1S (Sigma). Dissociation of neurons was continuously monitored and the cells were gently triturated with siliconized Pasteur pipettes every 10 min. After the ganglia dissociated into individual neurons (25-40 min.), the cell suspension was centrifuged for 10 min at 1200 rpm. The pellet was layered on 20 ml of 50% adult bovine serum (Sigma) and DMEM and centrifuged again at 800 rpm. This step removes most debris and broken cells. The pellet was then resuspended in DMEM containing 10% heat inactivated horse serum and 5% fetal bovine serum (Sigma), and plated on collagen coated 35 mm petri-dishes (Collaborative Research, Biocoat) or 35 mm Petri dishes with 10 mm glass bottom microwells (Mattek Corporation, Ashland, MA) for imaging experiments. Neurons were plated at low density (2000-3000 per dish) and the primary cultures were incubated in a 95% air, 5% CO_2 humidified incubator at 37°C for three to four days prior to infection with HSV-1 vectors.

2.2.3 Infection and transduction: A note on the terminology.

In this thesis, the term infection has been used to denote the process of attachment and entry of HSV-1 vectors with consequent virus replication in complementing 7B cell lines, while the term transduction has been used to denote HSV-1 vector attachment and entry and the consequent expression of transgenes in neurons, non-complementing Vero and U2OS cells. Thus, the difference between infection and transduction lies respectively in the presence or absence of replication after HSV-1 vector entry into the cell.

2.2.4 Methods for infection and cell transduction with HSV-1 vectors and general methodology for TRPV1 functional assays.

HSV-1 infections for complementing 7B cells were done in suspension in 15 ml conical tubes (Falcon) with DMEM media containing 10% FBS, and rocked on a nutator platform (Becton Dickinson) for 1 hour at 37°C. The vector-transduction of non-complementing Vero and U2OS cells was performed in a similar manner.

For TRPV1 functional studies, 250,000 cells per well were plated in 24 well plates containing required final concentrations of reagents in 1 ml of DMEM with 10% FBS, and incubated at 37°C in a humidified 5% CO_2 incubator. Supernatant samples collected at 24, 48 and 72 hrs post-infection (hpi) were titered by a standard viral plaque assay [59]. The number of plaques for each viral dilution was counted and titers were expressed as viral plaque forming units (PFU) per ml of viral suspension.

2.2.5 Transduction of primary neuronal cultures with HSV-1 vectors.

Primary neuronal cell cultures were incubated at 37˚C for three to four days prior to transduction with HSV-1 vectors. This allowed the growth of supporting fibrablasts and prevented sloughing of the neurons during and after transduction. Transduction was performed one day prior to the experiments. 10^7 PFU of vHG or vHDNP vectors were suspended in 600 µl of DMEM media containing 5% FBS and 10% heat inactivated HS. Media in the 35 mm Petri dishes was replaced with 600 µl of the above media containing 10^7 PFU of viral vectors. The viral inoculum (600 µl) was allowed to incubate overnight at 37˚C on the neuronal monolayer and experiments were performed the following day as required. Figure 5 is a schematic depicting the general methodology followed for the transduction of primary DRG neurons. As shown in the panels at the bottom of the figure, nearly 100% transduction efficiency of neurons and supporting cells in culture was achieved by following this method.

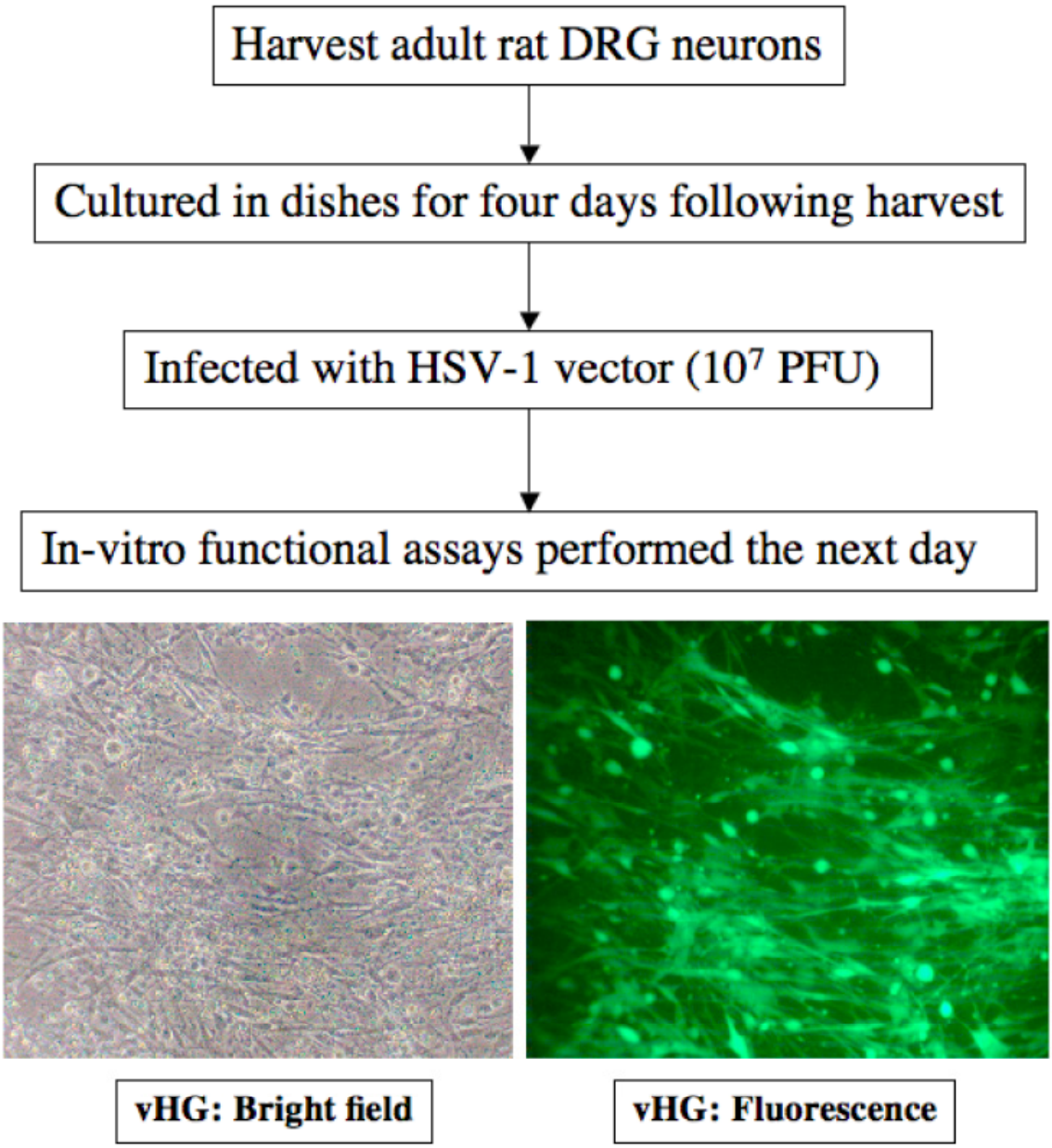

Figure 5. Method for transducing DRG neurons with HSV-1 vectors.

The figure is a schematic showing the methodology followed for transducing DRG neuronal cultures with HSV-1 vectors. The panels at the bottom of the figure show that nearly 100% of neurons were transduced by this method using the HSV-1 vector, vHG.

2.3 SOUTHERN BLOTTING

Viral DNA extracted by spooling from 3 million 7B cells infected at a multiplicity of infection (MOI = number of plaque forming units or PFU per cell) of 3 was used for Southern blotting [62]. Southern blotting was performed using a North2South kit (Pierce, Rockford, IL) as per the manufacturer's instructions. Briefly, ~1ug viral DNA extracted as above was digested with restriction enzymes and bands were electrophoretically separated. Following overnight transfer to a nitrocellulose membrane, hybridization with biotinylated probe was carried out overnight at 55˚C. The blot was then washed and developed with luminol. Signals were detected by autoradiography and scanned. A 10Kb biotinylated lambda plus marker (New England Biolabs, Catalogue # N75545) was used as the molecular weight marker for all southern blots.

2.4 WESTERN BLOTTING

Western blotting was performed to confirm the expression of GFP by vHG and DNP fused to GFP by vHDNP in vector-infected 7B, or vector-transduced Vero and U2OS cells. The cells were infected / transduced with the viral vectors, harvested with 1X NuPAGE LDS Sample Buffer in PBS (Invitrogen, Carlsbad, CA) and heated at 70^{o}C for 10 minutes. Each protein sample was loaded into duplicate wells on NuPAGE Novex Tris-Acetate gel (Invitrogen, Carlsbad, CA) and electrophoresed. The gel proteins were then transferred onto Immobilon-P PVDF membrane (Millipore, Billerica, MA). The membrane was cut into strips representing duplicate wells for a particular vector infection and cell line. The membranes were probed overnight at 4^{o}C with a 1:500 dilution of goat polyclonal antibody against GFP (Abcam,

Cambridge MA) in PBS containing 2% dry milk. The membranes were then washed with PBS containing 0.05% tween-20, incubated with a 1:7000 dilution of donkey anti-goat horseradish peroxidase conjugated antibody (Sigma, St. Louis, MO) in 2% milk for 1 h at 25^{o}C. After additional washes, the membranes were juxtaposed and the signals were developed on one X-ray film according to the standard protocol using the Amersham ECL kit (Amersham Pharmacia Biotech, Piscataway, NJ).

2.5 IMMUNOCYTOCHEMISTRY

For immunocytochemical analysis in Vero and complementing 7B cells, cells were infected with either vHG or vTT (18 hpi, 0.3 PFU/cell) and plated in an eight microwell glass bottom slide (Falcon). Following fixation in 4% formaldehyde at RT for 10 minutes, infected cells were washed twice with PBS, and then permeabilized in 0.001% Triton-X 100 for 10 minutes at RT. Slides were blocked with 10% horse serum (HS) in PBS for one hour at RT then incubated for one hour with either the TRPV1 (1:300, EMD Biosciences Oncogene Research Products, LA Jolla, CA) or an ICP0 (1:500, raised in rabbits against the 30 C-terminal residues of the ICP0 protein) antibody. Slides were washed in PBS and incubated at RT for one hour with a TRITC labeled goat anti-rabbit IgG secondary antibody (1:500, Sigma, St Louis, MO). After washing with PBS, coverslips were applied and images captured using a Zeiss inverted fluorescent microscope with Axiovision software (Carl Zeiss Microimaging Inc., Thornwood, NY).

For immunocytochemistry in adult rat DRG neurons were plated in a 35 mm petri dish with 10 mm glass bottom at a density of 200 cells per dish. Four days after culture, neurons were transduced in a monolayer with either vHG or vHDNP (10^7 PFU per petri dish). The

following day (16 hpi.), vector-transduced dishes were incubated with 5 μM phorbol dibutyrate (PDBu) for 2 min as required and then immediately fixed for 20 minutes at RT in 2% paraformaldehyde. Following two washes in PBS, cells were blocked with 10% HS in PBS for one hour and then incubated for one hour in 1% HS in a rabbit PKCε anitbody (1:300 dilution). The PKCε antibody used for this purpose is developed in rabbit using a synthetic peptide (Lys-Gly-Phe-Ser-Tyr-Phe-Gly-Glu-Asp-Leu-Met-Pro) corresponding to the C-terminal variable (V5) region (amino acids 726-737) of PKCε (Sigma St. Louis Missouri). Dishes were then washed with PBS and incubated for one hour with a Cy3 labeled goat anti-rabbit secondary antibody (1:300 dilution, Sigma). It should be noted that no permebealization was performed for PKCε immunostaining in order to prevent artifacts due to the disruption of protein subcellular localization that can occur following permebealization. Images were captured in multiple planes (4 to 6 planes) for each neuron with a Zeiss 510 meta inverted fluorescent microscope using green and red channels. Images are presented as stacked projections of multiple planes for each transduced neuron and were processed using the ImagePro image processing software.

2.6 LIVE CELL IMAGING

Vero and U2OS cells were transduced in suspension with the vHDNP vector (MOI 3) for 1 hour at 37˚C. Cells were plated in 10 mm glass bottom microwells of 35 mm Mattek petri dishes at a density of 40,000 cells per dish. For live cell imaging in neurons, cells were transduced in monolayer 4 days after plating freshly dissociated DRG neurons at a density of 500 cells per Mattek petri dish. Cells were visualized using a Leica TCS NT inverted fluorescent microscope. Phorbol myristate acetate (PMA) was added directly to the media in the Mattek petri

dishes to achieve a final concentration of 5μM PMA. Immediately after PMA stimulation, cell images were recorded at 2-second intervals, for the duration of the experiment, which lasted from 2 to 3-min. Translocation of the green fluorescent transgene product (DNP fused to GFP) was captured using a green fluorescent filter. The movies were recorded in Dr. Simon Watkins laboratory (Center for Biological Imaging, University of Pittsburgh, Pittsburgh PA).

2.7 WHOLE CELL PATCH CLAMP RECORDINGS

Gigaohm-seal whole-cell recordings of capsaicin induced currents were recorded in Vero cells and adult DRG neurons transduced with vTT, vHG or vHDNP vectors (20 hpi, 10 PFU/cell for Vero cell recordings and 16 hpi, 10^7 per petri dish for rat DRG neurons) or non-transduced cells using whole cell patch clamp techniques. Patch pipettes were pulled from capillary glass tubes (Accufil 90, Clay-Adams) and fire polished. Immediately before recording, the serum containing media was replaced with phosphate buffered saline. Whole cell currents were voltage clamped using an Axopatch 200A (Axon Instruments, Foster City, CA) amplifier. Pulse generation, current recording and data analysis used pClamp software (Axon Instruments). Currents were sampled at 500 μs, and filtered at 2 kHz. Capacitive currents and up to 80% of the series resistance were compensated. A p/4 protocol was used to subtract uncompensated capacitative currents and leak currents. The decay of TRPV1 currents in response to capsaicin and after addition of the phorbol ester, phorbol 12,13-dibutyrate (PDBu) or the PKC inhibitor bisindolylmaleimide I HCl (BIM) in the presence of capsaicin was fitted with single exponentials using pClamp software regression analysis. To determine the kinetics and voltage dependence of activation and inactivation of outward currents, a combined two pulse activation-inactivation

protocol was used, consisting of series of rectangular pre-pulses from a holding potential of -90 mV. The pre-pulse, 1000 ms in duration, ranging from –140 to +90 mV was used to generate current activation. The inactivation curve was measured after a brief, 23 ms interpulse at -80 mV and a second test pulse to +60 mV, 250 ms in duration. Peak current amplitudes were measured with pClamp software.

The extracellular solution was Dulbecco phosphate buffer (Sigma, St. Louis, MO). The pipette (intracellular) solution contained (mM): KCl 120, K_2HPO_4 10, NaCl 10, $MgCl_2$ 2, EGTA 1, HEPES 10, pH adjusted to 7.4 with HCl. To this solution Mg-ATP (3 mM), cAMP (0.3 mM) and tris-GTP (0.5 mM) were added just prior to the experiments. Capsaicin (Calbiochem, San Diego, CA), a TRPV1 antagonist (Neurogen, Branford, CT), the phorbol ester, phorbol 12,13-dibutyrate (Research Biochemicals, Natcik, MA), and the PKC inhibitor bisindolylmaleimide I HCl (Calbiochem, San Diego, CA) were dissolved in DMSO (100 mM) and used at less than 0.01% of their stock concentration. At these dilutions, DMSO alone had no effect on TRPV1 responses to capsaicin. Ruthenium Red (RuR) was prepared in aqueous solutions. Stock solutions in 10-100 mM were stored at -20^{o} C and diluted in the external recording solution just before use. The TRPV1 antagonist (diaryl piperazine, NDT9515223) was a gift from Neurogen (Branford, CT) and was shown previously to be a potent and selective TRPV1 inhibitor (K_i = 7 nM) [65]. Extracellularly applied drugs were pipetted from stock solutions at 10 to 100 times the final concentration and rapidly mixed in the recording chamber as described previously [64].

2.8 INTRACELLULAR CALCIUM MEASUREMENT

Free intracellular calcium was measured by photon scanning on a dual excitation fluorimeter (PTI, Lawrenceville, NJ). vTT or QOZ infected 7B cells were plated in 6 well plates containing 13.5 x 20 mm coverslips. Infected cells (8 hpi, 3 PFU/cell) were rinsed with 1X Hank's balanced salt solution (HBSS) and loaded with 2 μM FURA-2 (Molecular Probes Inc., Eugene, OR) [66] for 1 hour at 37˚C in a 5% CO_2 incubator. Coverslips with FURA-2 loaded cells were then placed in a cuvette containing HBBS and then separately subjected to capsaicin at either 3 or 0.3 μM concentrations. Calcium flux following the application of each concentration of capsaicin was measured at 2 Hz and graphed. Results were calibrated by adding 5 μM ionomycin to obtain the maximum fluorescence ratio, followed by addition of 10 mM EGTA to obtain the minimum fluorescence ratio. A K_d of FURA-2 for calcium of 224 nM was assumed.

2.9 DETECTION OF MITOCHONDRIAL PERMEABILITY TRANSITION AND CASPASE ACTIVATION

The DePsipher kit (R&D systems, Minneapolis, MN) was used to detect the initiation of mitochondrial permeability transition (MPT) in 7B cells. Briefly, vTT or QOZ infected cells (12 hpi, 0.1 PFU/cell) were incubated with 3 μm capsaicin for one hour at 37˚C in a 5 % CO_2 incubator. Cells were then loaded with 1 μl DePsipher/ml in pre-warmed culture media for 15-20 min at 37˚C in a 5% CO_2 incubator. Following two washes in prewarmed media, cells were immediately imaged using an inverted fluorescence microscope (Carl Zeiss Inc.).

For activated caspase detection, the CaspACE FITC-VAD-FMK *In- Situ* Marker kit (Promega, Madison, WI) was used. Briefly, CaspACE FITC-VAD-FMK was added to a final

concentration of 10 μM to 7B cells infected with vTT or QOZ virus (12 hpi, 0.3 PFU/cell). Cells were incubated for 20 minutes at 37˚C in a 5 % CO_2 incubator. Following two washes in PBS, cells were fixed for 30 minutes in 4 % formalin, washed three times with PBS and imaged using an inverted fluorescence microscope (Carl Zeiss Inc.).

2.10 VIRAL GROWTH ASSAYS

Infections for all TRPV1 functional studies were done in suspension in 15 ml conical tubes (Falcon) with DMEM media containing 10 % FBS, and rocked on a nutator platform (Becton Dickinson, San Diego, CA) for 1 hour at 37˚C. Cells were pelleted by centrifugation at 1000 rpm for 5 min and resuspended in 1ml of fresh DMEM. 250,000 cells per well were plated in 24 well plates containing required final concentrations of reagents in 1 ml of DMEM with 10 % FBS, and incubated at 37˚C in a humidified 5% CO_2 incubator. Supernatant samples collected at 24, 48 and 72 hrs post-infection (hpi) were titered by a standard viral plaque assay [59]. The number of plaques for each viral dilution was counted and titers were expressed as viral plaque forming units (PFU) per ml of viral suspension.

2.11 COBALT UPTAKE ASSAYS

Cobalt uptake assays were performed to identify TRPV1 activity in adult rat DRG neurons. The assay was performed according to a previously described method [67]. Briefly, non-transduced and vHG or vHDNP-transduced neurons in culture were washed twice in buffer A (NaCl, 57.5 mM; KCl 5 mM; $MgCl_2$, 2 mM; HEPES, 10 mM; Glucose, 12 mM; Sucrose, 139

mM; pH 7.4). Neurons were then incubated in a cobalt uptake assay buffer (buffer A plus 5 mM $CoCl_2$ and 0.5 μM capsaicin) for 8 min at room temperature. Following incubation in the cobalt uptake assay buffer, 0.2 % ammonium polysulphide (Sigma) was added and immediately washed off using buffer A. Ammonium polysulphide causes the intracellular precipitation of black, granular cobalt sulphide in the cytoplasm of neurons due to prior Co^{+2} ion uptake resulting from capsaicin-induced TRPV1 receptor activition. The number of black neurons is thus indicative of the percentage of TRPV1 expressing, capsaicin sensitive neurons in a culture. Following the assay, the number of black neurons was counted using a bright field microscope and this was expressed as a percentage of the total number of neurons counted.

2.12 CHEMICALS

Capsaicin, resiniferatoxin, ruthenium red, capsazepine, SB-366791, phorbol dibutyrate (PDBu), HYP-3-bradykinin (HYP3BK) and phorbol myristate actetate (PMA) were obtained from Sigma (St. Louis, MO). Micromolar and nanomolar dilutions for experiments were made by serial dilutions of stock solutions. Chemicals were added to media in the wells just prior to plating cells for selection studies.

2.13 *IN-VIVO* BEHAVIORAL TESTING

All *in-vivo* tests were performed on adult male Sprague-Dawley rats (200-225 g; Charles River, Boston, MA). Four days prior to performing behavioral tests, the animals were

subcutaneously injected with 100 µl of vHG, vHDNP (10^9 pfu/ml) or PBS (sham injection) into the plantar surface of the right hind paw. Uninjected animals were included as an additional control.

Tests for thermal hyperalgesia were performed using a Hargreaves apparatus on a platform with a baseline temperature of 25˚C. Each animal was placed on the platform in a 10 cm x 20 cm plastic container, positioned over a mirror tilted at a 45° angle. All rats were allowed to acclimatize to the plastic container and platform for 30 min prior to testing. During each evaluation of thermal hyperalgesia, a focused heat source using a light intensity of 30-lumen was aimed at the plantar surface of the foot and the time until the animal moved its foot in response to the heat measured. Three trials per testing period were made for each animal on both, the right and left foot with 1 min rest between each measurement. The average withdrawal time per foot was used for statistical comparisons. Data are presented as a ratio of the average time taken for withdrawal of the right foot versus the left foot for animals in each group.

To test for mechanical allodynia (painful response to an innocuous stimulus) each animal was placed in a clear plastic 10 cm x 20 cm container on top of a wire screen. After a 15-minute accommodation period the mechanical threshold was measured by applying a series of von Frey hairs to the midplantar surface of each hind paw. The von Frey hairs are a set of calibrated filaments of increasing diameter and stiffness. As they are pushed against the bottom of the paw, animals either retract their foot or not depending on whether or not the pressure from the von Frey hair is painful. Withdrawal of the hind paw within 5 seconds was inferred as a positive response; no paw withdrawal was inferred as a negative response. The up-down method was utilized to determine the 50% gram threshold [68]. In this method, a positive response is followed by application of the next grade higher filament and a negative response is followed by

presentation of the next grade lower filament. Approximately six responses from each animal were recorded. An algorithm together with the pattern of responses is used to calculate the 50% gram threshold response.

2.14 STATISTICS

Graphs for functional assays are based on data from four independent experiments (n=4). Error bars for all graphs including graphs for *in-vivo* behavioral tests are calculated as standard deviations. For patch clamp experiments, results are reported as mean ± SEM. For cobalt uptake assays, error bars are calculated based on standard deviations from a binomial distribution where a neuron with cobalt uptake is indicative of success and a neuron without uptake is indicative of failure. Statistical analysis for p values used t-test, 2 tail, and unequal variance. Data were considered to be statistically significant if $p < 0.05$. All images shown are representative results following multiple iterations of each experiment.

3.0 DESIGN AND DEVELOPMENT OF AN HSV-1 VECTOR-BASED SYSTEM FOR THE IDENTIFICATION AND SELECTION OF ION CHANNEL ANTAGONISTS

3.1 INTRODUCTION

The human genome expresses over 400 ion channels involved in almost every vital biological process including cardiac, renal and nervous system functions [69]. Ion channel inhibition is consequently gaining importance as an approach to treat many disorders. Ion channel antagonists such as lidocaine (sodium channel antagonist) to treat neuropathic pain, the anti-convulsant levetiracetam (N-type calcium channel blocker), the anti-arrhythmic carvedilol (L-type calcium channel blocker), anti-cancer agents such as carboxyamidotriazole (non-voltage operated calcium channel inhibitor), the anti-emetic ondansetron and numerous others are either established drugs or currently undergoing clinical trials [70-75]. The need for accelerated drug discovery has therefore resulted in high throughput screening (HTS) assays for ion channel antagonists [76]. Indeed, HTS assays identifying NMDA, AMPA and TRPV1 specific antagonists have been recently published [77-80].

Recent reports have uncovered the existence of several ion channels that are specifically upregulated in nociceptors during the development of chronic inflammatory and neuropathic pain states (Fig. 6) [5, 56]. The transient receptor potential (TRP) family of ion channels, sodium channel subtypes, purigenic receptors (P2X3), voltage gated calcium channels (VGCC) and the serotonin ionotropic receptor (5-HT3R) are among the pro-nociceptive receptors, while

potassium ion channel subtypes act as modulatory channels during nociception (Fig. 6). Although the mechanisms of channel activation are being revealed for many of these receptors, pro-nociceptive ion channel-specific antagonists and modulatory gene products are largely unknown. It follows that the discovery of specific antagonists or gene products that attenuate pro-nociceptive ion channel function may lead to a better understanding of nociceptive regulation at the periphery and can provide new drugs and avenues for the treatment of chronic pain states.

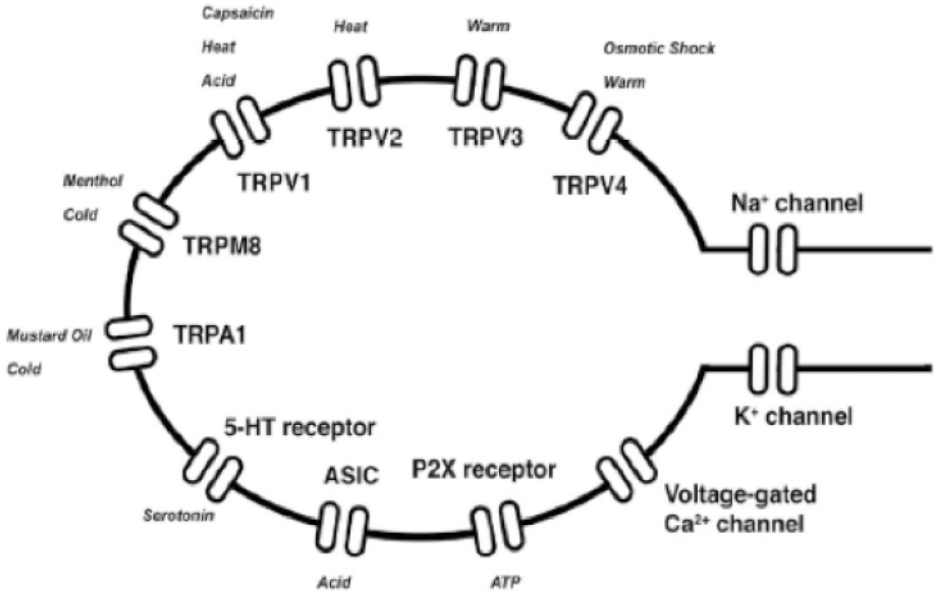

Figure 6. **Pro-nociceptive ion channels.**

The figure depicts ion channels upregulated in chronic pain states that are involved in nociception at the periphery of the pain pathway. These channels are directly activated by several components of the inflammatory soup such as protons, heat, ATP and bradykinin (From Lee et al, Mol. Cells, Vol.20(3) 315-324)

Fluorescence-based high throughput screening (HTS) assays are a mainstay for the discovery of molecules that specifically inhibit target ion channels. Current fluorescence based HTS assays for antagonists generally rely on a loss of signal following channel activation. This strategy results in significant numbers of false positives due to transient signals or signal

quenching by the candidate compound [81, 82]. As a result, subsequent secondary stage compound analyses increase both time and labor requirements. Other HTS assay drawbacks include the use of expensive reagents (e.g. FURA-2 in fluorescence based assays), low throughput (e.g. patch clamping) or low expression levels (e.g. stably transfected cell based assays). Specifically, assays utilizing stably transfected cell lines for cDNA expression exhibit declining expression levels with continual *in-vitro* culture or when applied to high throughput formats [83]. This can cause ambiguity when interpreting assay results. Given the difficulties with cell based assays, viral vector-based transient expression systems offer several advantages such as robustness due to ease of handling, high and uniform cDNA expression, excellent control over transgene expression achieved by varying parameters of infection and the ability to simultaneously express multiple transgenes, a property that can be exploited for ion channels possessing more than one type of subunit [83].

Replication defective herpes simplex virus-1 (HSV-1) vectors deleted for the essential immediate early genes ICP4 and ICP27 have been previously used for therapeutic gene transfer [44, 45]. This platform has proven useful to evaluate the ability to deliver a variety of anti-nociceptive gene products *in-vivo* in animal models of acute, chronic, and neuropathic pain [42]. In addition, replication defective HSV-1 vectors possess a large transgene capacity, the ability to simultaneously express multiple transgenes and an excellent control over transgene expression timing by using viral promoters with different kinetics of activation. The current chapter exploits these natural properties of HSV-1 viral vectors as a transgene expression tool in order to develop an HSV-1 based selection system using the vanilloid receptor as a target ion channel. The following paragraphs recap the role of the vanilloid receptor in nociception and the basis for HSV-1 vector-based selection.

The vanilloid receptor (transient receptor potential vanilloid 1, TRPV1, formerly known as VR1) plays important roles in nociception and physiology, making it an attractive therapeutic target for chemical library screens to identify novel receptor antagonists [79, 80]. TRPV1 is a peripheral pro-nociceptive Ca^{+2} ion channel belonging to the transient receptor potential (TRP) superfamily. TRPV1 is the peripheral sensor of inflammatory mediators such as ATP and bradykinin. In addition, TRPV1 is directly activated by heat (43˚C) [25], endovanilloids (anandamide) [23], low pH (protons), capsaicin and resiniferatoxin [25]. TRPV1 activation through this complex array of mechanisms results in the development of the neuronal hyperexcitability seen in chronic pain [84]. TRPV1 knockout mice exhibit reduced responses to noxious thermal stimuli [35, 85], which underscores the contribution of TRPV1 to the pain signaling pathway. Due to its vital role in nociception and the likely analgesic benefits of TRPV1 antagonism, this receptor was chosen as a model ion channel for developing an HSV-1 vector-based assay to identify novel antagonistic compounds.

In this chapter, a cell based assay was developed that utilizes herpes simplex virus 1 (HSV-1) vector expressed TRPV1 channels in which channel activation causes the influx of cytotoxic levels of Ca^{+2} ions into the cell. This Ca^{+2} influx induces cell death prior to the completion of the virus replicative cycle thereby blocking vector replication. TRPV1 antagonists in the presence of known receptor agonists reverse the inhibition of HSV-1 virus growth, thus allowing the identification of ion channel antagonists by selective vector replication. The HSV-1 vector may be engineered to co-express gene products such as green fluorescent protein (GFP) along with the ion channel. Vector replication resulting from channel antagonism will, in this case, cause a gain of fluorescence that can be read by an automated fluorometric plate reader (FLIPR). In addition to possessing advantages of a virus-based expression system, as a platform

the system is easily adaptable to a variety of ion channels such as the ligand gated TRP, NMDA, P2X3 and VGCC receptors.

3.2 RESULTS

3.2.1 Vector constructs and Southern Blotting.

To carry out these studies, two HSV vectors were created, a test vector (vTT) containing the TRPV1 gene replacing both copies of the essential immediate early (IE) gene ICP4 and a control vector (vHG) in which the ICP4 gene was replaced by an EGFP reporter gene cassette (Fig.7, top panel). The recombinant vector backbone is also deleted for the essential IE gene ICP27. Deletion of either ICP4 or ICP27 prevents subsequent expression of early or late viral genes and provides a platform for gene transfer (Fig. 7, top panel). Vector propagation and studies of TRPV1 function expressed from the vector genome were carried out in a complementing cell line (7B cells) that supply the ICP4 and ICP27 gene products *in-trans*.

The virus structures were confirmed by Southern blot analysis (Fig 7, bottom panels). All DNA digests were separately hybridized to probes for ICP27 (*BamH*1 to *Sac*1 fragment), ICP4 5' (*BamH*1 to *Bgl*II fragment), thymidine kinase promoter (TKp) (*Pvu*II to *Bgl*II fragment) or TRPV1 (*Asp*718 to *Not*1 cDNA fragment). Results confirm the correct insertion of the TRPV1 cDNA (TRPV1 probe) replacing EGFP at both ICP4 loci of vHG in vTT (Fig 7). The TKp and ICP4 5' probes confirm that TRPV1 cDNA is under transcriptional control of the viral early TK promoter at both ICP4 loci of vTT. Blots probed with the ICP27 validate the identical deletion of ICP27 in both vectors (Fig 7).

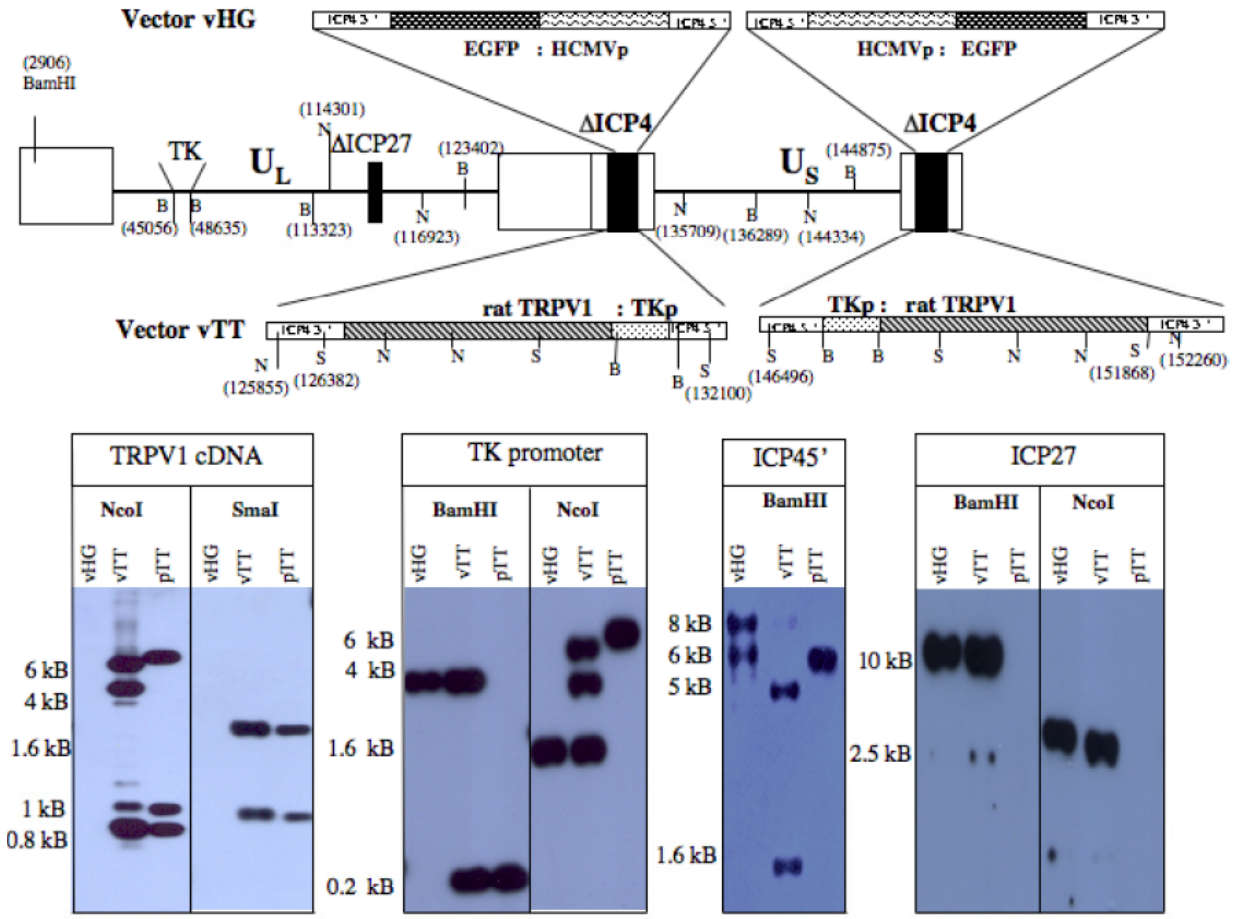

Figure 7. Genomic representation of the vectors vHG and vTT.

The top part of the figure shows schematic representations of the vTT and vHG vectors. Both vectors contain deletions of the immediate early (IE) genes, ICP4 and ICP27. In the genome of vHG, an HCMV immediate early promoter driving enhanced green fluorescent protein (HCMVp:EGFP cassette) is inserted into both ICP4 loci (top panel). In the genome of the vTT vector a TKp:TRPV1 cassette coding for the rat TRPV1 receptor, driven by the TK early promoter (TKp:TRPV1) resides in the ICP4 loci (top panel). The bottom panels depict Southern blotting to confirm viral genomic structure. vHG, vTT and the plasmid pTT used in vTT construction. Viral DNA probed for; 1) the TRPV1 cDNA demonstrates that vHG is negative for TRPV1 cDNA. *Nco*I (1 kb and 0.8 kb bands) and *Sma*I (1.6kb and 1kb bands) cut TRPV1 internally. The *Nco*I digest has 4 kb and 6 kb bands indicative of two TRPV1 copies at the ICP4 loci, 2) using the TK promoter (TKp) as a probe confirms vHG and vTT are positive for endogenous TKp. The *Nco*I digest for vTT has two bands, indicating successful insertion of TKp at both ICP4 loci, 3) using the 5' region of ICP4 demonstrates vHG and vTT display band shifts for *BamH*1 digests, confirming replacement of HCMVp:EGFP in vHG with TKp:TRPV1 in vTT at ICP4 loci, 4) Probing for ICP27 flanking sequences confirm identical deletions in vectors vTT and vHG.

3.2.2 Protein expression profiles for vectors vHG and vTT.

TRPV1 was expressed under control of the viral early (E) gene promoter (HSV thymidine kinase) and thus is not expressed in non-complementing cells. Expression of TRPV1 occurs in complementing cells since the virus is able to replicate and thus activate promoters with early (E) and late (L) kinetics. This engineered delay in expression of TRPV1 enhances virus replication since TRPV1 imparts some toxicity without activation. The EGFP gene was placed under control of the HCMV IE promoter that is expressed both in complementing and non-complementing cells and is used as a visual indicator of vector transduction. Expression of the individual transgenes from the vectors constructed above was confirmed prior to initiating functional experiments. Immunostaining for ICP0 in Vero cells at 18 hpi was positive for vHG and vTT viruses, confirming expression of ICP0 as an immediate early (IE) gene in both viral genomes as expected (Fig. 8). Complementing 7B cells infected with vTT were positive for TRPV1 receptor expression by immunofluoresence while the control vHG virus was negative indicating exclusive expression of TRPV1 from vTT. Non-complementing Vero cells infected with vTT were negative for TRPV1 at 18 hpi, confirming that TRPV1 driven by the thymidine kinase (TK) early (E) promoter is active only during viral replication (Fig. 8). In 7B cells, the vHG virus harbors GFP^+ plaques when viewed under fluorescence, while vTT plaquing is GFP^-, indicative of successful marker transfer in these viruses (Fig. 8).

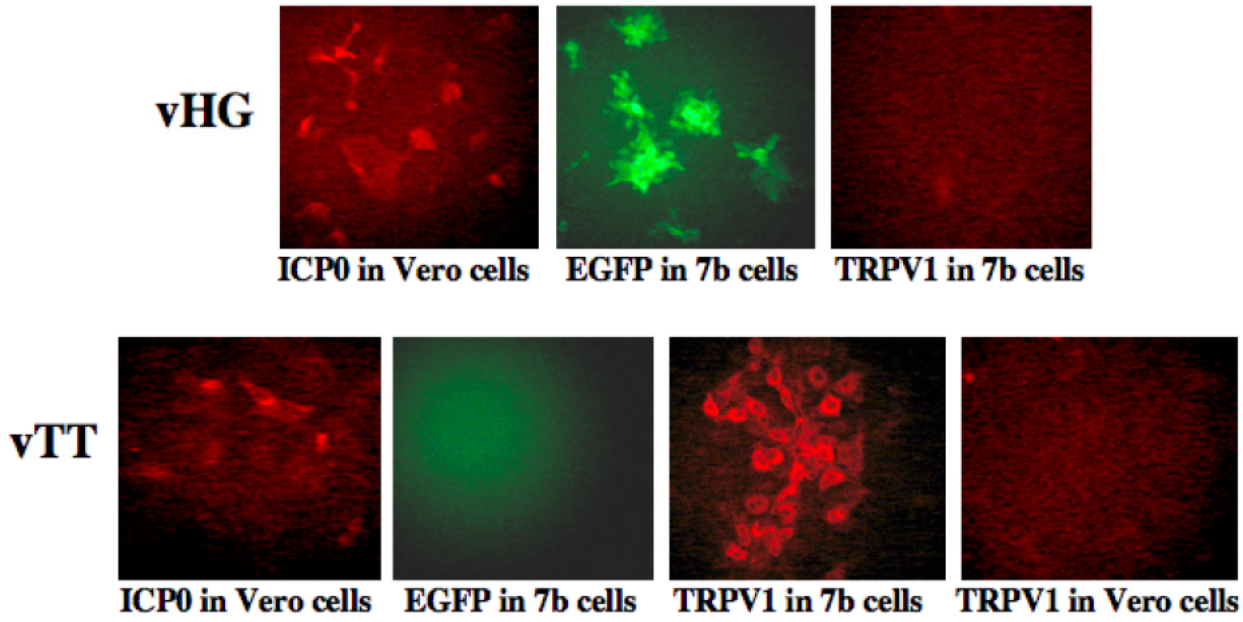

Figure 8. Protein expression profiles for vectors vHG and vTT.

The protein expression profiles in complementing 7B and non-complementing Vero cell lines are shown for the vector vHG (top three panels) and the vector vTT (bottom four panels). Since the natural HSV-1 immediate early (IE) promoter drives ICP0 protein expression, both vectors express ICP0 in non-complementing Vero cells. EGFP is exclusively expressed by vector vHG. TRPV1 is exclusively expressed by vector vTT and is limited to complementing 7B cells indicative of the early thymidine kinase (TK) gene promoter used to drive TRPV1 expression (all panels are at 20X magnification)

3.2.3 Functional demonstration of TRPV1 activity.

Whole cell electrophysiological recordings of vTT or vHG infected complementing 7B cells were done to demonstrate functional activity of the HSV-1 vector-expressed TRPV1 receptor. Infection of 7B cells was done at a high MOI (MOI of 10) to ensure that all cells in culture are infected with at least one virus particle. Figure 9 shows a representative trace of electrophysiological recordings from vHG or vTT infected 7B cells. Control vHG infected 7B cells did not respond to capsaicin. Capsaicin stimulation of vTT infected 7B cells resulted in

large current (nA range) that desensitized with time. The known TRPV1 antagonists, ruthenium red (RuR) and diaryl piperazine (NDT9515223, Neurogen) antagonized the vTT-specific currents. Table 2 summarizes electrophysiological recordings from vHG or vTT-infected and uninfected 7B cells. As seen in Table 2, the pre-incubation of vTT-infected 7B cells with bisindolylmaleimide (BIM), a PKC specific inhibitor resulted in significantly lower amplitude and rapidly desensitizing capsaicin-induced currents when compared to BIM untreated, vTT-infected cells. These data demonstrate the functionality of virally expressed TRPV1 in complementing Vero cells (7B cell line).

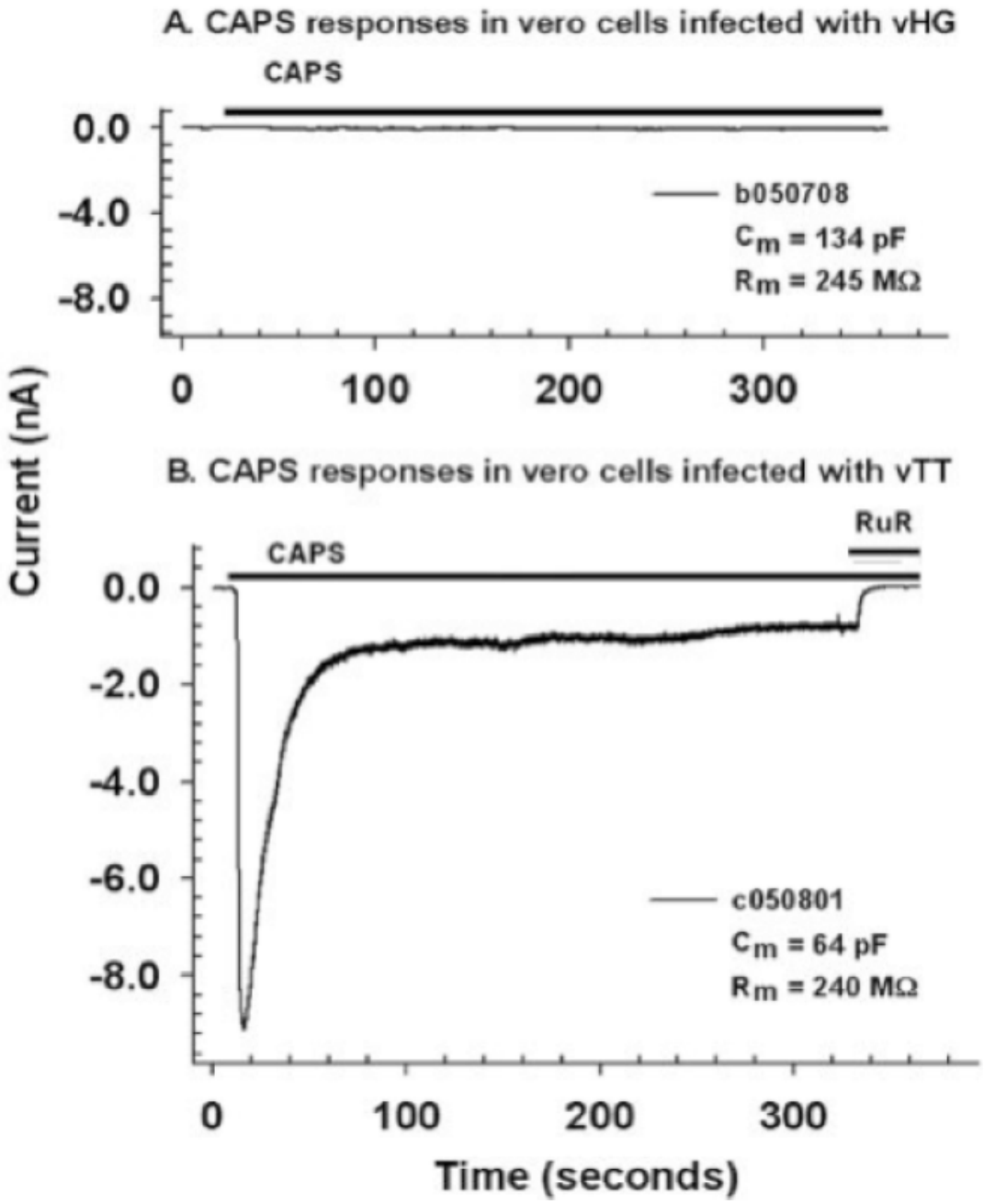

Figure 9. **Functional demonstration of TRPV1 activation by capsaicin.**

vHG infected 7B cells do not respond to capsaicin (CAPS) stimulation (upper trace). vTT infected 7B cells display a large inward current (9 nA) following stimulation with 0.5 μM capsaicin (CAPS) (lower trace). Addition of the TRPV1 antagonist, ruthenium red (RuR - 5 μM) brought the current back to baseline.

Table 2. Electrophysiological parameters in HSV-1 infected and uninfected 7b cells.

Parameters of excitability and K^+ currents were determined as in methods. Peak outward current amplitudes are for currents generated at +60 mV. The numbers of cells measured for each parameter are indicated in parentheses.

Infection	Membrane Capacitance	Membrane Resistance	Resting Potential	Outward Current Amplitude	Capsaicin	Capsaicin Desensitization Time-course
	C_m (pF)	R_m (MΩ)	RP (mV)	(nA)	(nA)	(tau, s)
vTT	71.8 ± 7.6	207.3 ± 26.9	0.04 ± 0.04	0.5 ± 0.4	-6.0 ± 0.6	280.6 ± 45.1
	(10)	(10)	(5)	(3)	(8)	(8)
vTT (BIM pre - incubation)	56.5 ± 2.5 (3)^{NS}	193.5 ± 76.5 (3)^{NS}	-	-	-2.2 ± 1.2 (3)**	53.4 ± 15.4 (3)***
vHG	171.5 ± 30.9	442.3 ± 109.8	0.8 ± 0.8	1.1 ± 0.1	No Response	-
	(4)	(4)	(4)	(4)		
no virus	34.0 ± 7.5	357.0 ± 122.1	-12.00 ± 2.8	0.7 ± 0.2	No Response	-
	(3)	(3)	(2)	(3)		

Level of significance: *NS* = not significant, ** = $p < 0.01$, or *** = $p < 0.001$

vTT = **v**ector **T**Kp: **T**RPV1; vHG = **v**ector **H**CMVp: E**G**FP ; BIM = PKC inhibitor, bisindolylmaleimide.

3.2.4 Demonstration of calcium influx following TRPV1 activation.

In order to demonstrate calcium influx through vTT vector-expressed TRPV1, intracellular calcium levels were monitored by FURA-2 loading, followed by stimulation of the vTT infected 7B cells with capsaicin. At 8 hpi, 3 μM capsaicin resulted in a massive increase of intracellular calcium (~900 nM range) in 7B cells infected with vTT virus (Fig. 10A). Ionomycin is calcium ionophore that disrupts the cell membrane, thus allowing a free flow of Ca^{+2} ions into the cellular cytoplasm. Ca^{+2} influx following ionomycin application is therefore indicative of the maximum amounts of extracellular Ca^{+2} ions that can enter a cell. Following the addition of 3 μM capsacin (CAP), the calcium influx response was sustained and did not further increase with 5 μM ionomycin (IONO) indicating that the Ca^{+2} influx with 3 μM CAP was maximal (Fig. 10A). Addition of 10 mM EGTA caused the signal to return to baseline levels indicating that a Ca^{+2} specific TRPV1 receptor was located on the cell membrane (Fig. 10A). Sub-maximal concentration of capsaicin (0.3 μM) caused a smaller response than that observed with 3 μM capsaicin (Fig. 10C). This response was further increased after the addition of 5 μM ionomycin (Fig. 10C). Since GFP would interfere with FURA-2 measurements, we used the GFP negative virus, QOZ as a negative control for intracellular Ca^{+2} measurements and the demonstration of apoptosis. QOZ possesses a similar backbone to vHG, but lacks the HCMVp:EGFP cassette at the ICP4 loci. QOZ instead contains an ICP0p-LacZ cassette at the UL41 locus. QOZ infected cells displayed a maximal calcium influx in response to 5μM ionomycin, but no effect with 0.3 or 3μM capsaicin (Fig. 10B and 10D).

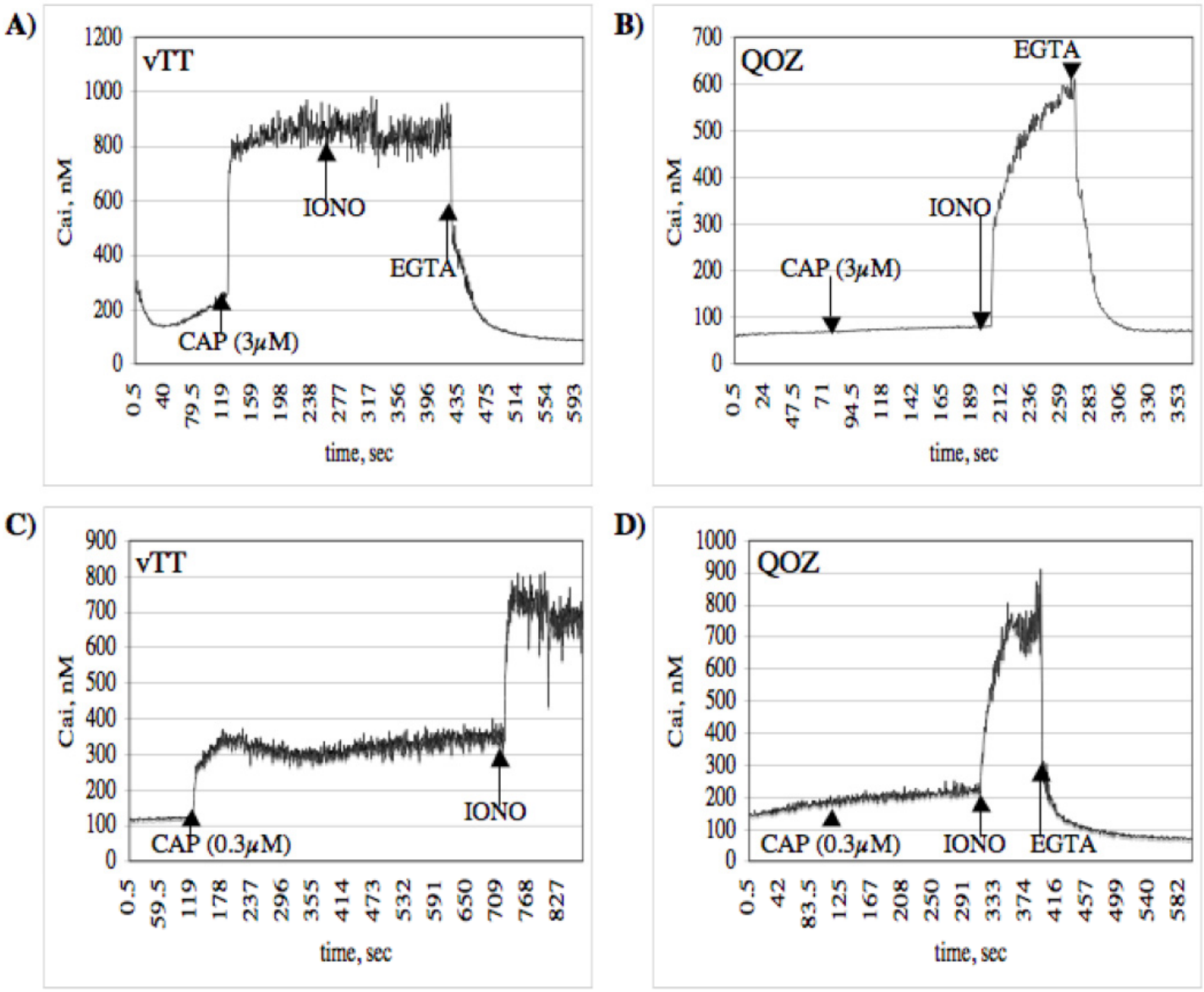

Figure 10. **Demonstration of calcium influx through TRPV1.**

Intracellular calcium concentrations (Cai, nM) graphed against time (sec) in response to stimulation with 3μM (Fig. 9A; 9C) or 0.3 μm (Fig. 9B; 9D) capsaicin (CAP), 5 μM ionomycin (IONO) and 10 mM EGTA are shown for vTT and QOZ infected cells.

3.2.5 Cell death following calcium influx through activated TRPV1.

Mitochondrial permeability transition (MPT) is often the first change that occurs during the initiation of cell death and is a major component of the apoptotic cascade induced by TRPV1 activation in several cell types. Ca^{+2} overload through activated TRPV1 has been specifically and uniquely linked to the development of MPT with the subsequent activation of caspases [86-88]. In order to demonstrate the development of MPT due to intracellular calcium overload in our system, we assayed for MPT and caspase activation following capsaicin exposure in 7B cells infected with vTT as described in materials and methods. Following stimulation with 3 μM capsaicin for one hour, MPT was specifically seen in vTT infected 7B cells at 12 hpi as evidenced by green fluorescent areas corresponding to mitochondria in the perinuclear region of dying cells (Fig. 11B is a bright field image of vTT infected 7B cells stimulated with 3 μM capsaicin and Fig. 11C is a green fluorescence image of the same field). Cell death and MPT were not observed in QOZ infected 7B cells following stimulation with 3 μM capsaicin (Fig. 11D). The QOZ vector was used as a control for this experiment since the MPT assay is based on a green fluorescent readout, thus disallowing the use of a GFP expressing vHG control vector. In addition to the development of MPT, vTT infected cells were positive for activated caspases following overnight capsaicin (3 μm) stimulation while QOZ infected 7B cells did not show a significant activation of caspases at 16 hpi (personal observation, data not shown). These data provide direct evidence for activated TRPV1 triggering Ca^{+2} overload, leading to MPT, caspase activation and the initiation of cell death.

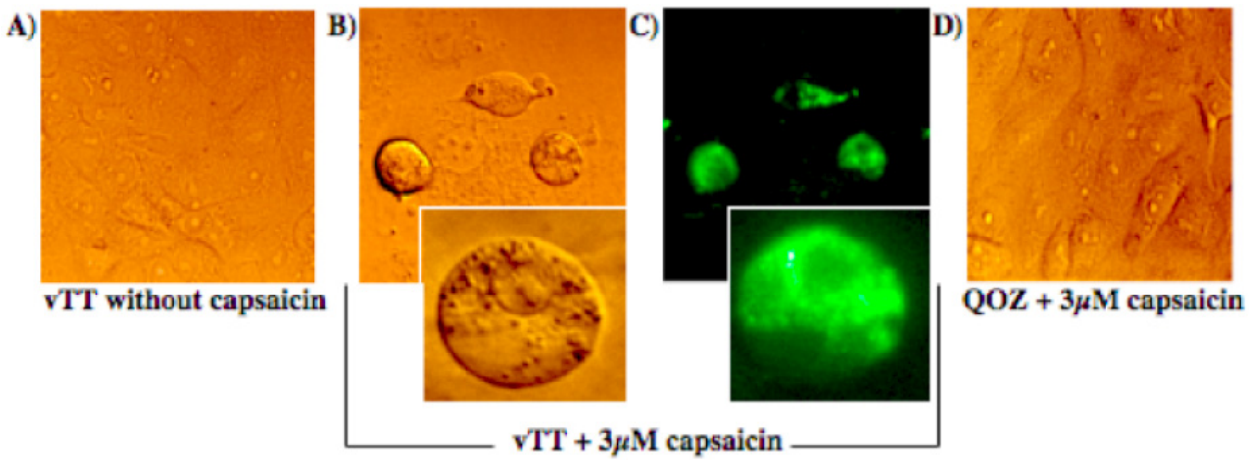

Figure 11. Demonstration of MPT and cell death.

(A) vTT infected 7B complementing cells without capsaicin. (B) Bright field image of vTT infected 7B complementing cells incubated with 3 μm capsaicin for 60 min and (C) Flourescent image of the same cells loaded with DePsipher dye to detect MPT. (D) Bright field image of vHG (control) infected 7B complementing cells incubated with 3 μm capsaicin (all images at 20X magnification, enlarged images are at 40X magnification).

3.2.6 TRPV1 activation blocks vector replication.

With the influx of cytotoxic levels of calcium into vTT infected cells and the consequent initiation of cell death as demonstrated above, it was anticipated that vector expression and the subsequent activation of TRPV1 would induce cell death prior to completion of the virus replicative cycle, thus blocking virus growth. In the absence of TRPV1 agonists, vector vTT replicated less robustly (~0.1 log) than vHG at 24 and 48 hpi, however, the final yield of these vectors was similar at 72 hpi. To quantify the effects of TRPV1 activation on viral replication, complementing 7B cells were infected at 0.01 PFU/cell and incubated in the presence of increasing concentrations (0.1 to 40 μM final) of the TRPV1-specific agonist, capsaicin. To display the differences in replication between vHG (control) and vTT (TRPV1 expressing)

vectors, the effect of capsaicin concentration was determined at 24, 48 and 72 hpi based on the ratio of vHG to vTT virus particle yield (growth ratio, GR). Significant differences in replication between vHG and vTT were observed at concentrations as low as 0.3 μM capsaicin (Fig. 12). The greatest GR differential (approximately 500 fold; $p < 0.05$, n=4) was observed with a 3 μM capsaicin concentration at 72 hpi (Fig. 12). In order to demonstrate the relative potency of selective replication using multiple TRPV1 agonists, the above experimental procedure was repeated with resiniferatoxin (RTX), an ultrapotent TRPV1 agonist. Nanomolar concentrations of RTX caused a reduction in vTT viral titers, similar to that seen with ~100 fold higher doses of capsaicin at all time points (Fig. 13). The highest observed difference in growth rate (GR = 474; $p < 0.05$, n=4) was seen with 1 μM RTX at 72 hpi (Fig. 13).

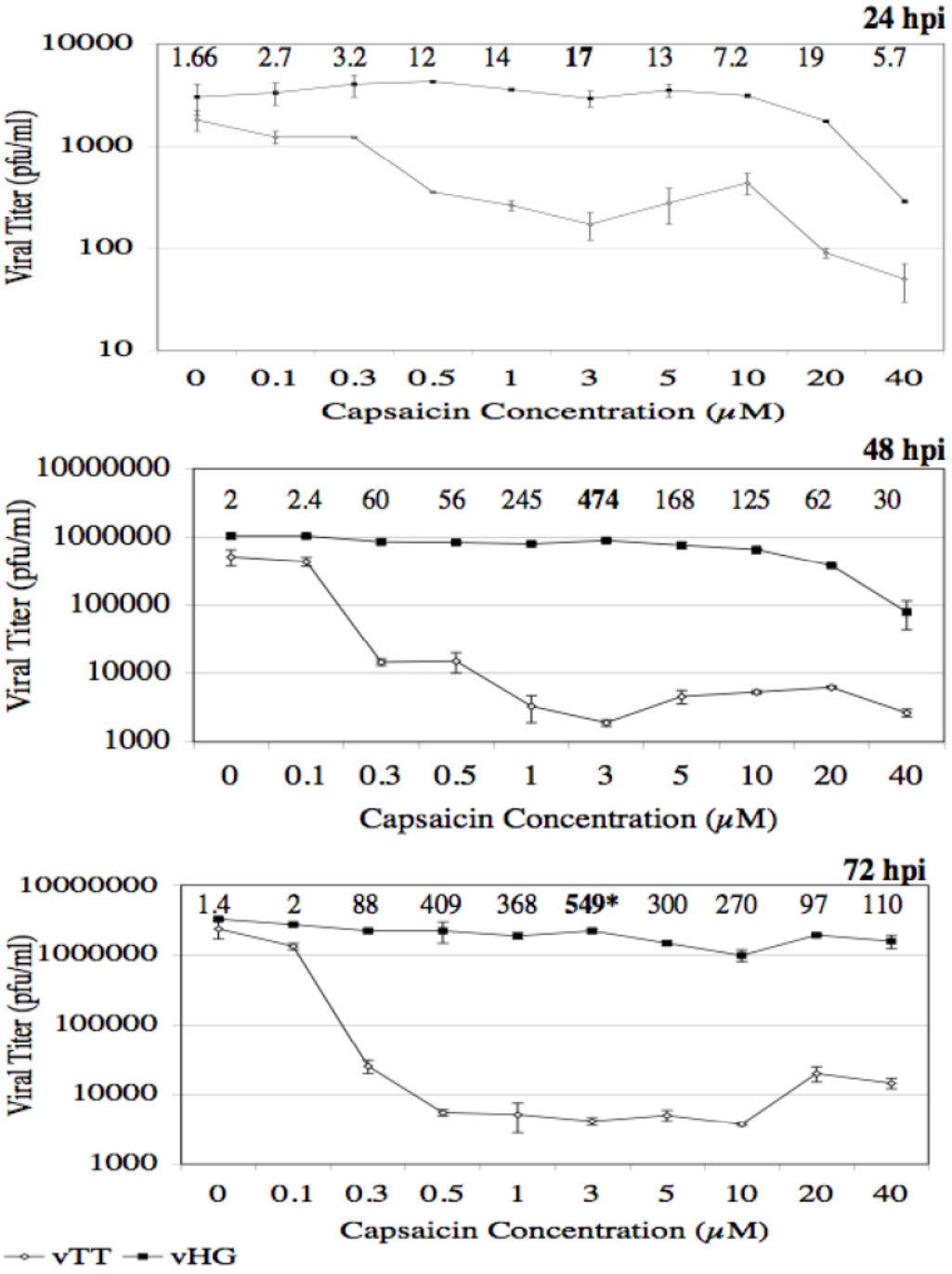

Figure 12. **Effect of capsaicin on vTT viral growth.**

7B complementing cells were infected with vTT or vHG (control) virus. Infected cells were plated in culture media containing increasing doses of capsaicin (0 to 40 μM final). Viral titers determined from supernatant media at 24, 48 and 72 hours post-infection (hpi) are plotted against capsaicin concentration. Growth ratios, calculated as the ratio of vHG to vTT viral titers at each concentration of capsaicin are shown for each graph (* $p < 0.05$, $n = 4$).

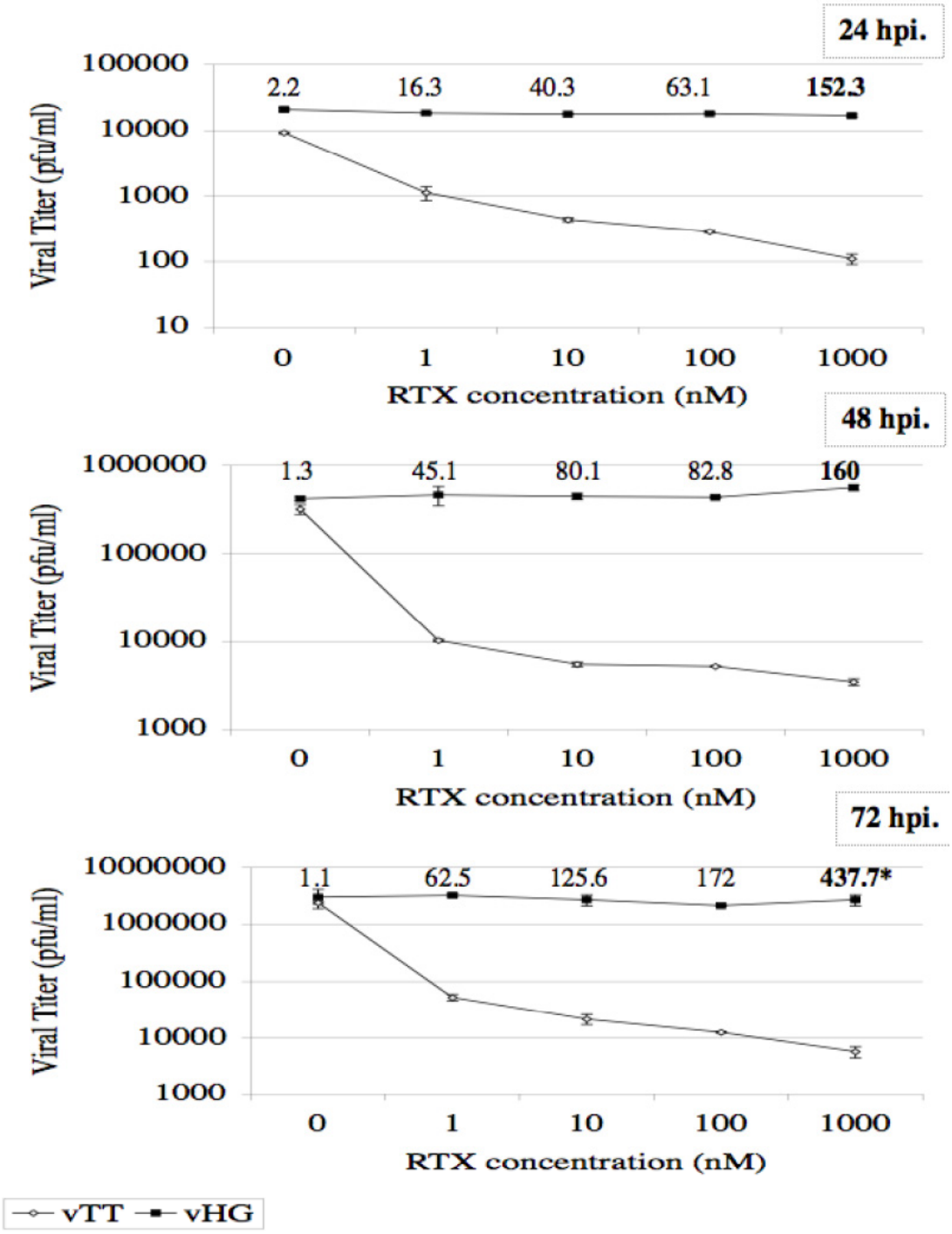

Figure 13. Effect of resiniferatoxin (RTX) on vTT viral growth.

7B cells infected with vTT or vHG (control) virus were plated in culture media containing increasing doses of resiniferatoxin (0 to 1000 nM final). Viral titers determined from supernatant samples are plotted against the RTX concentration at 24, 48 and 72 hours post-infection. Growth ratios for each concentration of resiniferatoxin are indicated at the top of each graph (* $p < 0.05$, $n = 4$).

3.2.7 TRPV1 antagonism rescues vector replication.

While TRPV1 activation by capsaicin significantly blocks vector replication, antagonism of TRPV1 receptor activation by capsaicin should rescue vector replication. The recovery of vector replication following TRPV1 antagonism could then be used as a read-out in a selection system to identify additional TRPV1 receptor antagonists from a chemical compound library. In order to provide proof of principle data for the above rationale, viral yields were determined for infections in the presence of capsaicin alone or in cultures containing both capsaicin and known TRPV1 antagonists.

To assess non-competitive antagonism of viral growth inhibition, ruthenium red (RuR), a known TRPV1 channel pore blocker was added to replication assays along with capsaicin (CAP). vHG or vTT vector-infected 7B cells were plated in the presence of 3 μM CAP, 5 μM RuR, or 3 μM CAP + 5 μM RuR and samples taken daily for viral titration. Vector replication was unaffected by 5 μM RuR alone at 24, 48 and 72 hours post infection (Figs. 14A and 14B). The presence of CAP specifically inhibited vTT replication (Fig. 14A) without affecting vHG titers. (Fig. 14B). In the presence of both 3 μM CAP and 5 μM RuR, replication of vTT was completely restored ($p < 0.05$, n=4) (Fig. 14A).

In order to demonstrate competitive antagonism of TRPV1 activation by capsaicin, similar assays were carried out using the known competitive capsaicin antagonist, SB-366791 [79]. Addition of SB-366791 alone (at 1, 5 and 10 μM concentrations) did not affect replication of vHG (data not shown) or vTT (Fig. 15B). Addition of both CAP and SB-366791 did not affect replication of the control vector, vHG (data not shown). A dose dependent rescue of viral titers with 1 μM, 5 μM and 10 μM SB-366791 in the presence of 0.5 μM capsaicin was observed at all time points post-infection ($p < 0.05$, n=4) (Fig. 15A). It should be noted that a similar experiment

was performed using another known competitive capsaicin antagonist, capsazepine, however, a small and insignificant vTT growth recovery following capsaicin (0.5 μM) stimulation was observed with a very high dose of capsazepine (40 μM) at all post-infection time points tested (data not shown).

These data provide proof-of-principle for the growth recovery of a TRPV1 expressing HSV-1 vector using known non-competitive and competitive TRPV1 antagonists in the presence of the known TRPV1 agonist, capsaicin.

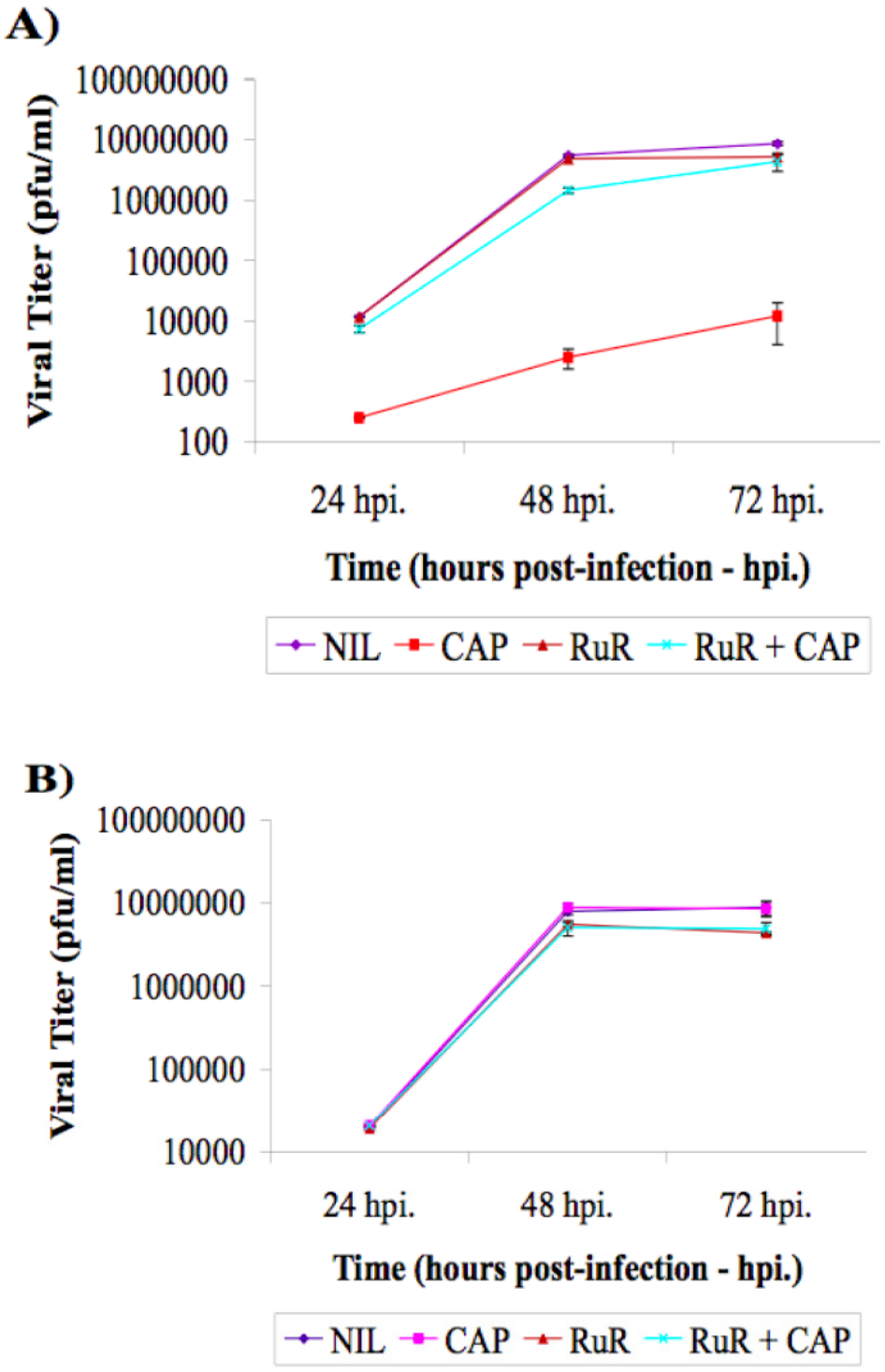

Figure 14. vTT growth recovery due to non-competitive antagonism of TRPV1 activation.

Growth curves from vTT infected (Graph A) and vHG infected (Graph B) 7B cells at 24, 48 and 72hours post-infection (hpi) are shown after separate incubation with either nothing (NIL), 3 μM capsaicin (CAP), 5 μM Ruthenium Red (RuR), or 5 μM ruthenium red + 3 μM capsaicin (RuR+CAP) (Details in text).

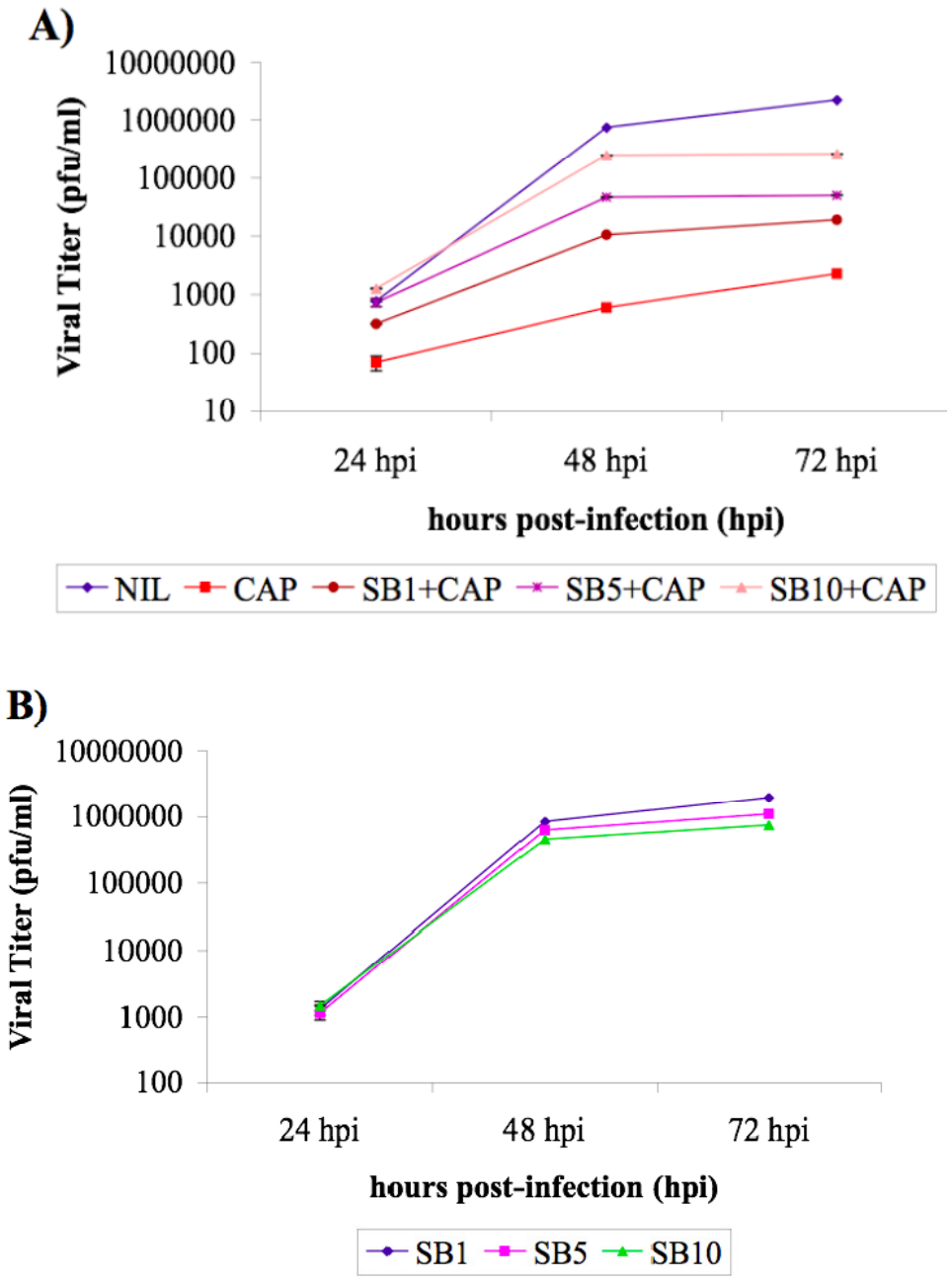

Figure 15. vTT growth recovery due to competitive antagonism of TRPV1 activation.

Titers from vTT infected 7B cells are represented as growth curves at 24, 48 and 72 hours post-infection (hpi), after separate incubation with chemicals as follows. Graph A: vTT infection with nothing (NIL), 0.5 μM capsaicin (CAP), 1 μM SB-366791 + 0.5 μM capsaicin (SB1+CAP), 5 μM SB-366791 + 0.5 μM capsaicin (SB5+CAP) and 10 μM SB-366791 + 0.5 μM capsaicin (SB10+CAP); Graph B: vTT infection with 1 μM SB-366791 (SB1), 5 μM SB-366791 (SB5) and 10 μM SB-366791 (SB10). See text for details.

3.2.8 Selection against vTT in mixed infections.

The vTT virus described in this study should prove useful in chemical selection assays to identify novel antagonists of TRPV1. With this in mind, and to determine the sensitivity of capsaicin based genetic selection against TRPV1 activation, mixed infections of 7B cells with varying ratios of vTT and vHG viruses were carried out with or without 3 μM capsaicin (0.4 PFU/cell). Cells were harvested at 72 hpi, after a cytopathic effect was observed and titered. Plaques were then counted for each dilution of mixed vTT:vHG infections, and scored as a percentage of GFP positive (GFP^+ vHG) versus GFP negative (GFP^- vTT) plaques. Samples from the first passage were then re-passaged in complementing cells with or without 3 μM capsaicin (0.4 PFU/cell), followed by rescoring for GFP positive plaques. Figure 16 is a schematic depicting the methodology followed for the mixed infection experiments along with representative images of the harvests that were titered following serial passages with capsaicin. The images are from titers of a 1:200 infection ratio of vTT:vHG.

Results are presented in Figure 17 as percent input versus percent output of green fluorescent viral plaques. Starting with a 0.005% vHG input (1:20,000 vHG:vTT), 66% after one passage and 95% vHG (GFP^+) after two passages were obtained in the presence of capsaicin ($p < 0.05$, $n = 4$) (Fig. 17), demonstrating a very effective selective pressure against TRPV1 in the presence of capsaicin. Starting with as little as 1:100,000 vHG, cultures were found to contain significant proportions (40%) of vHG after two passages in capsaicin (Fig. 17). This data demonstrates the sensitivity of using HSV-1 vectors in a capsaicin-based chemical or genetic selection strategy to identify TRPV1 antagonists.

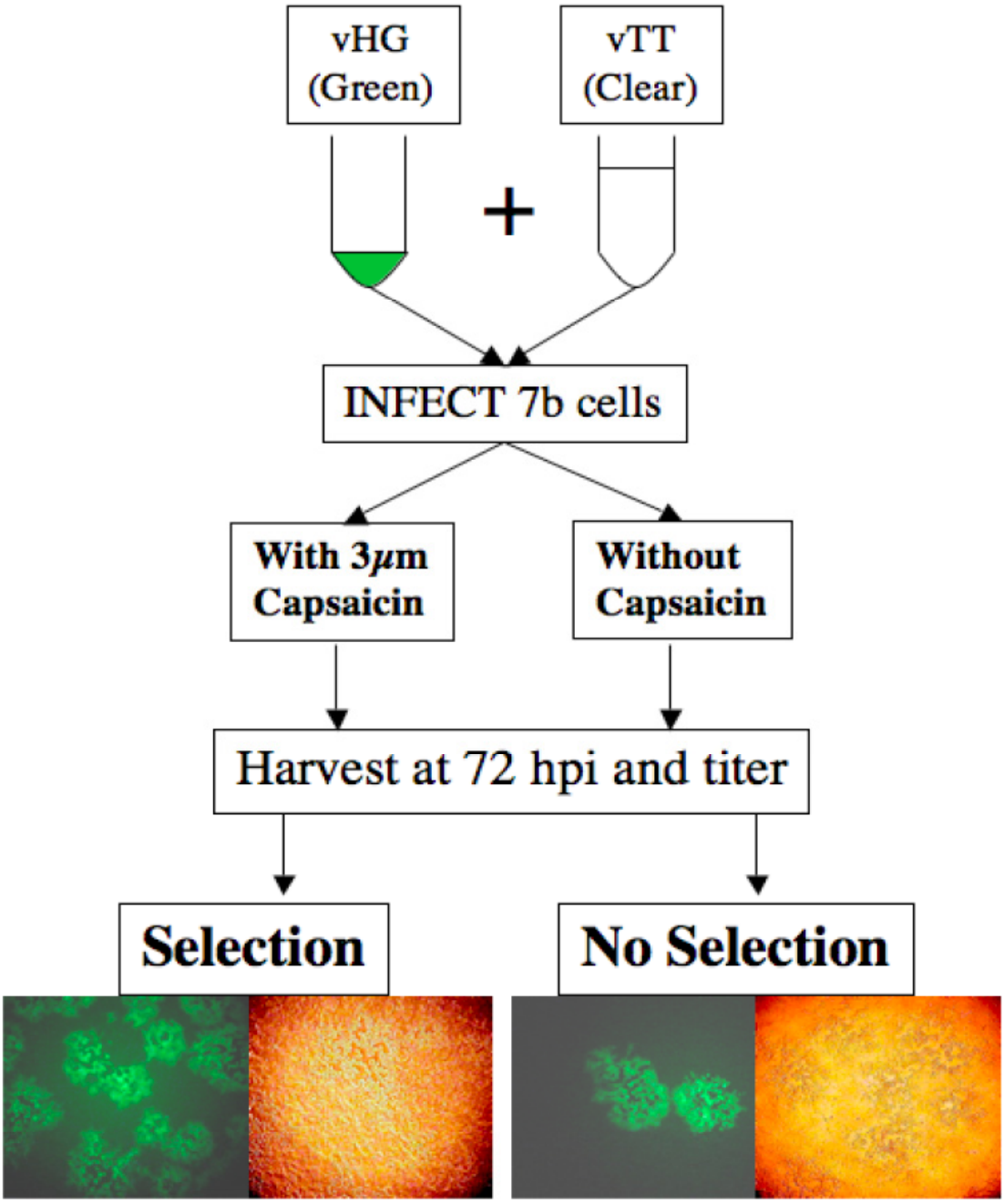

Figure 16. **Selection methodology with capsaicin using mixed virus infections.**

The figure depicts the method for selection against vTT following mixed infections with the vHG vector. The panels at the bottom of the figure show a selection for GFP^+ vHG plaques with 3 μM capsaicin (selection panels), while GFP^- clear vTT plaques outgrow GFP^+ vHG plaques in the absence of capsaicin (no selection panels).

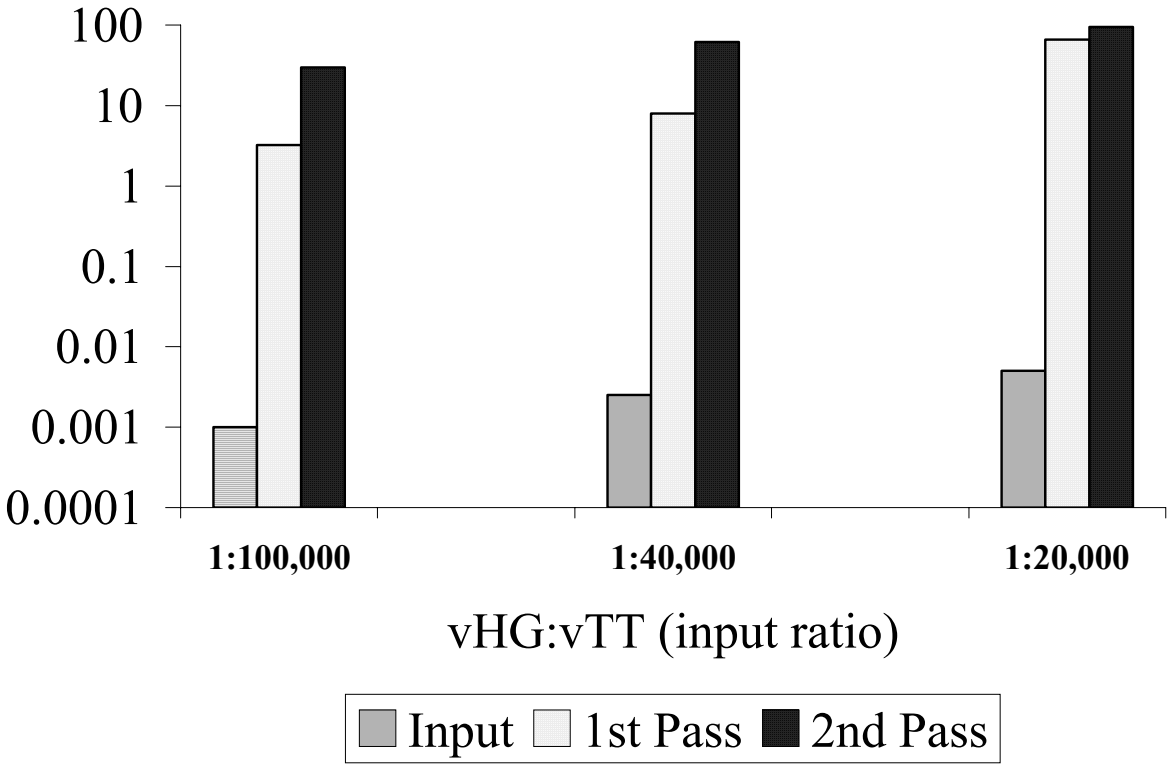

Figure 17. **Capsaicin selection sensitivity.**

Mixed infections on 7B cells at indicated ratios (input ratio) of vHG:vTT vectors were passaged with 3 μM capsaicin (1st Pass), harvested and titered at 72 hours post-infection (72 hpi). Harvests from 1st passage were passaged a second time (2^{nd} Pass) with 3 μM capsaicin, harvested at 72 hpi and titered. The relative output of the vHG vector was quantified and is presented as percent output (vHG %). (Note: Error bars are small and cannot be seen in this figure; $p<0.05$, $n=4$)

3.3 DISCUSSION

The current chapter describes the engineering of a novel herpes simplex virus 1 (HSV-1) vector based assay system utilizing selective virus replication as a read-out of channel inactivation. In particular, it was shown that agonist-mediated activation of virally over-expressed TRPV1 in an infected, complementing cell results in the rapid influx of cytotoxic amounts of calcium ions into the cytoplasm. Intracellular calcium overload opens mitochondrial transition pores, leading to caspase activation and the initiation of an apoptotic cascade within the cell. Calcium influx through activated TRPV1 in infected complementing cells causes cellular apoptosis before viral replication occurs, ultimately preventing vector replication. Lowered viral titers are therefore an indicator of TRPV1 activation, and molecules that antagonize TRPV1 activation will conversely rescue virus replication. Replication of vTT is substantially suppressed by incubation with capsaicin and viral particles that are able to replicate remain sensitive to capsaicin.

Initial experiments demonstrated that the TRPV1 expression vector performed as expected. Immunostaining of 7b complementing cells infected with vTT was positive for TRPV1 at 18 hpi and localized to the cellular plasma membrane and cytoplasm. Replication of vTT in the absence of agonists was comparable to vHG (control) viral growth at all post-infection time points, indicating minimal toxicity due to transgene expression in this system. Patch clamp recordings of vTT infected complementing cells demonstrated large currents at all post-infection time points tested following the application of 0.5 μM capsaicin, while vHG infected control cells did not respond to capsaicin indicating that virally expressed TRPV1 assembled as a functional ion channel. The currents were TRPV1 specific since they were blocked by application of known TRPV1 antagonists, ruthenium red and diaryl piperazine. Desensitization is

a property of ion channels whereby the channel pore closes and stops conducting ions despite the agonist being bound to the channel. Desensitization rates of activated TRPV1 are known to slow down when the receptor is phosphorylated. This phenomenon is called receptor sensitization. Conversely, TRPV1 de-phosphorylation increases desensitization rates. The enhancement or attenuation of TRPV1 function thus depends on a dynamic interplay between kinase-mediated receptor phosphorylation and phosphatase-mediated de-phosphorylation [15, 89]. In the HSV-1 vector-based TRPV1 expression system, currents desensitized slowly when compared to desensitization rates of neuronally expressed TRPV1 [65] indicating that the virally expressed receptor was maximally phosphorylated. Moreover, the pre-incubation of vTT infected cells with BIM, a PKC inhibitor caused significant reductions in current amplitude and accelerated desensitization rates following capsaicin application (Table 2). This data points to PKC as the kinase that phosphorylates HSV-1 vector-expressed TRPV1 in the experimental system described here. It is interesting to note that this increased phosphorylation of TRPV1 mimics a pathological state of increased TRPV1 phosphorylation in *in-vivo* models of neuropathic pain and bladder cystitis [65, 90]. Activation of the over-expressed TRPV1 receptor after stimulation with capsaicin caused a rise in intracellular calcium after addition of 0.3 and 3 μM capsaicin. The failure to enhance maximal responses with the calcium ionophore, ionomycin indicated very high levels of Ca^{+2} influx following the application of 3 μM capsaicin. All capsaicin responses were sustained and sub-maximal responses could be enhanced with the calcium ionophore ionomycin. This suggests that TRPV1 activation in the HSV-1 expression system was concentration dependent. Further, the response returned to baseline levels upon application of EGTA showing that this effect was caused by calcium ions. These data demonstrated that HSV-1 vector-expressed TRPV1 functioned as a calcium ion channel.

Calcium overload following capsaicin stimulation of TRPV1 has been shown by others to cause mitochondrial permeability transition (MPT) followed by caspase activation and apoptosis [88]. Consistent with these observations, vTT infected cells also demonstrated a similar apoptotic cascade initiating with MPT following capsaicin treatment, further confirming functionality of the HSV-1 based assay system. A source of potential false positives in this assay can be the identification of MPT and/or apoptosis inhibitors that may allow vector replication in the presence of capsaicin. However, these compounds are also of great interest as a therapeutic approach to treat neuronal apoptosis due to spinal cord injury or degenerative disorders [91]. Moreover, these compounds would be identified by standard second round intracellular calcium measurement methods [82].

The effect of the TRPV1 agonists, capsaicin and resiniferatoxin on vTT replication were next studied. Both capsaicin and resiniferatoxin caused a significant (500-fold) and dose dependent reduction in vTT replication when compared to the control vHG vector at 72 hpi, indicative of a specific effect of these agonists on the TRPV1 receptor. Resiniferatoxin was effective in reducing vTT viral titers at nanomolar concentrations (1 nM to 1000 nM final concentration) compared to micromolar concentrations (0.1 μM to 40 μM) of capsaicin. This dosage phenomenon agreed with other studies in which resiniferatoxin has been shown to be several fold more potent than capsaicin as an activator of TRPV1. The non-competitive capsaicin antagonist ruthenium red (5 μM) significantly rescued vTT replication in the presence of 3 μM capsaicin. Ruthenium red antagonism of capsaicin was almost complete, thus validating the HSV-1 vector-based system for selection of chemical antagonists of the TRPV1 receptor. Similarly, a concentration dependent reversal of the capsaicin effect with the competitive antagonist SB-366791 was found.

The vTT virus described in this study could prove useful to express a cDNA library such that each virion expresses a unique molecule among which TRPV1 inhibitory cDNA products may be selected and captured on the basis of virus replication. With this in mind, and to determine the sensitivity of genetic selection against TRPV1 activation, mixed infections infections with vTT and a control vHG vector that is negative for TRPV1 expression were performed. When one PFU vHG was mixed with 20,000 vTT, a selection for vHG by sequential passage in the presence of capsaicin, yielding greater than 95% vHG (GFP^+) was achieved. With a 1:100,000 vHG:vTT mixture, significant amplification of the selected vHG particle to approximately 40 % occurred after two passages in the presence of capsaicin, indicating that the selection system was highly sensitive and robust. It can be noted that no obvious TRPV1 mutants in vTT were observed during these experiments. This is supported by the fact that a second passage in the presence of capsaicin resulted in further selection for the TRPV1 negative and GFP^+ control vector vHG. The absence of TRPV1 viral mutants allows continuous agonist-based selection strategies to be devised.

Modulation of ion channel activity has gained recognition as a viable approach to treat numerous disorders including epilepsy, cancer and pain [70-75]. Significant difficulties remain in current assay systems including signal quenching or transient signals for fluorescent readouts, resulting in many false positive and false negative outcomes [81, 82]. Other assay drawbacks such as low throughput, inefficient transgene expression, expensive reagents and inadaptability to miniaturized formats reduce assay efficiency and increase screening costs for antagonistic compounds. A previous study has addressed the issue of transient signals by using calcium ion chelating agents such as BAPTA to increase signal duration following channel activation [81]. Similarly, assays that employ transfection to express ion channels could be improved using

baculovirus-based transient expression systems [83] or other viral platforms such as HSV-1 vectors.

The HSV-1 based assay system described here could be used to identify novel TRPV1 antagonists from a chemical compound library. The assay can be adapted to a fluorescence read-out high throughput screen by co-expressing the target ion channel and green fluorescent protein (GFP). Virus replication following channel inactivation should result in increased fluorescence that can be monitored using a fluorometric imaging plate reader. Potential advantages of the HSV-1 based assay include the ability to simultaneously express multiple genes, efficient transgene expression, robustness and cost-effectiveness due to the use of inexpensive reagents. Other applications for the system described in this study include identification of novel TRPV1 antagonists from cDNA, gene-knockout based (e.g. RNAi) or random peptide libraries with potential therapeutic applications in the field of pain management as well as providing basic scientific understanding of targeted ion channels in chronic pain.

4.0 DEVELOPMENT AND CHARACTERIZATION OF HSV-1 VECTOR-EXPRESSED DOMINANT NEGATIVE PKCε FOR CHRONIC PAIN THERAPY

4.1 INTRODUCTION

Chronic pain occurs as a result of a variety of disorders and is a debilitating condition with over 80 million sufferers in the United States (section 1.2.2). Following a resolution of the causative pathology, chronic pain states often persist and are accompanied with a distinct set of signs and symptoms such as hyperalgesia, allodynia, reduced activity and depression (section 1.2.1). A recent declaration by the European Federation of the International Association for Pain (IASP) chapters states that chronic pain should be recognized as a distinct disease entity and treated as such (section 1.2.1). Current analgesics used to treat pain target the nociceptive pathway at various levels, but are accompanied by side effects resulting from effects on other biological systems (Table 1). An approach to address this problem is to develop a better understanding of plastic nociceptive changes that occur during the pathophysiological progress of chronic pain and to achieve the targeted inhibition of pro-nociceptive molecules in DRG neurons that are the well-known sensory seat of nociception.

The vanilloid receptor (transient receptor potential vanilloid 1 or TRPV1, formerly known as VR1) has emerged as an important integrator of various inflammatory mediators (section 1.2.5) and is likely to be a link in the transition between acute and chronic pain. The TRPV1 receptor assembles at the plasma membrane as a tetramer of six transmembrane-

spanning subunits and is an inward rectifying ion channel that preferentially conducts Ca^{+2} ions through a pore loop between domains 5 and 6 (Fig. 18). TRPV1 is a directly activated by protons, pH and heat (43˚C) and is indirectly modulated by several inflammatory mediators like ATP and bradykinin via G-protein coupled mechanisms (section 1.2.5). The G-protein coupled functional modulation of the TRPV1 and other TRPV channels is achieved through cytoplasmic receptor domains possessing consensus sites for the action of kinases and phosphatases (Fig. 18). In addition, TRPV1 is subject to unknown modulatory mechanisms by several other molecules (Fig. 18) [84]. Recent evidence suggests that like many other ion channels, TRPV1 activity is controlled, in part, by the phosphorylation state of the receptor [84, 92]. TRPV1 activation is enhanced following receptor phosphorylation, a phenomenon known as receptor sensitization, while de-phosphorylation results in rapid receptor desensitization and a consequent attaenation of function. This dynamic interplay between receptor phosphorylation and de-phosphorylation is mediated by intracellular kinases and phosphatases [89].

TRPV1 sensitization results in an increased activation of the receptor with sub-maximal doses of agonists, such that the receptor becomes activated by room temperature, physiological pH and lower doses of capsaicin. This hyperactivation or sensitization causes a release of calcitonin gene related peptide (CGRP), substance P (SP) and other inflammatory mediators from peripheral neuronal terminals [93]. CGRP and SP are known to enhance neurogenic inflammation in the surrounding tissue [94]. A positive-feedback cycle consisting of a loop of TRPV1 hyperactivity, the release of SP and CGRP and a consequent increase in the levels of inflammatory mediators resulting in further increase in TRPV1 function is thus established, creating a pathological microenvironment that results in a self-perpetuating chronic pain state.

Among the kinases that sensitize TRPV1, protein kinase C epsilon (PKCε) has emerged as an important pro-nociceptive kinase that phosphorylates TRPV1 at the S502 and S800 residues. Phosphorylation results in an enhanced *in-vitro* and *in-vivo* activation of TRPV1 [15, 30]. A recent study in TRPV1 knockout mice demonstrated significant reductions in nocisposive behavior following stimulation with the PKC specific activator, phorbol myristate acetate (PMA) [39], while another study has reported reduced pain behavior in response to heat application in PKCε knockout mice [38]. Additional reports have shown that PKCε is specifically activated downstream of the bradykinin receptor 2 in nociceptive neurons, thus providing a molecular link between bradykinin (BK) and nociception [95, 96]. Finally, *in-vitro* electrophysiological recordings in neurons demonstrate an enhanced TRPV1 function in neurons following pre-incubation with BK, mediated by PKC [27]. Taken together, these results have uncovered a unique nociceptive pathway in which PKCε is activated downstream of the bradykinin receptor 2 and phosphorylates TRPV1 resulting in the sensation of pain [96]. Thus, the inhibition of PKCε is a potential strategy to break this positive feedback cycle and consequently attenuate TRPV1 function *in-vivo*.

The herpes simplex virus-1 (HSV-1) virus is neurotropic and therefore ideally suited as a delivery vehicle for the targeted expression of therapeutic transgene products in nociceptive neurons. Replication defective HSV-1 vectors have been previously used as a gene delivery vehicle to attenuate pain in several animal models (sections 1.2.7 and 1.2.8). In the current chapter, the neurotropism of replication defective HSV-1 mutant vectors is exploited as a means to attenuate TRPV1 function at the periphery of the nociceptive pathway by the targeted delivery of a dominant negative form of PKCε to DRG neurons. Chapter 4 describes the design, development and characterization of an HSV-1 vector engineered to express a dominant negative

form of PKCε and its use to attenuate TRPV1 function *in-vitro* and *in-vivo*. This study may provide future avenues for the development of analgesics for chronic pain that exert their effects via the targeted inhibition of pro-nociceptive gene products at the periphery of the nociceptive pathway.

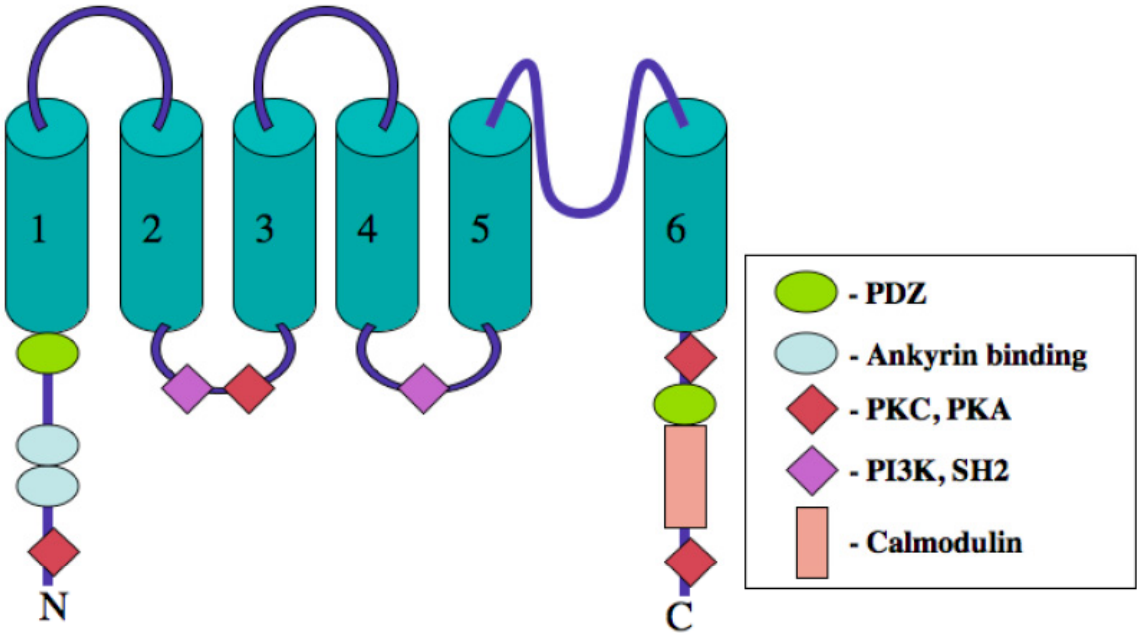

Figure 18. Subunit structure of the TRPV1 receptor.

The figure shows a TRPV1 receptor subunit structure. Putative sites for the action of several modulatory gene products are highlighted. The PDZ domain (green oval) is a scaffolding domain that links components of signaling complexes. The ankyrin binding site (blue oval) may also perform a scaffolding function by tethering the receptor to intracellular cytoskeletal elements. The kinase domains (red diamonds) for protein kinase C (PKC) and protein kinase A (PKA) are present at the T144 (PKC), S502 (PKC and PKA), T704 (PKC and PKA) and S800 (PKC) residues of TRPV1. The PI3-kinase (PI3K) and SH2 domains (purple diamonds) are putative sites for phosphorylation by PI3K and tyrosine kinase repectively and may play a role in receptor sensitization. The calmodulin binding domain (pink rectangle) plays a role in receptor desensitization by recruiting calcineurin to de-phosphorylate TRPV1 in a calcium dependent manner. (Figure modified from Pedersen et al, Cell Calcium 38 (2005), 233-252)

4.2 RESULTS

4.2.1 Vector constructs.

The two vectors used throughout this study are called vHDNP and vHG. vHDNP is the experimental vector (**v**ector **H**CMVp:**D**ominant **N**egative **P**KCε) containing a dominant negative PKCε (DNP) construct fused to green fluorescent protein (GFP) at the UL41 locus of a replication defective HSV-1 vector deleted for ICP27 and both copies of ICP4 (Fig. 19A). DNP and vHDNP were engineered as described in materials and methods (section 2.1.1). Figure 19A shows the full-length PKCε structure and the deletions in the DNP construct, driven by an HCMV IE promoter. Prior to starting experiments, the UL41 locus of vector vHDNP was PCR amplified and the correct insertion of the HCMVp:DNP transgene cassette was confirmed by sequencing. Successful DNP insertion into vHDNP was also confirmed by Southern blotting using a PKCε cDNA probe (*Bgl*II to *Sal*I fragment) (data not shown). The vector, vHG shown in figure 19A was used as a control for all experiments. vHG has been described in materials and methods (section 2.1.2) and in chapter 3.

4.2.2 Dominant negative PKCε (DNP) protein expression by vHDNP.

vHDNP-mediated expression of DNP was first confirmed by Western blotting. vHDNP infected 7B cells (MOI of 3 at 16 hpi) were positive for a 47 KDa band when probed with a GFP antibody, while vHG infected 7B cells (MOI of 3 at 16 hpi) were positive for a 27 KDa GFP band (Fig. 19B). The 20 KDa shift between vHDNP-infected and vHG-infected 7B cells when probed with the same GFP antibody corresponded with the size of the DNP construct without a

GFP fusion, thus indicating successful vHDNP-mediated expression of the DNP transgene fused to GFP in complementing 7B cells. A similar result was obtained using vHDNP or vHG-transduced non-complementing Vero and U2OS cells (Fig. 19B). Expression in non-complementing cell lines indicated that the DNP transgene in vHDNP was driven by an HCMV immediate early promoter.

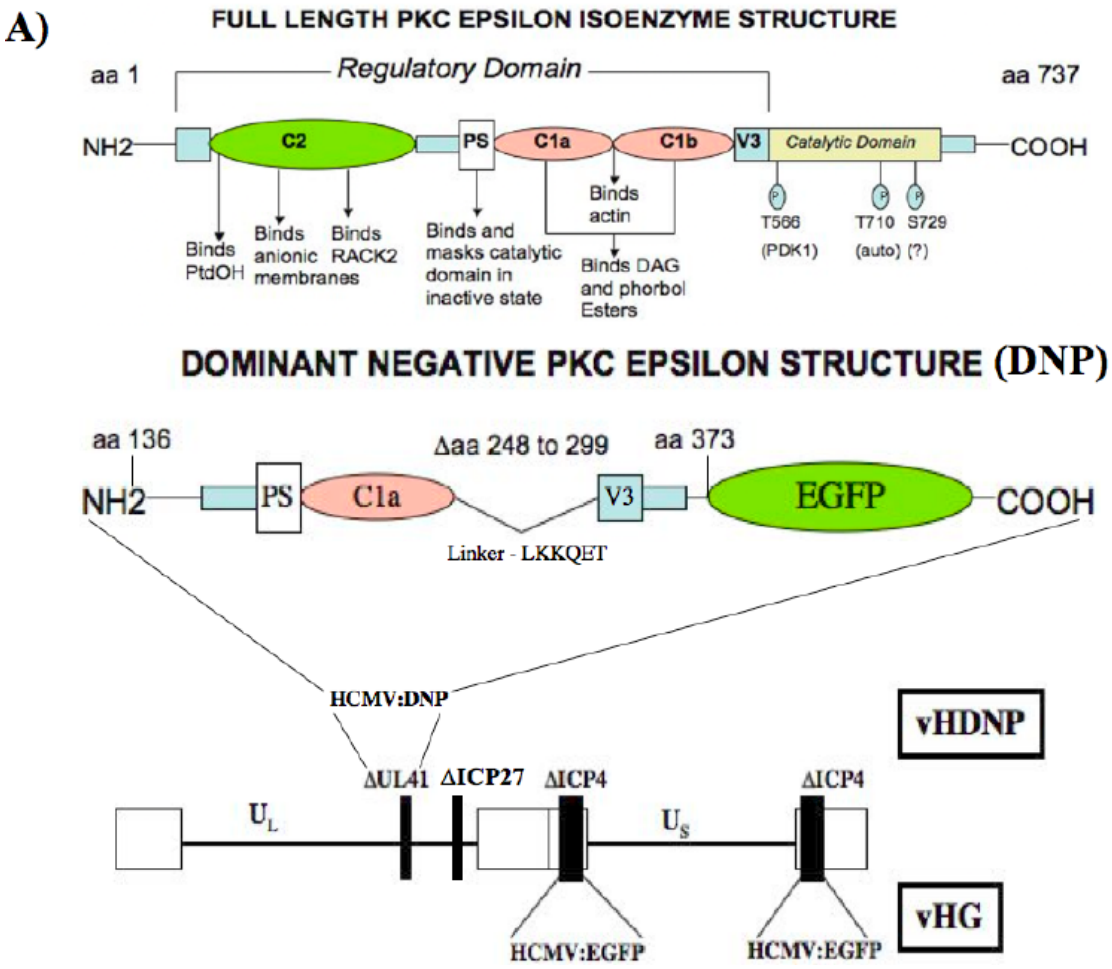

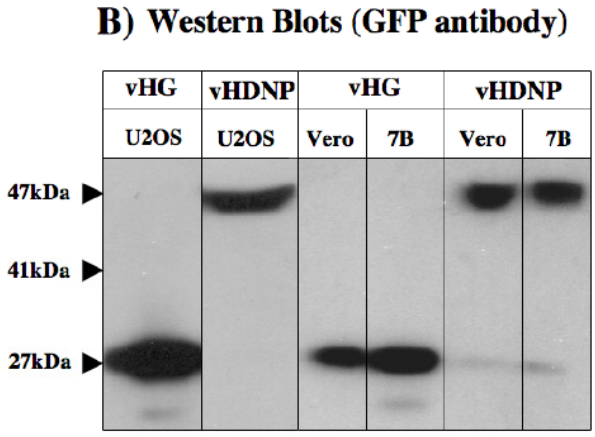

Figure 19. **Dominant negative PKCε (DNP) structure and transgene expression.**

(A) Full length PKCε with sub-domain functions and phosphorylation sites are shown (top). The dominant negative PKCε (DNP) + GFP fusion construct along with vector (vHDNP and vHG) genomic structures are also shown. (B) Western blots to confirm DNP transgene expression from vHDNP or vHG in the indicated cell lines are shown. See text for details.

4.2.3 Demonstration of vHDNP-expressed dominant negative PKCε (DNP) translocation in U2OS and Vero cells.

Following a confirmation of vector-mediated DNP expression in complementing and non-complementing cell lines, the functionality of vector-expressed DNP was studied in U2OS and Vero cells. PKC-specific activators like phorbol myristate actetate (PMA) bind to the regulatory domain of PKCs resulting in kinase translocation to the plasma membrane. Membrane translocation is an indirect indicator of kinase function as the PKCs mediate most of their signaling functions following localization near surface receptors. Since the PMA binding sub-domain (C1a) is retained in the DNP construct, it was anticipated that the stimulation of vHDNP-transduced cells with PMA would result in the membrane translocation of DNP. Translocation can be visualized by live cell imaging with green fluorescence emitted by the DNP construct.

To study the functionality of the DNP construct, vHDNP vector-transduced non-complementing Vero and U2OS cells (MOI of 3 at 16 hpi) were visualized for DNP expression by live cell imaging using a fluorescent microscope. Following transduction with vHDNP, Vero and U2OS cells displayed a distinct perinuclear localization of the DNP transgene product prior to PMA stimulation (Fig. 20A,C). 5 μM PMA was added to the media and cells were immediately imaged as described in materials and methods (section 2.6). PMA stimulation caused DNP to completely translocate to the plasma membrane in Vero and U2OS cell (Fig. 20B,D). Translocated DNP appeared to localize in specific structures morphologically resembling microvilli in Vero cells, while DNP uniformly translocated to the plasma membrane in U2OS cells. This data confirmed functionality of the vHDNP vector-expressed dominant

negative PKCε in non-complementing cell lines and encouraged further studies of DNP function in DRG neurons.

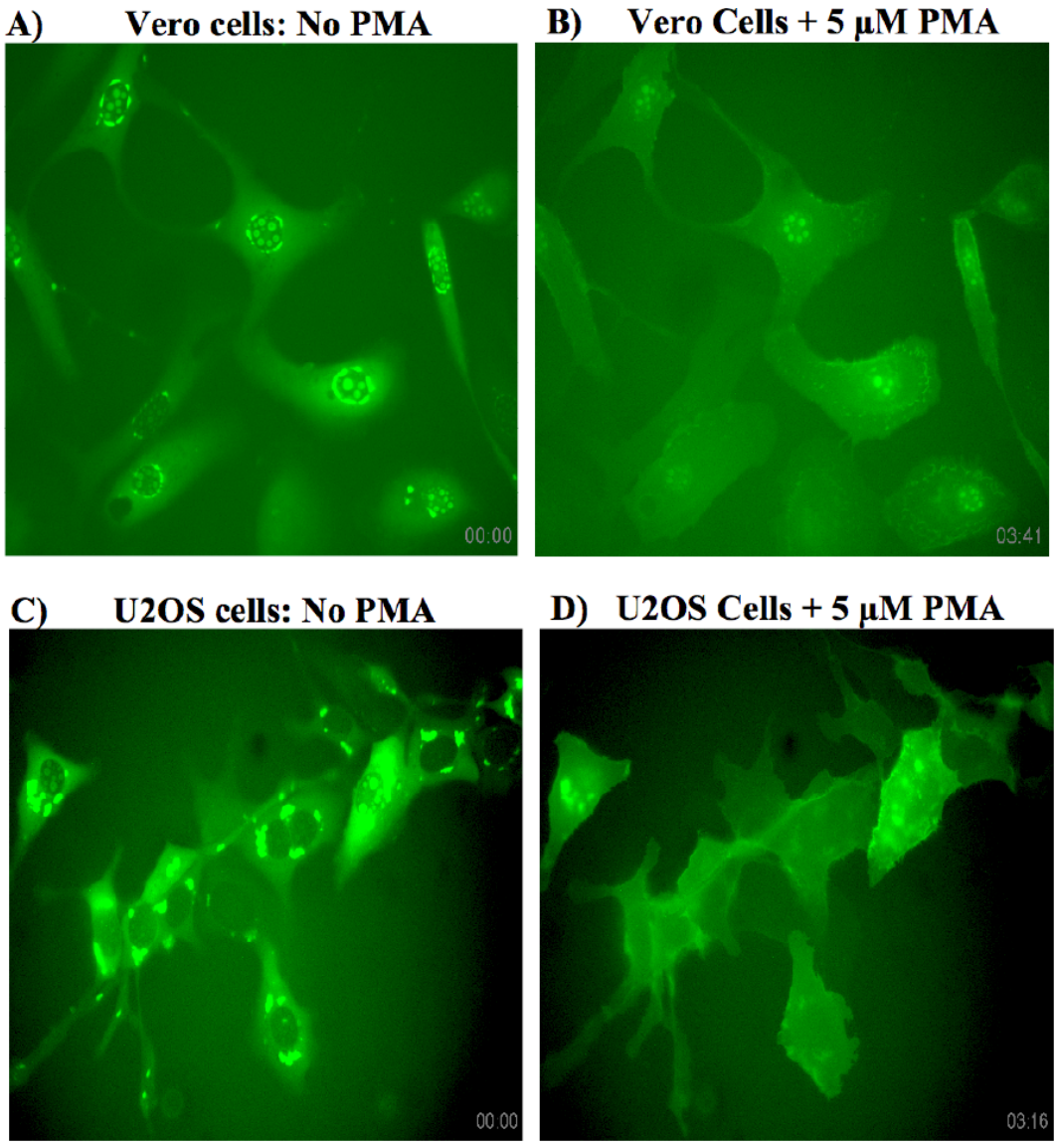

Figure 20. PMA-induced functional translocation of vHDNP vector-expressed dominant negative PKCε (DNP) in Vero and U2OS cells.

The figure shows the following vHDNP vector-transduced cells: A) Vero cells without PMA, B) Same field of Vero cells at 3 min 41 sec after 5 µM PMA addition, C) U2OS cells without PMA and D) Same field of U2OS cells at 3 min 16 sec after 5 µM PMA addition. Panel A shows a perinuclear localization of vHDNP-expressed dominant negative PKCε in all Vero. Panel C shows a perinuclear as well as cytoplasmic localization of DNP in U2OS cells prior to PMA stimulation. The intranuclear fluorescence in these cells is an optical artefact.

4.2.4 vHDNP-expressed dominant negative PKCε (DNP) inhibits endogenous PKCε translocation in DRG neurons.

Following the functional demonstration of vector-expressed DNP in Vero and U2OS cells, the ability of DNP to inhibit the translocation of endogenous PKCε in adult rat DRG neurons was examined. The assay utilized for this purpose is shown in Figure 21 and is based on the rationale that following activation with a PKC activator in vHDNP-transduced neurons, DNP will translocate to the plasma membrane and consequently inhibit the translocation of endogenous PKCε. vHG-transduced control neurons will by contrast, display a normal translocation of endogenous PKCε along with a cytoplasmic localization of GFP, thus confirming the ability of DNP to inhibit endogenous PKCε in DRG neurons.

vHG or vHDNP-transduced neurons were stimulated with 5 μM of the PKC-specific activator, phorbol myristate acetate (PDBu) for 2 min, fixed and immunostained for endogenous PKCε. Immunostaining was done with a primary antibody that recognizes the C-terminal domain of PKCε and is consequently specific for endogenous PKCε (see section 2.5 for details). A red fluorescent Cy3 secondary antibody was used to visualize endogenous PKCε staining. Unstimulated vHG and vHDNP vector-transduced neurons immunostained for endogenous PKCε were used as a negative control for this experiment. Figure 22 shows representative images of vector-transduced neurons with and without PDBu stimulation. As seen in Figure 22, unstimulated vHG-transduced neurons displayed a diffuse localization of vector-expressed GFP (Fig. 22A), while DNP localized to perinuclear regions in unstimulated vHDNP-transduced neurons (Fig. 22G). Unstimulated vHG and vHDNP-transduced neurons also showed a diffuse localization of endogenous PKCε (Fig. 22 B,H). Following stimulation with 5 μM PDBu,

endogenous PKCε translocated to the plasma membrane in vHG-transduced neurons (Fig. 22E), while the localization of GFP in these neurons remained unaffected (Fig. 22D). Following stimulation with 5 μM PDBu, DNP completely translocated to the plasma membrane in vHDNP-transduced neurons (Fig. 22J) while the translocation of endogenous PKCε in these neurons was almost completely inhibited (Fig. 22K). Merged images show a significant co-localization of DNP and endogenous PKCε (yellow-orange color) at perinuclear regions of unstimulated vHDNP-transduced neurons (Fig. 22I). DNP and endogenous PKCε did not significantly co-localize in neurons following stimulation with PDBu (Fig. 22L). Finally, the GFP in merged images of unstimulated and PDBu stimulated vHG-transduced neurons did not co-localize with endogenous PKCε (Fig. 22 C,F). These data clearly demonstrate that the dominant negative PKCε (DNP) construct expressed by the vHDNP vector prevented the translocation of endogenous PKCε in adult rat DRG neurons.

It should be noted that all experiments performed in DRG neurons utilized PDBu as the PKC activator in place of PMA. The reason for this is that PMA, unlike PDBu is known to directly bind to and activate the TRPV1 receptor (Bhave et al, PNAS, 2003;100(21):12480-85). The use of PDBu thus prevented possible sources of error arising from PMA-mediated direct activation of TRPV1 in later experiments.

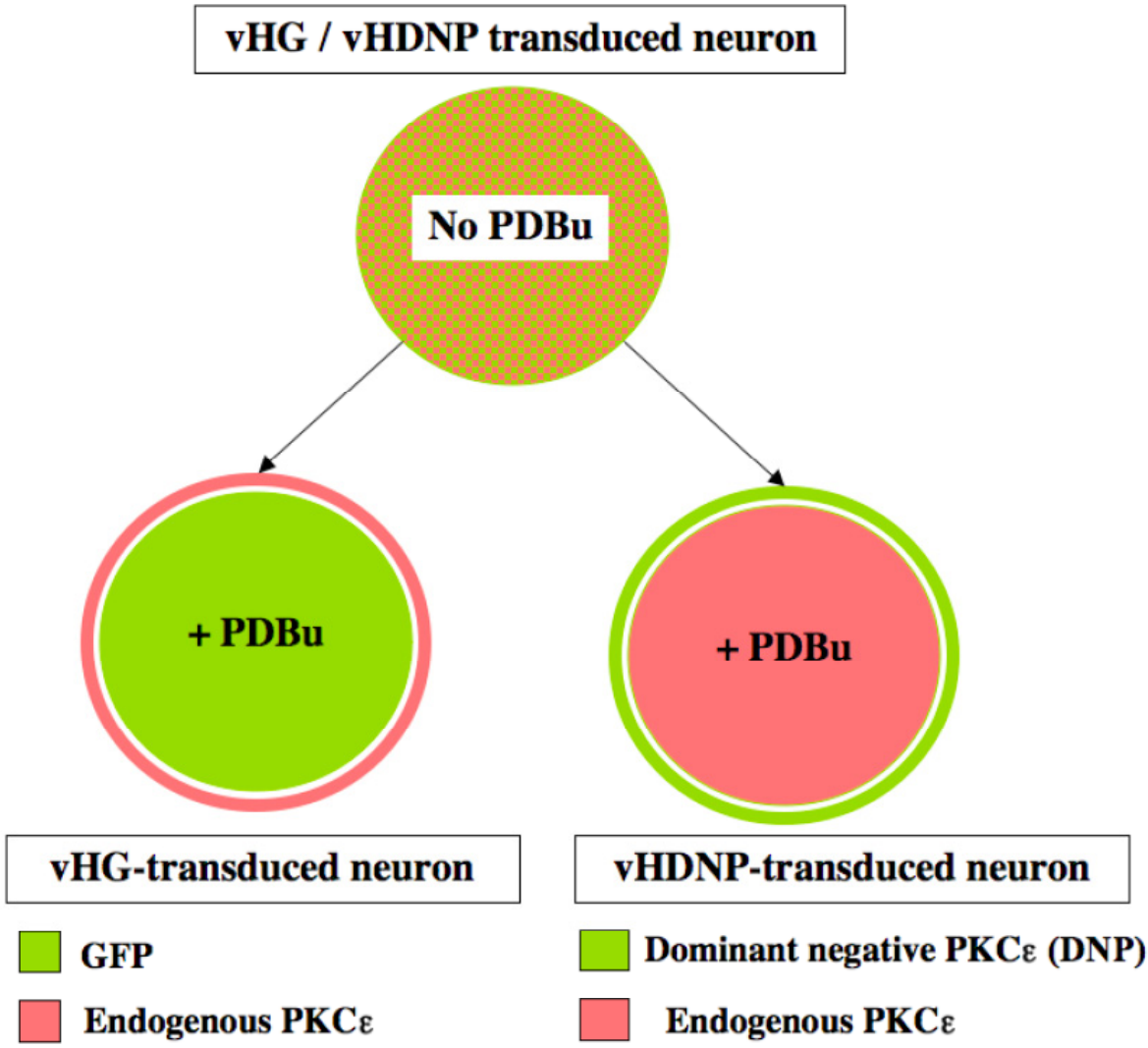

Figure 21. Assay rationale for the demonstration of DNP function in neurons.

The figure is a schematic of the assay rationale to demonstrate the DNP-mediated inhibition of endogenous PKCε in neurons. vHG or vHDNP vector-transduced neurons are either left unstimulated (No PDBu) or are stimulated with 5 μM PDBu (+PDBu) and immunostained for endogenous PKCε (red). An unstimulated (No PDBu) vHG or vHDNP vector-transduced neuron (shown at the top) will display a diffuse localization of DNP or GFP (green speckles) and endogenous PKCε (red speckles). Following PDBu stimulation (+PDBu), a vHG-transduced neuron (bottom left neuron) will show a complete translocation of endogenous PKCε to the plasma membrane, while the GFP protein will remain unaffected. PDBu stimulation (+PDBu) of a vHDNP-transduced neuron (bottom right neuron) will by contrast display a complete plasma membrane translocation of the DNP product (green) and an inhibition of endogenous PKCε translocation, thus confirming the functional inhibition of endogenous neuronal PKCε by DNP.

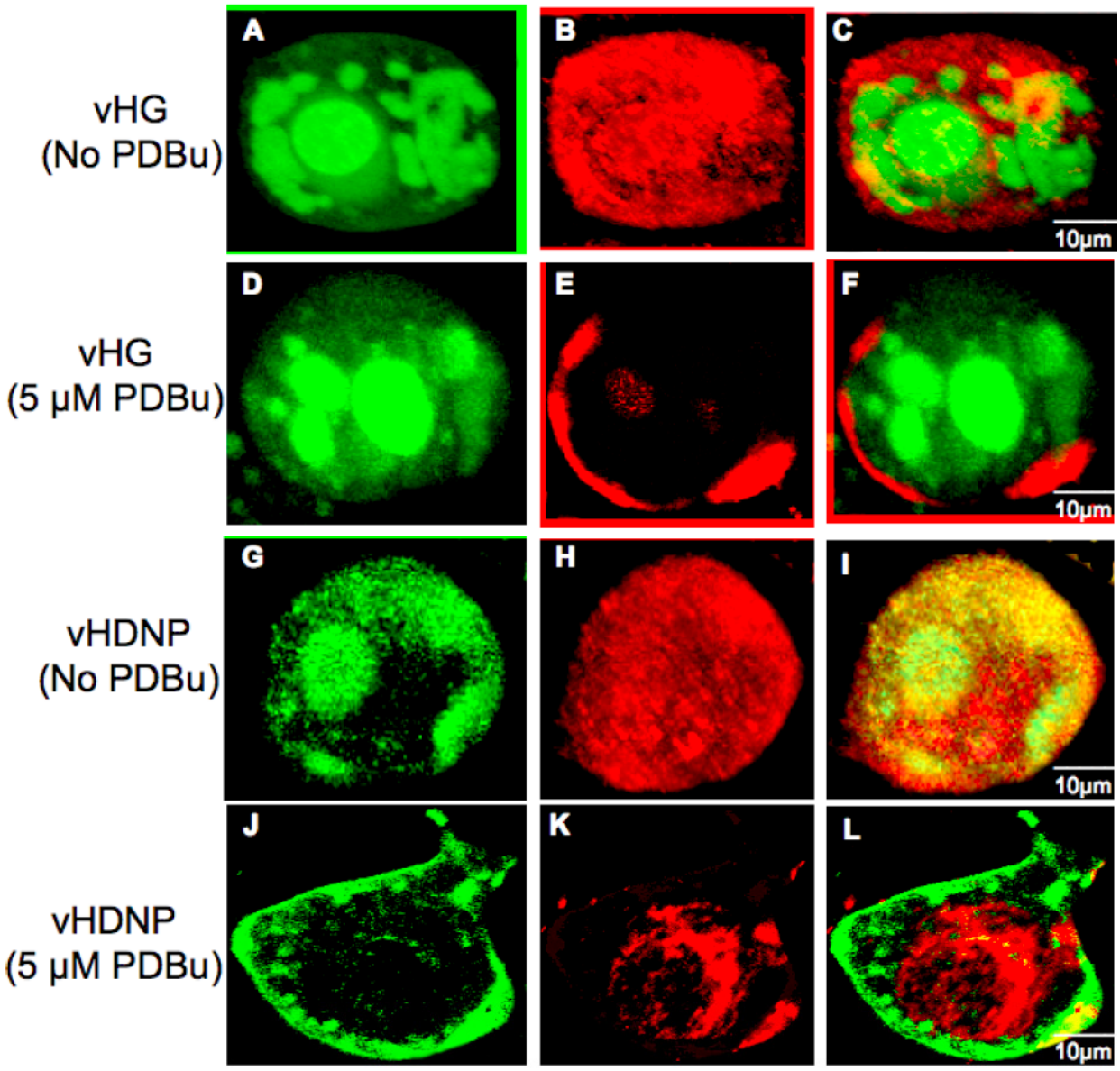

Figure 22. vHDNP-mediated inhibition of endogenous PKCε in adult rat DRG neurons.

vHG (panels A to F) or vHDNP (panels G to L) transduced neurons were fixed and immunostained for endogenous PKCε (red fluorescence) (panels B,E,H,K). Projections of multiplanar stacked images for each transduced neuron (approx. 30 μm diameter) before (No PDBu) and after (+PDBu) stimulation with PDBu are shown. Merged images show that GFP expressed from vHG does not affect PDBu induced endogenous PKCε translocation (panel F), while DNP expressed from the vHDNP-transduced neuron almost completely inhibits PDBu-induced endogenous PKCε translocation (Panel L). Vectors used to transduce the neurons and PDBu treatments for each neuron and indicated at the left of the figure. See text (section 4.2.4) for a detailed explanation.

4.2.5 vHDNP-expressed dominant negative PKCε (DNP) inhibits TRPV1 activity in rat DRG neurons.

With the demonstration of dominant negative PKCε (DNP)-mediated inhibition of endogenous PKCε translocation to the plasma membrane of neurons, it was anticipated that the DNP transgene product might attenuate TRPV1 activity since the vanilloid receptor function is coupled to PKCε-mediated receptor phosphorylation (section 4.1). The cobalt uptake assay provides a means for the quick and efficient assay of TRPV1 activity in a large number of DRG neurons in culture [97]. With this in mind and to determine the effect of DNP on TRPV1 activity *in-vitro*, cobalt uptake assays were done to examine adult rat DRG neuronal TRPV1 activity in vHDNP-transduced cells. Non-transduced and vHG-transduced neurons were used as controls for this experiment. Cobalt uptake assays were performed as described in materials and methods (section 2.11). The transduction of neurons with vHG and vHDNP vectors was performed as described in section 2.2.5 in order to ensure that 100% of the neurons in culture were transduced with HSV-1 vectors.

Figure 23A depicts the rationale for cobalt uptake assays. Vector-transduced or non-transduced DRG neurons in culture are incubated for 8 min with a cobalt chloride (CoCl) buffer containing capsaicin (0.5 μM). Capsaicin-mediated activation of neuronal TRPV1 receptors will cause Co^{+2} ions to flux into neurons that express functional TRPV1 receptors at the plasma membrane. Co^{+2} is then precipitated with ammonium polysulphide that reacts with the intracellular Co^{+2} ions in TRPV1 positive cells forming a black precipitate of cobalt sulphide (CoS). Thus, black intracellular precipitates are an indirect indicator of neurons expressing functional TRPV1 receptors. These neurons can then be counted with a light microscope and are

presented as a percentage of capsaicin sensitive neurons. Figure 23 also shows a representative image of a TRPV1 negative neuron with no cobalt uptake (Fig. 23B) and representative images of non-transduced, vHG-transduced and vHDNP-transduced capsaicin sensitive neurons with cobalt uptake (Fig. 23 C,D,E). It should be noted that the cobalt precipitate in vHDNP-transduced neurons was lighter than that seen in non-transduced or vHG-transduced neurons. These neurons were counted as capsaicin sensitive.

Figure 24 summarizes results of cobalt uptake assays. The type of neuron (x-axis: non-transduced or vHG-transduced or vHDNP-transduced) is plotted against the percentage of capsaicin sensitive neurons by cobalt uptake (y-axis). The numbers of neurons counted for each group are shown in parentheses. As seen in the graph (Fig. 24), approximately 44% of non-transduced neurons were capsaicin sensitive, while 33% of vHG-transduced neurons demonstrated capsaicin sensitivity. By contrast, only 12% of the vHDNP-transduced neurons were capsaicin sensitive. The result was significant when compared with the number of capsaicin sensitive vHG-transduced neurons ($p<0.001$). This data demonstrates the HSV-1 vector expressed dominant negative PKCε (DNP)-mediated *in-vitro* attenutation of TRPV1 activity in response to capsaicin stimulation in adult rat DRG neurons.

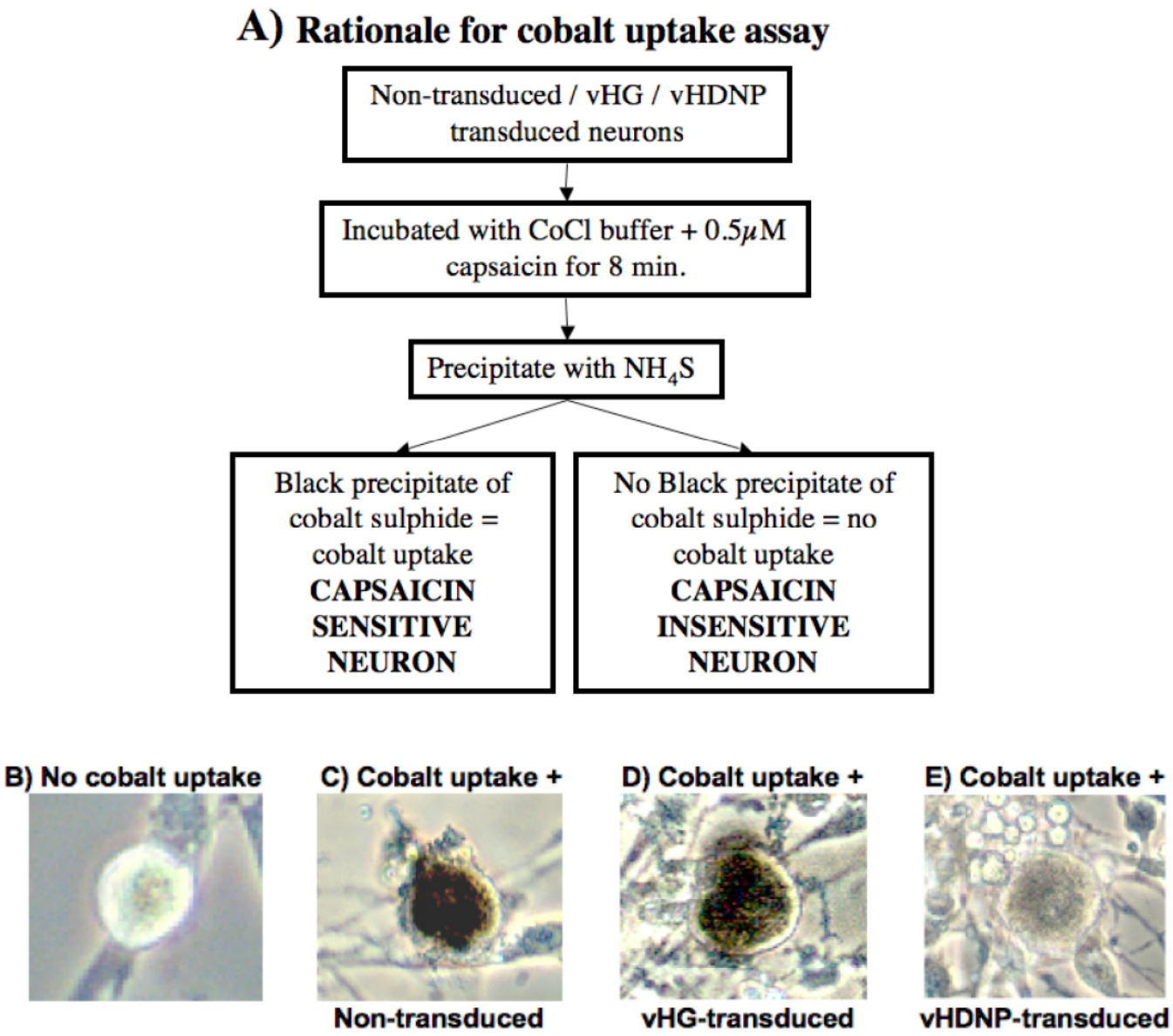

Figure 23. **Rationale for cobalt uptake assay.**

(A) The rationale for cobalt uptake assay to determine the number of capsaicin sensitive neurons in culture is shown. Non-transduced or vector-transduced neurons are stimulated with a buffer containing cobalt chrloride (CoCl) and 0.5 μM capsaicin for 8 min. Intracellular Co^{+2} ions in TRPV1 positive neurons are treated with ammonium polysulphide (NH_4S) to form a black cobalt sulphide precipitate. These capsaicin sensitive black neurons can be counted under a microscope. Representative images of (B) a neuron with no cobalt uptake, (C) a non-transduced neuron with cobalt uptake, (D) a vHG-transduced neuron with cobalt uptake and, (E) a vHDNP-transduced neuron with cobalt uptake are shown.

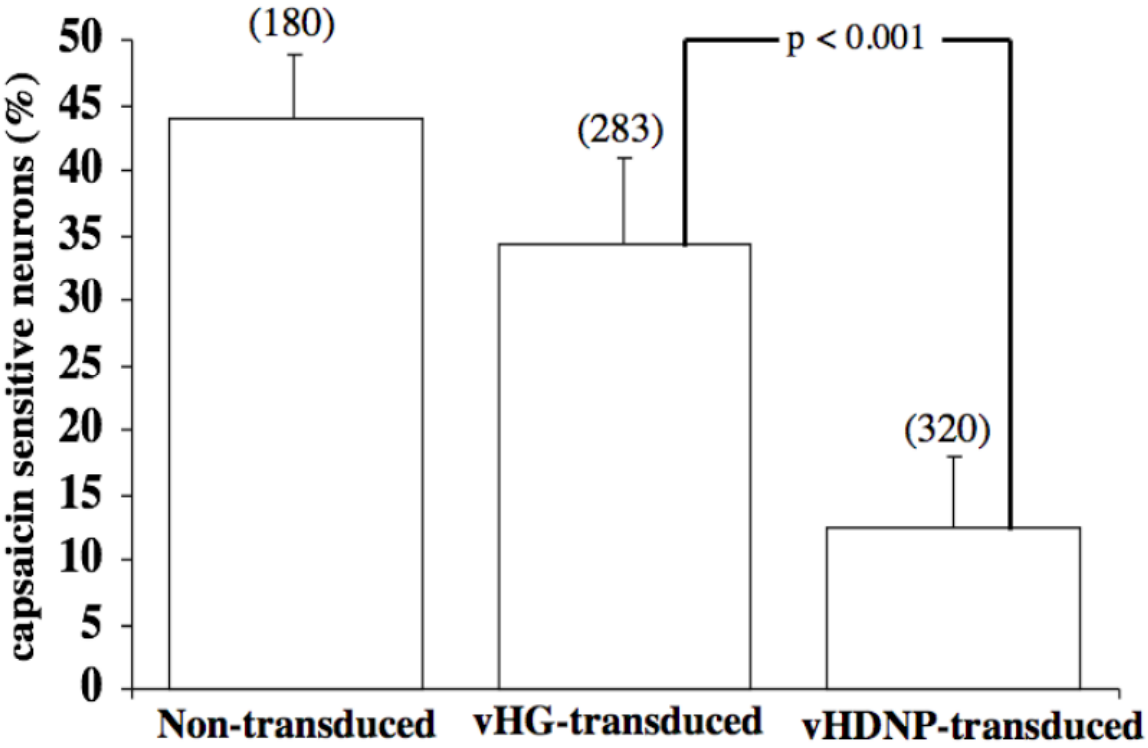

Figure 24. **Demonstration of vHDNP-mediated inhibition of TRPV1 activity by cobalt uptake assays.**

The graph plots the percentage of capsaicin sensitive neurons (%) counted by cobalt uptake (y-axis) for groups of non-transduced, vHG-transduced or vHDNP-tranduced neurons (x-axis). 44% of non-transduced and 33% of vHG-transduced neurons were capsaicin sensitive. The number of capsaicin sensitive neurons was significantly reduced to 12% following transduction with vHDNP ($p<0.001$). The number of neurons counted for each group are indicated in parantheses.

4.2.6 vHDNP-expressed dominant negative PKCε (DNP) inhibits and modulates TRPV1 currents in rat DRG neurons.

Cobalt uptake assays demonstrated an *en-masse*, quantitative reduction in TRPV1 activity mediated by HSV-1 vector-expressed dominant negative PKCε (DNP). This encouraged qualitative studies addressing the ability of DNP to modulate TRPV1 currents in single neurons.

With this in mind, whole cell electrophysiological recordings of capsaicin-induced currents were performed in vHG and vHDNP vector-transduced neurons.

For these studies, adult rat DRG neurons in culture were transduced with either vHG or vHDNP as described in materials and methods (section 2.2.5). Putative nociceptive neurons were chosen based on their diameter (small to medium diameter of 30 to 40 μm), an elongated morphology and the emission of green fluorescence by the neuron following vector transduction. The elongated small to medium diameter neurons neurons in non-transduced control DRG cultures were found to be capsaicin sensitive approximately 50 percent of the time. Figure 25 A,B,C and D show representative bright field and fluorescent images of vHG- and vHDNP-transduced neurons that were chosen for whole cell electrophysiology. Gigaohm-seal whole-cell recordings of capsaicin-induced currents were done in these neurons as described in materials and methods (section 2.7).

Figure 26A is a representative recording of capsaicin-induced currents obtained from vHG-transduced neurons. As seen in Figure 26A, the application of capsaicin (CAPS, 0.5 μM) caused an inward TRPV1-mediated current (500 pA amplitude) in these neurons. This current was significantly enhanced by addition of the bradykinin receptor 2-specific agonist, HYP-3-bradykinin (HYP3BK, 5 μM). Addition of the non-specific PKC activator, PDBu (5 μM) did not further enhance the TRPV1 current, while an application of the PKC-specific inhibitor bisindolylmaleimide (BIM, 5 μM) accelerated the TRPV1 current desensitization rates. The current was completely antagonized and returned to baseline values following application of the TRPV1-specific agonist, diaryl piperazine or NDT9515223 (TRPV1 Ant, 5 μM). This indicated that the current enhancement by HYP3BK was specific to the TRPV1 receptor. It should be noted that the addition of PDBu alone without prior incubation with HYP3BK caused an

enhancement of the TRPV1 current in other recordings of vHG-transduced neurons, indicating that PDBu-induced current enhancement was obliterated when HYP3BK was used.

Figure 26B is a representative recording of capsaicin-induced currents in vHDNP transduced neurons. As seen in the figure, in contrast to recordings in vHG-transduced neurons, vHDNP-transduced neurons consistently displayed diminished (50 pA amplitude), rapidly desensitizing currents following application of capsaicin (CAPS, 0.5 μM). This current was not enhanced following the application of HYP3BK. The application of 5 μM PDBu consistently caused a slow onset drift like enhancement of TRPV1 currents. This effect was antagonized by the application of 5 μM BIM. Incubation with the TRPV1 anatgonist diaryl piperazine (TRPV1 Ant, 5 μM) completely returned the currents to baseline values indicating that the drift current caused by PDBu was TRPV1 specific.

Figure 27 A,B and C summarize the findings from electrophysiological studies. As seen in Figure 27A, vHDNP caused a significant reduction in capsaicin-induced current amplitudes in DRG neurons when compared with non-transduced (control) or vHG-transduced neurons ($p<0.01$). vHDNP transduction also resulted in significantly accelerated desensitization rates of capsaicin currents ($p<0.01$) when compared with non-transduced and vHG-transduced controls (Fig. 27B). The time taken for current amplitudes to peak following PDBu stimulation was significantly reduced in vHDNP-transduced neurons when compared with non-transduced or vHG-transduced controls ($p<0.001$), indicating that the PKC translocation and consequent TRPV1 phosphorylation in vHDNP-transduced neurons was inefficient when compared with controls. Figure 28 is a graph showing comparisons of desensitization rates and effects of PDBu application between vHDNP-transduced and non-transduced neurons. As seen in the figure, desensitization rates of vHDNP-transduced neurons were ~10-fold faster that the rate at which

the non-transduced neuron desensitized. In addition to these findings, a significant reduction in the number of capsaicin-reponsive vHDNP-transduced neurons was observed in comparison with controls (data not shown). Taken together, these results demonstrate that HSV-1 vector-expressed DNP qualitatively inhibits and modulates the current responses to capsaicin in rat DRG neurons and results in an overall *in-vitro* attenuation of neuronal TRPV1 function.

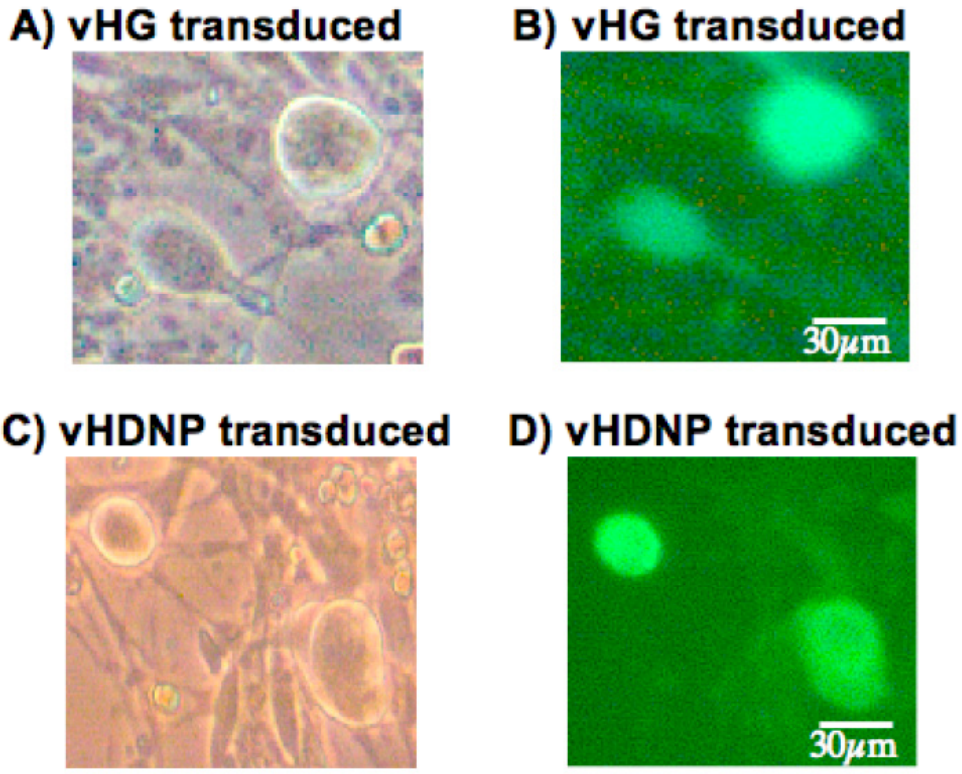

Figure 25. **Neurons chosen for whole cell electrophysiological recordings.**

The figure shows representative images of adult rat DRG neurons chosen for whole cell electrophysiology. Putative nociceptive neurons that were between 30 to 40 μm in diameter and emitted green fluorescence as a result of GFP or DNP transgene expression following vector transduction were chosen for recordings of capsaicin currents. The panels in this figure show a bright field image of vHG-transduced neurons (panel A), a fluorescent image of the same field displaying vHG-transduced neurons with green fluorescence from the GFP transgene product (panel B), a bright field image of vHDNP-transduced neurons (panel C), and a fluorescent image of the same field displaying vHDNP-transduced neurons with green fluorescence from the DNP transgene product.

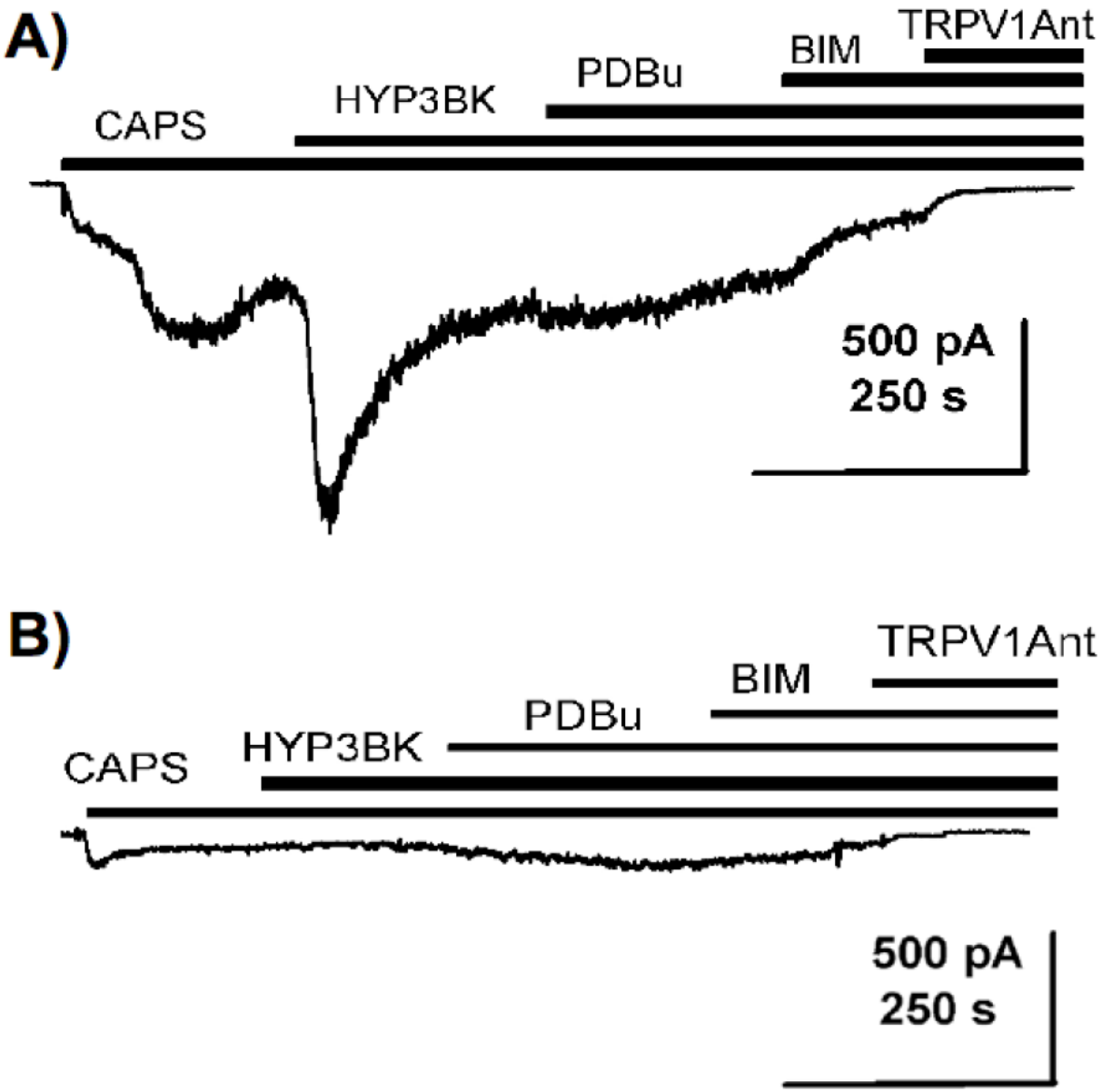

Figure 26. **Whole cell capsaicin currents in vHG and vHDNP-transduced neurons.**

Representative recordings of capsaicin currents in vHG- and vHDNP-transduced neurons are shown. A) Capsacin currents in vHG-transduced neurons were enhanced by a bradykinin receptor 2 agonist (HYP3BK, 5 μM). Application of 5μM PDBu did not further enhance the current. Addition of the PKC inhibitor, bisindolylmaleimide (BIM, 5μM) partially blocked the current. The current was completely antagonized by a TRPV1-specific antagonist (TRPV1 Antag). B) vHDNP1-transduced neurons displayed diminished capsaicin (CAP) currents that were not enhanced by HYP3BK. 5 μM PDBu caused a drift current that was partially antagonized by 5μM BIM. TRPV1 antagonist (TRPV1 Ant) completely returned the current to baseline values. Scales showing time (sec) and current amplitude (pA) are indicated for each recording.

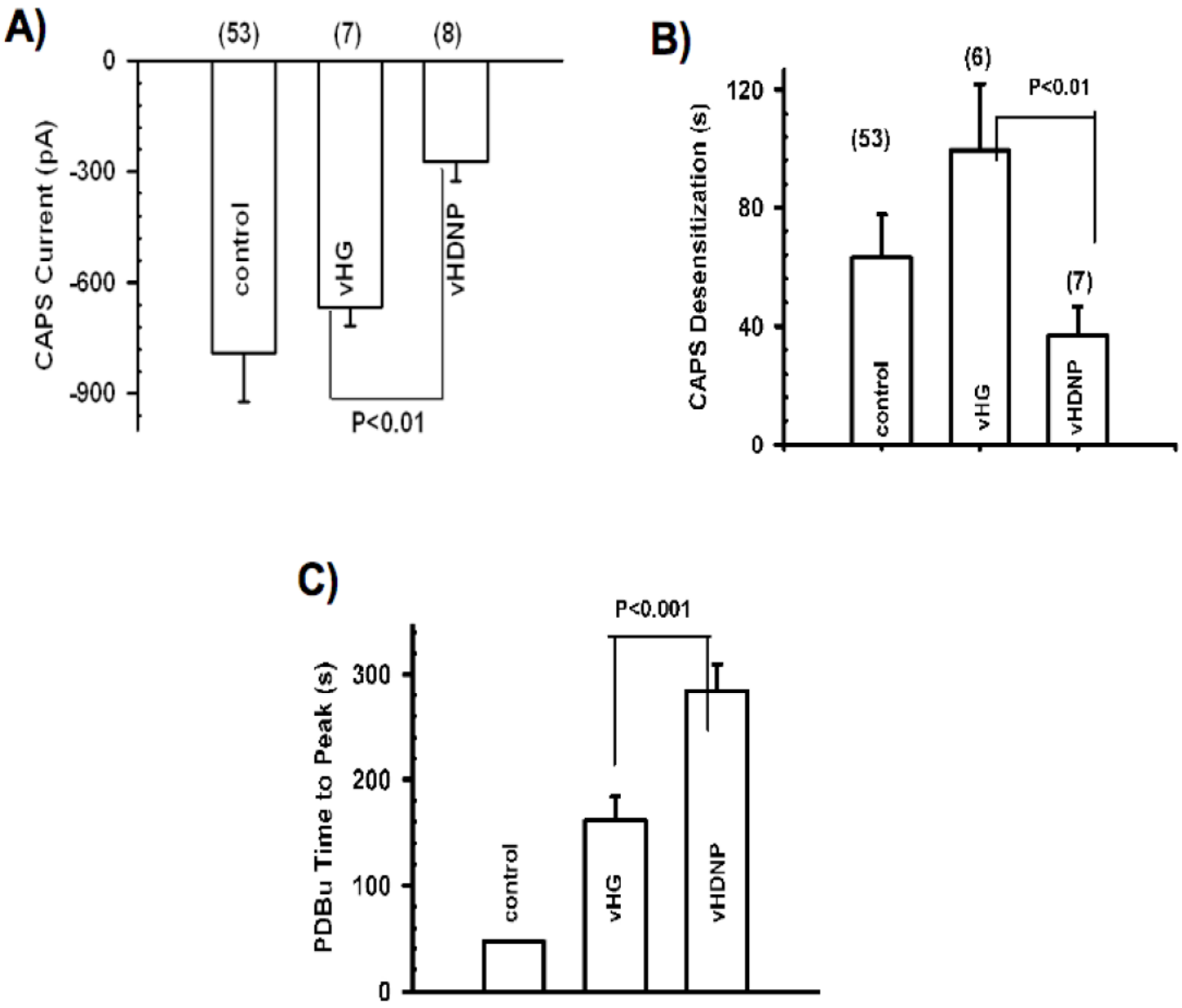

Figure 27. **Summary of vHDNP-mediated TRPV1 current inhibition.**

A) vHDNP-transduced neurons displayed significantly diminished ($p<0.01$) current amplitudes when compared with vHG-transduced or non-transduced (control) neurons. B) vHDNP transduction of neurons resulted in faster desensitization rates of capsaicin-induced TRPV1 currents when compared with vHG-transduced or non-transduced (control) neurons. C) PDBu stimulation of vHDNP-transduced neurons resulted in a significantly increased time for the capsaicin currents to reach peak amplitude when compared with vHG-transduced or non-transduced (control) neurons ($p<0.001$). The number of neurons measured for each parameter are indicated in parantheses.

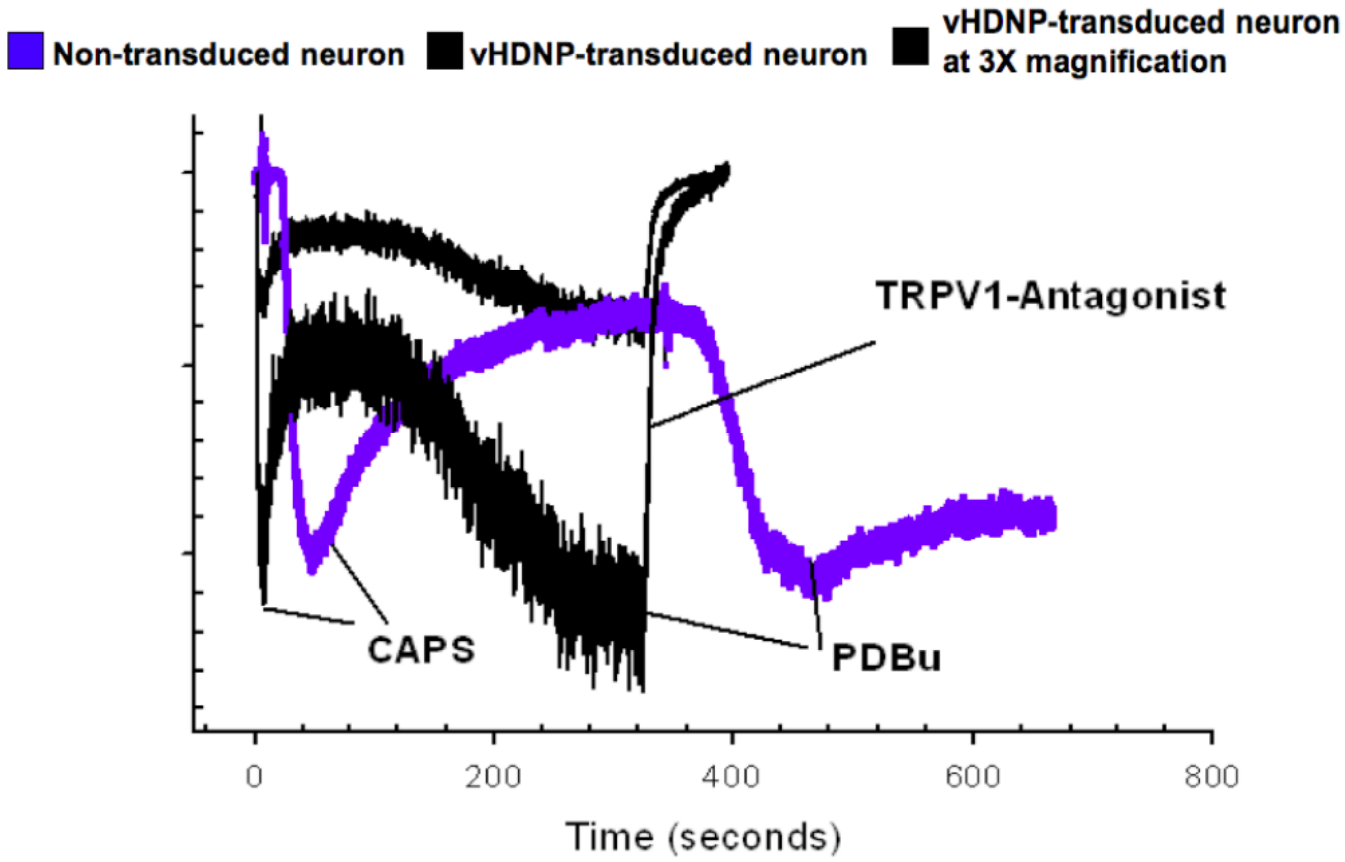

Figure 28.Comparison of desensitization rates and PDBu effects between non-transduced and vHDNP-transduced neurons.

The graph depicts a representative recording of the capsaicin (CAPS) current response in a non-transduced neuron in blue. The capsaicin current in this neuron desensitizes over a period of several seconds. PDBu application greatly enhances current amplitude and results in a non-desensitizing current. In contrast, vHDNP-transduced neurons display small currents in response to capsaicin (CAPS) (black trace). The currents show a drift with PDBu application that can be antagonized with a TRPV1-Antagonist. Also shown is a 3X magnification of the same vHDNP-transduced neuronal recording (larger black trace). As seen, the desensitization rate is significantly faster in the vHDNP-transduced neuron (approximately 20 sec) when compared with the non-transduced neuron (approximately 150 sec).

4.2.7 vHDNP-expressed dominant negative PKCε (DNP) inhibits TRPV1 function *in-vivo*.

Experiments performed so far revealed a vHDNP-mediated inhibition of endogenous PKCε translocation in adult rat DRG neurons. This was accompanied by quantitative and

qualitative reductions in the TRPV1 activity of cultured DRG neurons as shown by results from cobalt uptake assays and electrophysiological recordings. Together, these results confirm the ability of HSV-1 vector-expressed dominant negative PKCε to inhibit endogenous PKCε function in rat DRG neurons and thereby attenuate TRPV1 function *in-vitro*. Following the *in-vitro* demonstration of TRPV1 inhibition by vHDNP, the next step was to examine the *in-vivo* attenuation of TRPV1 function by vHDNP. Since the TRPV1 receptor is a known sensor of noxious heat (43˚C), *in-vivo* tests examined nociceptive responses of vector-inoculated rats following the application of an intense heat source.

For *in-vivo* experiments, young adult male Sprague-Dawley rats were subcutaneously injected with 100 µl of vHG, vHDNP (10^9 pfu/ml) or PBS (sham injection) into the plantar surface of the right hind paw. Uninjected animals were included as an additional control. Animals were placed on a temperature-controlled platform and tested for thermal hyperalgesia by the application of an intense light source to the footpad. A focused heat source (30-lumen light intensity) was aimed at the plantar surface of the foot and the time until the animal moved its foot in response to the heat was measured. Figure 29A shows the paw withdrawal latency times (y-axis) presented as ratios of the average time taken for withdrawal of the right foot versus the left foot for animals in each group (x-axis). As seen in the figure, the ratio for paw withdrawal latency in the uninoculated and PBS injected control rats was around 1, while the ratio in vHG-inoculated rats was 0.85. When compared with the vHG-inoculated group, rats inoculated with the vHDNP vector displayed a significantly increased paw withdrawal ratio of 1.25 ($p<0.05$).

Immediately following the tests for thermal hyperalgesia, the rats were also tested for mechanical allodynia using von Frey hair stimulation as described in materials and methods

(section 2.13). Figure 29B summarizes findings from tests for mechanical allodynia where data are presented as a ratio of 50% gram threshold responses between right and left paws for each group. As seen in the figure, there were no significant differences in the ratios of 50% gram threshold responses between the three groups of rats.

These data indicate a subtle inhibitory effect of vHDNP on the sensory responses of rats to noxious heat stimuli.

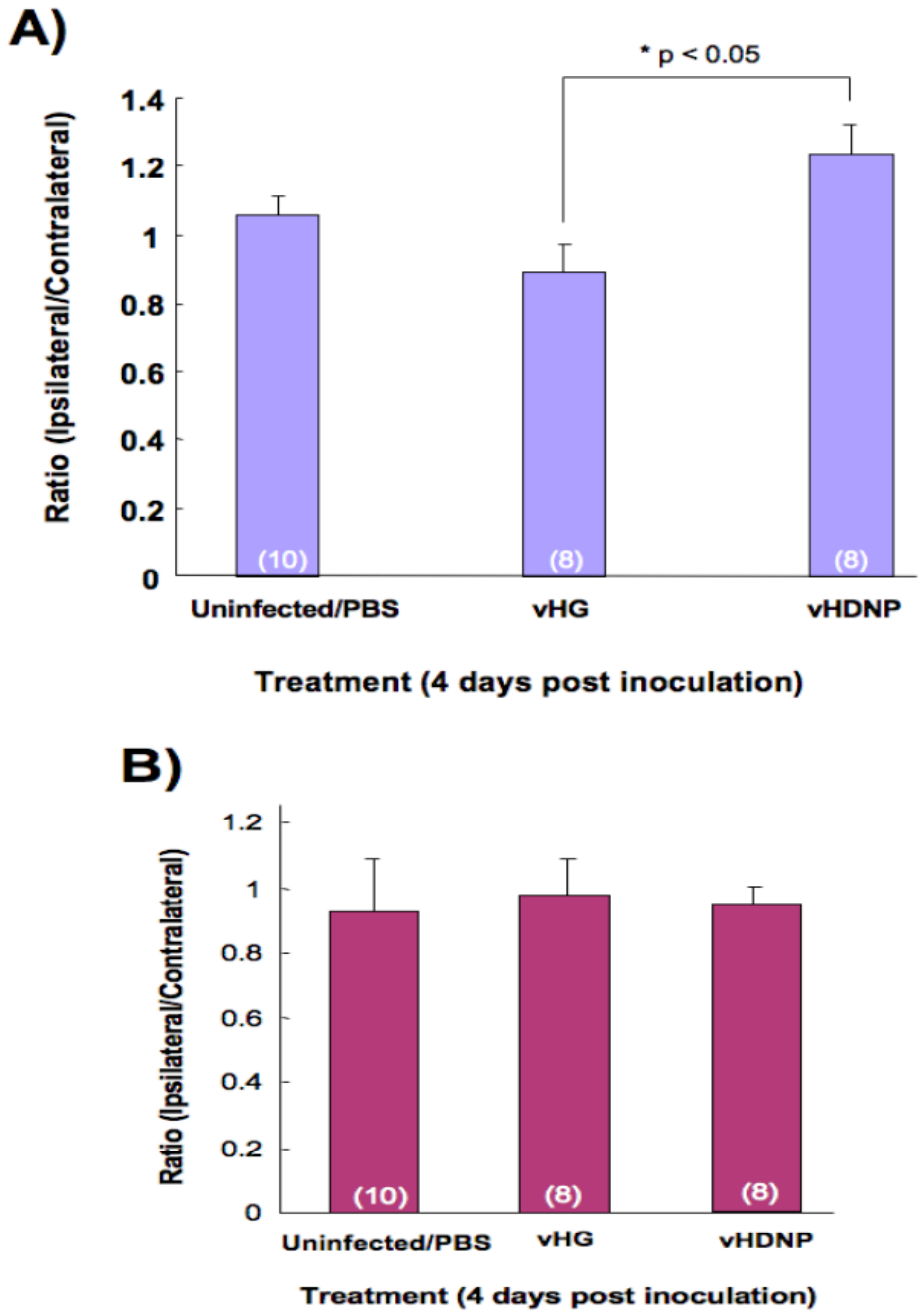

Figure 29. ***In-vivo*** **effects of vHDNP in adult rats.**

Vector-inoculated, sham injected and uninfected rats were examined for painful behaviors in response to heat (thermal hyperalgesia) and innocuous mechanical stimuli (mechanical allodynia). A) Data are presented as the ratio of right to left paw withdrawal latencies (y-axis) for each group of rat (x-axis). A significant difference was observed in the ratios of paw withdrawal latencies between the vHG and vHDNP vector-inoculated rats. B) The graph plots the right to left paw ratios of 50% gram threshold responses (y-axis) for each group of rat (x-axis). No significant differences were observed between the three groups of rats. The number of rats for each group are indicated in parantheses for each graph.

4.3 DISCUSSION

Protein kinase C epsilon (PKCε) is a pro-nociceptive molecule that potentiates TRPV1 activation in DRG neurons, leading to the development of a chronic pain state. The targeted inhibition of PKCε function in nociceptive afferent neurons therefore represents a novel strategy to attenuate TRPV1 function in order to prevent the development of chronic pain. In this chapter, the neurotropism of herpes simplex viral vectors have been exploited for the targeted delivery of a dominant negative PKCε (DNP) transgene product to DRG neurons. The design, development and functional effects of HSV-1 vector-expressed DNP on neuronal TRPV1 receptor function *in-vitro* and *in-vivo* have been described.

Initial experiments demonstrated the successful expression of dominant negative PKCε (DNP) from the HSV-1 vector, vHDNP. The PKC-specific activator, PMA caused a translocation of DNP to the plasma membrane of vHDNP-transduced Vero and U2OS cells, thus confirming the functionality of this transgene product.

Interestingly, DNP translocated to specific regions resembling microvilli in Vero cells, while the translocation in U2OS cells occurred uniformly along the plasma membrane. The C2 sub-domain of PKCε is known to confer signaling specificity to this isozyme by binding to the receptor for activated kinases (RACK2) at the plasma membrane [98]. However, the DNP construct used in this study is deleted for the C2 domain and still translocates to specific structures in Vero cells, suggesting that there may be other unknown cell specific determinants of subcellular localization and the consequent signaling specificity of PKCε. Indeed, studies have shown that specific subcellular localization of PKCε can be mediated by the pseudosubstrate (PS) region or the variable 3 (V3) region, both of which are retained in the DNP construct [99-102]. Prior to PMA-

mediated enzyme activation, the HSV-1 vector-expressed DNP construct localized to perinuclear regions of U2OS, Vero and neuronal cells while perinuclear localization of DNP was not observed in Vero and U2OS cells transfected with a DNP expressing plasmid (p41HDNP). Figure 30 shows vector vHDNP-transduced Vero cells with a distinct perinuclear localization of the DNP transgene product in all cells (Fig. 30A), while plasmid p41HDNP transfected Vero cells display a uniform and non-specific localization of DNP in all the cells (Fig. 30B). This points to the idea that the HSV-1 vector may mediate perinuclear DNP localization in these cells. In support of this theory, a recent study has shown that PKC isoenzymes localize to areas surrounding the nuclear lamina in HSV-1 infected HEp-2 cells [103].

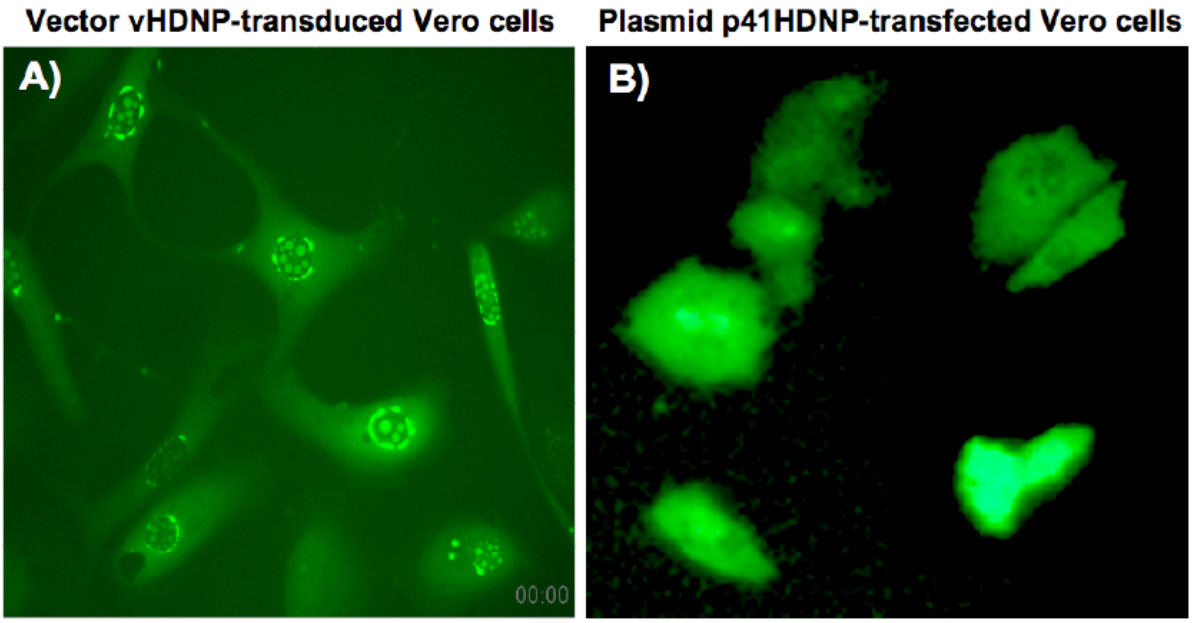

Figure 30. Subcellular localization of DNP in vHDNP-transduced and p41HDNP plasmid-transfected Vero cells.

A) vHDNP vector-transduced cells show a distinct perinuclear localization of DNP in all cells, and B) DNP displays is uniformly localized throughout the cells following transfection with a DNP expressing plasmid, p41HDNP (Images are at 40X magnification).

Following the confirmation of vHDNP vector-mediated DNP expression and functionality, the ability of DNP to inhibit the translocation of endogenous PKCε in cultured DRG neurons was examined. Results from *in-vitro* experiments in PDBu-stimulated neurons transduced with vHDNP showed that following activation, DNP translocated to the neuronal plasma membrane and inhibited the translocation of endogenous PKCε. The DNP translocation in neurons occurred uniformly across the plasma membrane and was much faster than that observed in Vero and U2OS cells. The addition of 1 μM cytochalasin 30 min prior to PDBu activation in neurons resulted in a reduction in the rate of DNP translocation (personal observation, data not shown). Since cytochalasin disrupts the actin cytoskeleton, this observation suggests that DNP translocation may occur via binding to the actin cytokeleton. This theory agrees with the fact that PKCε possesses a unique actin-binding site in the regulatory domain that is retained in the DNP construct [104].

As mentioned earlier, PKCε is known to phosphorylate and potentiate TRPV1 receptor function in a variety of painful inflammatory and neuropathic conditions, making PKCε inhibition a potential strategy to treat chronic pain states. The demonstration of vector-expressed DNP functionality in Vero and U2OS cells and the DNP-mediated inhibition of endogenous PKCε in cultured DRG neurons encouraged further studies to evaluate the effects of vector-expressed DNP on TRPV1 receptor activity in cultured DRG neurons. The cobalt uptake assay allows a quick evaluation of ion channel activity in a large number of DRG neurons in culture and was therefore used to determine the effect of DNP on TRPV1 activity. Since PKCε is an indirect downstream potentiator, and not a direct activator of TRPV1, the assays were expected to reveal comparatively normal levels of TRPV1 activity in vHDNP-transduced neurons following an activation with the direct receptor agonist, capsaicin. However, surprisingly,

vHDNP-transduced neurons showed a marked reduction in capsaicin-induced TRPV1 activity when compared with non-transduced or vHG-transduced control neurons. Moreover, vHDNP-transduced neurons that were positive for cobalt uptake showed a lighter staining when compared with non-transduced and vHG-transduced neurons. This observation meant that either the TRPV1 receptor was desensitizing rapidly due to the inhibition of endogenous PKCε or that the expression of functional TRPV1 receptors at the neuronal plasma membrane was reduced. In order to dissect out these possibilities, qualitative whole cell electrophysiological recordings of capsaicin-induced TRPV1 currents in vHDNP-transduced neurons were performed. Cobalt uptake studies in vHG-transduced neurons displayed near normal TRPV1 activity in response to capsaicin stimulation and were therefore used as a control for these experiments. The following paragraphs will describe molecular mechanisms thought to be responsible for the various effects of capsaicin currents in control vHG-transduced neurons followed by a discussion of the capsaicin current recordings in vHDNP-tranduced neurons.

vHG-transduced neurons demonstrated capsaicin-induced currents of a normal amplitude. Addition of the bradykinin receptor 2 (BK2R) specific agonist, HYP-3-bradykinin (HYP3BK) enhanced the capsaicin current. The increase in TRPV1 function and current amplitudes following stimulation of the BK2R receptor has been previously reported in several studies described in the introduction of chapter 4. Briefly, BK2R is a G-protein coupled receptor that, when stimulated results in the downstream activation of PKCε. Activated PKCε translocates to the membrane and phosphorylates the TRPV1 receptor, resulting in a potentiation of TRPV1 function and the consequent enhancement of current amplitude. This enhancement of current with HYP3BK could not be further enhanced with the addition of a non-specific PKC activator, PDBu, indicating that PKCε is likely to be the major isoform that phosphorylates and enhances

TRPV1 function in cultured DRG neurons. This result contradicts a previous study showing that PKCα and not PKCε is the isoform coupled to the enhancement of TRPV1 function in DRG neurons [105]. As mentioned in the introduction of this chapter, the dynamic interplay between receptor phosphorylation and de-phosphorylation by kinases and phosphatases is thought to govern TRPV1 function [89]. The constitutive activity of kinases within the neuron may be responsible for both receptor sensitization as well as the ability of TRPV1 to remain in an optimal capsaicin responsive configuration. The inhibition of kinases is therefore likely to attenuate capsaicin responses in TRPV1 due to a comparatively greater constitutive activity of phosphatases. The phosphatase mediating this effect is likely to be calcineurin because of the presence of a calmodulin binding site at the C-terminal domain of TRPV1. In accord with this theory, the addition of a non-specific PKC inhibitor, bisindolylmaleimide (BIM) resulted in an acceleration of TRPV1 current desensitization due to the unchecked activity of endogenous neuronal phosphatases in the cell. Finally, the addition of a TRPV1 specific agonist returned the current to baseline levels indicating that the effects of HYP3BK and BIM were due to a TRPV1-mediated current.

In stark contrast to the vHG-transduced neuronal capsaicin currents, the capsaicin responsiveness in vHDNP-transduced neurons was significantly reduced. This correlated with the reduction in capsaicin sensitive neurons seen by cobalt uptake. vHDNP-transduced neurons that responded to capsaicin consistently demonstrated diminished, rapidly desensitizing currents. These results indicate that the inhibition of endogenous PKCε in neurons severely diminishes the ability of capsaicin to activate TRPV1. To my knowledge, this phenomenon has not been previously reported and it is likely that PKC-mediated phosphorylation may be a requirement for capsaicin-induced TRPV1 activation. Moreover, TRPV1 phosphorylation by Ca+2/Calmodulin

dependent kinase was shown to be a requirement for TRPV1 activation by capsaicin and resiniferatoxin in a previous study [106]. It is therefore likely that variations in the combinations of receptor phosphorylation and de-phosphorylation sites regulate vanilloid receptor sensitivity to different agonists.

In contrast to vHG-transduced neurons, the addition of HYP3BK following the onset of capsaicin-induced currents consistently failed to enhance current amplitude, thus confirming the complete inhibition of endogenous PKCε activation downstream of bradykinin receptor 2 (BK2R).

The addition of PDBu following HYP3BK in vHDNP-transduced neurons consistently caused a slow onset drift-like current that was antagonized by the addition of the non-specific PKC inhibitor, BIM. Addition of a TRPV1 antagonist returned the current to baseline levels indicating that a TRPV1-specific current caused the PDBu-induced drift. Mechanistically, this may translate into either the inefficient phosphorylation of TRPV1 by other isoforms or a delayed onset, inefficient phosphorylation of TRPV1 by endogenous PKCε. Since PKCε was the major isoform contributing to the enhancement of capsaicin-induced TRPV1 currents as described earlier, the later case of inefficient receptor phosphorylation by endogenous PKCε is more likely.

Taken together, findings from electrophysiological recordings show that following transduction of neurons, HSV-1 vector-expressed DNP severely inhibits capsaicin-induced TRPV1 currents and that this inhibition is accompanied by significant changes in endogenous PKC activation profiles.

Following the successful domonstration of the vHDNP-mediated inhibition of TRPV1 activity in cultured DRG neurons, the effects of vHDNP on *in-vivo* nociceptive behaviors in

adult rats was examined. Since the TRPV1 receptor is a known direct sensor of noxious heat (43˚C), the paw withdrawal responses of rats following an application of noxious heat to the rat footpad was used as a behavioral model. A subtle but significant effect of delayed withdrawal responses was observed in vHDNP-inoculated rats when compared with uninoculated and vHG-inoculated rats. The absence of a complete loss of heat sensitivity is in agreement with the fact that several other TRP receptors, expressed nociceptive neurons directly sense heat [20] and also with the idea that PKCε may act exclusively through the TRPV1 receptor to cause pain [39]. Moreover, mice without TRPV1 and TRPV2 receptors have been shown to possess normal heat responses, suggesting that there may be other unknown heat sensing receptors in nociceptive neurons [107]. The results obtained in this chapter thus suggest that a specific knockdown of TRPV1 function *in-vivo* may have been achieved using the vHDNP vector. This can be beneficial if the inhibition of PKCε is to be used as a strategy to treat pain, since acute pain responses to heat are protective and must be preserved.

It should be noted that several pieces of data in this study point toward a unique mechanism that might involve the inadequate assembly of a TRPV1-bradykinin receptor 2 (BK2R)-PKCε signaling complex in neurons transduced with vHDNP. These data are summarized as follows: A drastic reduction of the capsaicin current amplitudes in vHDNP-transduced along with rapid current desensitization was observed by combined results from cobalt uptake studies and electrophysiological recordings. This fits with the idea that a reduced number of surface TRPV1 receptors, when activated, will cause a reduction in whole cell current amplitudes or a quantitative fall in the Co^{+2} ions that flux into the cell. In addition, HYP3BK failed to cause any enhancement of current, while PDBU stimulation resulted in an inefficient TRPV1 current enhancement. This can be interpreted as a complete absence of the bradykinin 2

receptor at the cell surface. The consequently inefficient anchoring and phosphorylation mechanism for PKC following stimulation with PDBu in vHDNP-transduced neurons is read as slow, inefficient drift-like currents by electrophysiology. Finally, the number of capsaicin responsive vHDNP-transduced neurons were greatly reduced when compared with controls. This points towards an overall reduction in the assembly of functional TRPV1 receptors on the plasma membrane of DNP expressing DRG neurons. The theory of a possible disassembly of the TRPV1-BK2R-PKC signaling complex following an inhibition of PKCε function in nociceptive neurons is supported by studies of TRP signaling complexes in drosophila. These studies show that eye-specific PKC null mutant flies possess an inadequate assembly of the TRP signaling complex with the consequent loss of visual function [108]. A series of studies by the same group have also shown that the TRP receptor assembles in drosophila photoreceptors as a large signaling complex called the transducisome which consists of a multivalent scaffolding protein called INAD that tethers TRP receptors to phospholipase C and PKC subunits. Further, it was shown that a disruption of any of these transducisome components including PKC caused a mislocalization of the complex and a consequent loss of function [109-111]. Indeed, the association of ion channels with signaling complexes in neurons is a field of growing interest [112]. With the plethora of recent literature showing that TRP receptors and other ion channels associate with large signaling complexes, it is likely that the DNP product used in this study mediates the inhibition of TRPV1 by a disruption of the signaling complex associated with this receptor. Support for this viewpoint can also be gained a study showing that PKC is involved in the trafficking of TRPV1 receptor in neurons [113]. Although I have not addressed the aspect of TRPV1-PKC assembly in my dissertation, this thesis provides future avenues and tools for research into the area of TRPV1 transducisome assembly in DRG neurons.

5.0 SUMMARY AND CONCLUSIONS

Chronic pain is a complex process caused by peripheral plastic changes in nociceptive neurons. These changes are largely mediated by the activation of receptors that detect the release of inflammatory mediators from damaged tissue at the periphery of the nociceptive pathway. Recent research has uncovered the existence of several ion channels and pro-nociceptive molecules that are specifically upregulated in chronic pain states. Among these, the vanilloid receptor (TRPV1) is an important calcium ion channel activated by several noxious stimuli and protein kinase C epsilon (PKCε) is a pro-nociceptive kinase that potentiates and enhances TRPV1 function. Following activation, TRPV1 initiates plastic changes in neurons that ultimately result in a chronic pain state. The inhibition of TRPV1 function can therefore be an effective strategy to treat chronic pain. This dissertation focuses on the development of methods and tools that can be used to identify inhibitors of the TRPV1 receptor in chapter three, while an inhibition of TRPV1 function by the HSV-1 vector-mediated expression of dominant negative PKCε is described in chapter four.

In chapter three, a selection system using the rationale of selective HSV-1 vector replication following the antagonism of vector-expressed receptor function was developed. The TRPV1 receptor was used as a model gene to develop this system. Salient features of this system are as follows:

1) The HSV-1 vector-expressed TRPV1 receptor was activated by capsaicin, resulting in an influx of cytotoxic levels of calcium ions into the cell.

2) Calcium influx following TRPV1 activation caused cell death prior to the completion of the HSV-1 replicative cycle. This resulted in a fall of viral titers as an indirect effect of TRPV1 activation.

3) Antagonism of TRPV1 activation with known receptor inhibitors reversed this blockage of viral replication thus providing a model system whereby ion channel inhibitors can be identified by virtue of their ability to cause a recovery in HSV-1 viral growth.

4) The system was highly sensitive to capsaicin selection since it was possible to select for one particle of a GFP expressing vector among 100,000 background viral particles that expressed TRPV1.

In conclusion, the HSV-1 vector-based selection system described in chapter three is a powerful platform system that can be applied to other ion channels involved in nociception. The system can also be used in cDNA and RNAi library screens to identify novel biological products that inhibit ion channel function. The identification of nociceptive ion channel inhibitors and modulatory gene products can provide novel treatments for chronic pain and help develop a better understanding of regulatory mechanisms in nociception.

Chapter four of this dissertation describes the use of a dominant negative PKCε construct to inhibit TRPV1 function *in-vitro* and *in-vivo*. Salient findings from this study are summarized below:

1) HSV-1 vector expressed dominant negative PKCε (DNP) was functional and translocated to the membrane in Vero and U2OS cells following activation with the known PKC activator, PMA.

2) Following stimulation with the known PKC activator, PDBu, HSV-1 vector-expressed DNP translocated to the plasma membrane of DRG neurons in culture and as a result, inhibited the functional translocation of endogenous PKCε.

3) Neurons transduced with HSV-1 vectors expressing DNP displayed marked reductions in capsaicin sensitivity and also showed several changes in the responses of capsaicin currents to the PKC activators, PDBu and HYP3BK when compared with controls. This indicated that vector-expressed DNP inhibits TRPV1 function *in-vitro*.

4) Behavioral studies in rats demonstrated that HSV-1 vector-expressed DNP caused a small reduction in nociceptive responses to noxious heat, thus indicating a knockdown of TRPV1 function *in-vivo*.

In conclusion, chapter four demonstrates the use of HSV-1 vectors as a valuable expression tool to inhibit TRPV1 function *in-vitro* and *in-vivo*. In addition, mechanisms for the inhibition of TRPV1 function by HSV-1 expressed DNP were partially dissected, providing several avenues for future research in this area.

BIBLIOGRAPHY

1. Pain terms: a list with definitions and notes on usage. Recommended by the IASP Subcommittee on Taxonomy. Pain 6, 249 (1979).

2. Deleo, J. A. Basic science of pain. J Bone Joint Surg Am 88 Suppl 2, 58-62 (2006).

3. Melzack, R. & Wall, P. D. Pain mechanisms: a new theory. Science 150, 971-9 (1965).

4. Rainville, P. Brain mechanisms of pain affect and pain modulation. Curr Opin Neurobiol 12, 195-204 (2002).

5. Lee, Y., Lee, C. H. & Oh, U. Painful channels in sensory neurons. Mol Cells 20, 315-24 (2005).

6. Julius, D. & Basbaum, A. Molecular mechanisms of nociception. Nature 413, 203-210 (2001).

7. Schaible, H. G. & Richter, F. Pathophysiology of pain. Langenbecks Arch Surg 389, 237-43 (2004).

8. Dworkin, R. H. et al. Advances in neuropathic pain: diagnosis, mechanisms, and treatment recommendations. Arch Neurol 60, 1524-34 (2003).

9. Zeilhofer, H. U. Synaptic modulation in pain pathways. Rev Physiol Biochem Pharmacol 154, 73-100 (2005).

10. Woolf, C. J. & Salter, M. W. Neuronal plasticity: increasing the gain in pain. Science 288, 1765-9 (2000).

11. Stewart, W. F., Ricci, J. A., Chee, E., Morganstein, D. & Lipton, R. Lost productive time and cost due to common pain conditions in the US workforce. Jama 290, 2443-54 (2003).

12. Strunin, L. & Boden, L. I. Family consequences of chronic back pain. Soc Sci Med 58, 1385-93 (2004).

13. Bailey, C. P. & Connor, M. Opioids: cellular mechanisms of tolerance and physical dependence. Curr Opin Pharmacol 5, 60-8 (2005).

14. Premkumar, L. S. & Ahern, G. P. Induction of vanilloid receptor channel activity by protein kinase C. Nature 408, 985-90 (2000).

15. Mandadi, S. et al. Increased sensitivity of desensitized TRPV1 by PMA occurs through PKCepsilon-mediated phosphorylation at S800. Pain 123, 106-16 (2006).

16. Montell, C. The TRP Superfamily of Cation Channels. Sci STKE 2005, re3 (2005).

17. Clapham, D. E. TRP channels as cellular sensors. Nature 426, 517-24 (2003).

18. Moran, M. M., Xu, H. & Clapham, D. E. TRP ion channels in the nervous system. Curr Opin Neurobiol 14, 362-9 (2004).

19. Patapoutian, A., Peier, A. M., Story, G. M. & Viswanath, V. ThermoTRP channels and beyond: mechanisms of temperature sensation. Nat Rev Neurosci 4, 529-39 (2003).

20. Dhaka, A., Viswanath, V. & Patapoutian, A. TRP Ion Channels and Temperature Sensation. Annu Rev Neurosci (2006).

21. Caterina, M. J. et al. The capsaicin receptor: a heat-activated ion channel in the pain pathway. Nature 389, 816-24 (1997).

22. Smart, D. & Jerman, J. C. Anandamide: an endogenous activator of the vanilloid receptor. Trends Pharmacol Sci 21, 134 (2000).

23. Smart, D. et al. The endogenous lipid anandamide is a full agonist at the human vanilloid receptor (hVR1). Br J Pharmacol 129, 227-30 (2000).

24. Szallasi, A. & DiMarzo, V. New perspectives on enigmatic vanilloid receptors. TINS 23, 491-497 (2000).

25. Tominaga, M. et al. The cloned capsaicin receptor integrates multiple pain-producing stimuli. Neuron 21, 531-43 (1998).

26. Kress, M. & Zeilhofer, H. U. Capsaicin, protons and heat: new excitement about nociceptors. Trends Pharmacol Sci 20, 112-8 (1999).

27. Sugiura, T., Tominaga, M., Katsuya, H. & Mizumura, K. Bradykinin lowers the threshold temperature for heat activation of vanilloid receptor 1. J Neurophysiol 88, 544-8 (2002).

28. Tang, H. B., Inoue, A., Oshita, K. & Nakata, Y. Sensitization of vanilloid receptor 1 induced by bradykinin via the activation of second messenger signaling cascades in rat primary afferent neurons. Eur J Pharmacol 498, 37-43 (2004).

29. Amaya, F. et al. NGF and GDNF differentially regulate TRPV1 expression that contributes to development of inflammatory thermal hyperalgesia. Eur J Neurosci 20, 2303-10 (2004).

30. Numazaki, M., Tominaga, T., Toyooka, H. & Tominaga, M. Direct phosphorylation of capsaicin receptor VR1 by protein kinase Cepsilon and identification of two target serine residues. J Biol Chem 277, 13375-8 (2002).

31. Wood, J. N., Boorman, J. P., Okuse, K. & Baker, M. D. Voltage-gated sodium channels and pain pathways. J Neurobiol 61, 55-71 (2004).

32. Mohapatra, D. P. & Nau, C. Regulation of Ca2+-dependent desensitization in the vanilloid receptor TRPV1 by calcineurin and cAMP-dependent protein kinase. J Biol Chem (2005).

33. Chuang, H. H. et al. Bradykinin and nerve growth factor release the capsaicin receptor from PtdIns(4,5)P2-mediated inhibition. Nature 411, 957-62 (2001).

34. Wilson-Gerwing, T. D., Dmyterko, M. V., Zochodne, D. W., Johnston, J. M. & Verge, V. M. Neurotrophin-3 suppresses thermal hyperalgesia associated with neuropathic pain and attenuates transient receptor potential vanilloid receptor-1 expression in adult sensory neurons. J Neurosci 25, 758-67 (2005).

35. Caterina, M. J. et al. Impaired nociception and pain sensation in mice lacking the capsaicin receptor. Science 288, 306-13 (2000).

36. Ohno, S. & Nishizuka, Y. Protein kinase C isotypes and their specific functions: prologue. J Biochem (Tokyo) 132, 509-11 (2002).

37. Akita, Y. Protein kinase C-epsilon (PKC-epsilon): its unique structure and function. J Biochem (Tokyo) 132, 847-52 (2002).

38. Khasar, S. G. et al. A novel nociceptor signaling pathway revealed in protein kinase C epsilon mutant mice. Neuron 24, 253-60 (1999).

39. Bolcskei, K. et al. Investigation of the role of TRPV1 receptors in acute and chronic nociceptive processes using gene-deficient mice. Pain 117, 368-76 (2005).

40. Zhou, Y., Li, G. D. & Zhao, Z. Q. State-dependent phosphorylation of epsilon-isozyme of protein kinase C in adult rat dorsal root ganglia after inflammation and nerve injury. J Neurochem 85, 571-80 (2003).

41. Moriyama, T. et al. Possible involvement of P2Y2 metabotropic receptors in ATP-induced transient receptor potential vanilloid receptor 1-mediated thermal hypersensitivity. J Neurosci 23, 6058-62 (2003).

42. Glorioso, J. C. & Fink, D. J. Herpes vector-mediated gene transfer in treatment of diseases of the nervous system. Annu Rev Microbiol 58, 253-71 (2004).

43. Honess, R. & Roizman, B. Regulation of herpes simplex virus macromolecular synthesis. I. Cascade regulation of the synthesis of three groups of viral proteins. J Virol 14, 8-19 (1974).

44. Marconi, P. et al. Replication-defective herpes simplex virus vectors for gene transfer in vivo. Proc Natl Acad Sci U S A 93, 11319-20 (1996).

45. Marconi, P. et al. Replication-defective HSV vectors for gene transfer in vivo. Proc Natl Acad Sci, USA 93, 11319-11320 (1996).

46. Burton, E. A. et al. Multiple applications for replication-defective herpes simplex virus vectors. Stem Cells 19, 358-77 (2001).

47. Fink, D., DeLuca, N., Yamada, M., Wolfe, D. & Glorioso, J. Design and application of HSV vectors for neuroprotection. Gene Ther 7, 115-120 (2000).

48. Wolfe, D. et al. Herpesvirus-mediated systemic delivery of nerve growth factor. Mol Ther 3, 61-9 (2001).

49. Wilson, S. P. et al. Antihyperalgesic effects of infection with a preproenkephalin-encoding herpes virus. Proc. Natl. Acad. Sci. USA 96, 3211-3216 (1999).

50. Braz, J. et al. Therapeutic efficacy in experimental polyarthritis of viral-driven enkephalin overproduction in sensory neurons. J Neurosci 21, 7881-7888 (2001).

51. Goss, J. R. et al. Antinociceptive effect of a genomic herpes simplex virus-based vector expressing human proenkephalin in rat dorsal root ganglion. Gene Ther 8, 551-6 (2001).

52. Hao, S., Mata, M., Goins, W., Glorioso, J. C. & Fink, D. J. Transgene-mediated enkephalin release enhances the effect of morphine and evades tolerance to produce a sustained antiallodynic effect in neuropathic pain. Pain 102, 135-42 (2003).

53. Goss, J. R. et al. Herpes vector-mediated expression of proenkephalin reduces bone cancer pain. Ann Neurol 52, 662-5 (2002).

54. Hao, S. et al. HSV-mediated gene transfer of the glial cell-derived neurotrophic factor provides an antiallodynic effect on neuropathic pain. Mol Ther 8, 367-75 (2003).

55. Liu, J. et al. Peripherally delivered glutamic acid decarboxylase gene therapy for spinal cord injury pain. Mol Ther 10, 57-66 (2004).

56. Wood, J. N. et al. Ion channel activities implicated in pathological pain. Novartis Found Symp 261, 32-40; discussion 40-54 (2004).

57. Lee, S. Y. et al. Sensitization of vanilloid receptor involves an increase in the phosphorylated form of the channel. Arch Pharm Res 28, 405-12 (2005).

58. Tominaga, M. et al. Regulation mechanisms of vanilloid receptors. Novartis Found Symp 261, 4-12; discussion 12-8, 47-54 (2004).

59. Goins, W. F., Krisky, D. M., Wolfe, D. P., Fink, D. J. & Glorioso, J. C. Development of replication-defective herpes simplex virus vectors. Methods Mol Med 69, 481-507 (2002).

60. Chen, X. et al. Herpes simplex virus type 1 ICP0 protein does not accumulate in the nucleus of primary neurons in culture. J Virol 74, 10132-41 (2000).

61. Samaniego, L. A., Neiderhiser, L. & DeLuca, N. A. Persistence and expression of the herpes simplex virus genome in the absence of immediate-early proteins. J Virol 72, 3307-20 (1998).

62. Niranjan, A. et al. Treatment of rat gliosarcoma brain tumors by HSV-based multigene therapy combined with radiosurgery. Mol Ther 8, 530-42 (2003).

63. Zeidman, R., Lofgren, B., Pahlman, S. & Larsson, C. PKCepsilon, via its regulatory domain and independently of its catalytic domain, induces neurite-like processes in neuroblastoma cells. J Cell Biol 145, 713-26 (1999).

64. Sculptoreanu, A. & de Groat, W. C. Protein kinase C is involved in neurokinin receptor modulation of N- and L-type Ca2+ channels in DRG neurons of the adult rat. J Neurophysiol 90, 21-31 (2003).

65. Sculptoreanu, A., de Groat, W. C., Buffington, C. A. & Birder, L. A. Protein kinase C contributes to abnormal capsaicin responses in DRG neurons from cats with feline interstitial cystitis. Neurosci Lett 381, 42-6 (2005).

66. Sneddon, W. B., Liu, F., Gesek, F. A. & Friedman, P. A. Obligate mitogen-activated protein kinase activation in parathyroid hormone stimulation of calcium transport but not calcium signaling. Endocrinology 141, 4185-93 (2000).

67. Sathianathan, V. et al. Insulin induces cobalt uptake in a subpopulation of rat cultured primary sensory neurons. Eur J Neurosci 18, 2477-86 (2003).

68. Chaplan, S. R., Bach, F. W., Pogrel, J. W., Chung, J. M. & Yaksh, T. L. Quantitative assessment of tactile allodynia in the rat paw. J Neurosci Methods 53, 55-63 (1994).

69. Hubner, C. A. & Jentsch, T. J. Ion channel diseases. Hum Mol Genet 11, 2435-45 (2002).

70. Kalso, E. Sodium channel blockers in neuropathic pain. Curr Pharm Des 11, 3005-11 (2005).

71. Reis, J. et al. Levetiracetam influences human motor cortex excitability mainly by modulation of ion channel function--a TMS study. Epilepsy Res 62, 41-51 (2004).

72. Lipton, S. A. Failures and successes of NMDA receptor antagonists: molecular basis for the use of open-channel blockers like memantine in the treatment of acute and chronic neurologic insults. NeuroRx 1, 101-10 (2004).

73. Cheng, J. H., Kamiya, K. & Kodama, I. Carvedilol and vesnarinone: new antiarrhythmic approach in heart failure therapy. Acta Pharmacol Sin 22, 193-200 (2001).

74. Dutcher, J. P. et al. Phase II study of carboxyamidotriazole in patients with advanced renal cell carcinoma refractory to immunotherapy. Cancer (2005).

75. Ye, J. H., Ponnudurai, R. & Schaefer, R. Ondansetron: a selective 5-HT(3) receptor antagonist and its applications in CNS-related disorders. CNS Drug Rev 7, 199-213 (2001).

76. Zheng, W., Spencer, R. H. & Kiss, L. High throughput assay technologies for ion channel drug discovery. Assay Drug Dev Technol 2, 543-52 (2004).

77. Bednar, B. et al. Kinetic characterization of novel NR2B antagonists using fluorescence detection of calcium flux. J Neurosci Methods 137, 247-55 (2004).

78. Nikam, S. S. & Kornberg, B. E. AMPA receptor antagonists. Curr Med Chem 8, 155-70 (2001).

79. Gunthorpe, M. J. et al. Identification and characterisation of SB-366791, a potent and selective vanilloid receptor (VR1/TRPV1) antagonist. Neuropharmacology 46, 133-49 (2004).

80. El Kouhen, R. et al. A-425619 [1-isoquinolin-5-yl-3-(4-trifluoromethyl-benzyl)-urea], a novel and selective transient receptor potential type V1 receptor antagonist, blocks channel activation by vanilloids, heat, and acid. J Pharmacol Exp Ther 314, 400-9 (2005).

81. Grant, S. K. et al. Delay of intracellular calcium transients using a calcium chelator: application to high-throughput screening of the capsaicin receptor ion channel and G-protein-coupled receptors. Anal Biochem 294, 27-35 (2001).

82. Jager, S., Brand, L. & Eggeling, C. New fluorescence techniques for high-throughput drug discovery. Curr Pharm Biotechnol 4, 463-76 (2003).

83. Ames, R. et al. BacMam recombinant baculoviruses in G protein-coupled receptor drug discovery. Receptors Channels 10, 99-107 (2004).

84. Cortright, D. N. & Szallasi, A. Biochemical pharmacology of the vanilloid receptor TRPV1. An update. Eur J Biochem 271, 1814-9 (2004).

85. Szabo, A. et al. Role of transient receptor potential vanilloid 1 receptors in adjuvant-induced chronic arthritis: in vivo study using gene-deficient mice. J Pharmacol Exp Ther 314, 111-9 (2005).

86. Dedov, V. N., Mandadi, S., Armati, P. J. & Verkhratsky, A. Capsaicin-induced depolarisation of mitochondria in dorsal root ganglion neurons is enhanced by vanilloid receptors. Neuroscience 103, 219-26 (2001).

87. Jambrina, E. et al. Calcium influx through receptor-operated channel induces mitochondria-triggered paraptotic cell death. J Biol Chem 278, 14134-45 (2003).

88. Shin, C. Y. et al. Essential role of mitochondrial permeability transition in vanilloid receptor 1-dependent cell death of sensory neurons. Mol Cell Neurosci 24, 57-68 (2003).

89. Mandadi, S. et al. Activation of protein kinase C reverses capsaicin-induced calcium-dependent desensitization of TRPV1 ion channels. Cell Calcium 35, 471-8 (2004).

90. Hong, S. & Wiley, J. W. Early painful diabetic neuropathy is associated with differential changes in the expression and function of vanilloid receptor 1. J Biol Chem 280, 618-27 (2005).

91. Stavrovskaya, I. G. & Kristal, B. S. The powerhouse takes control of the cell: is the mitochondrial permeability transition a viable therapeutic target against neuronal dysfunction and death? Free Radic Biol Med 38, 687-97 (2005).

92. Pedersen, S. F., Owsianik, G. & Nilius, B. TRP channels: an overview. Cell Calcium 38, 233-52 (2005).

93. Massaad, C. A. et al. Involvement of substance P, CGRP and histamine in the hyperalgesia and cytokine upregulation induced by intraplantar injection of capsaicin in rats. J Neuroimmunol 153, 171-82 (2004).

94. Holzer, P. Neurogenic vasodilatation and plasma leakage in the skin. Gen Pharmacol 30, 5-11 (1998).

95. Cesare, P., Dekker, L. V., Sardini, A., Parker, P. J. & McNaughton, P. A. Specific involvement of PKC-epsilon in sensitization of the neuronal response to painful heat. Neuron 23, 617-24 (1999).

96. Ferreira, J., da Silva, G. L. & Calixto, J. B. Contribution of vanilloid receptors to the overt nociception induced by B2 kinin receptor activation in mice. Br J Pharmacol 141, 787-94 (2004).

97. Hu-Tsai, M., Winter, J. & Woolf, C. J. Regional differences in the distribution of capsaicin-sensitive target-identified adult rat dorsal root ganglion neurons. Neurosci Lett 143, 251-4 (1992).

98. Csukai, M. & Mochly-Rosen, D. Pharmacologic modulation of protein kinase C isozymes: the role of RACKs and subcellular localisation. Pharmacol Res 39, 253-9 (1999).

99. Lehel, C. et al. Protein kinase C epsilon subcellular localization domains and proteolytic degradation sites. A model for protein kinase C conformational changes. J Biol Chem 270, 19651-8 (1995).

100. Lehel, C., Olah, Z., Jakab, G. & Anderson, W. B. Protein kinase C epsilon is localized to the Golgi via its zinc-finger domain and modulates Golgi function. Proc Natl Acad Sci U S A 92, 1406-10 (1995).

101. Lehel, C., Olah, Z., Petrovics, G., Jakab, G. & Anderson, W. B. Influence of various domains of protein kinase C epsilon on its PMA-induced translocation from the Golgi to the plasma membrane. Biochem Biophys Res Commun 223, 98-103 (1996).

102. Quittau-Prevostel, C., Delaunay, N., Collazos, A., Vallentin, A. & Joubert, D. Targeting of PKCalpha and epsilon in the pituitary: a highly regulated mechanism involving a GD(E)E motif of the V3 region. J Cell Sci 117, 63-72 (2004).

103. Park, R. & Baines, J. D. Herpes simplex virus type 1 infection induces activation and recruitment of protein kinase C to the nuclear membrane and increased phosphorylation of lamin B. J Virol 80, 494-504 (2006).

104. Prekeris, R., Mayhew, M. W., Cooper, J. B. & Terrian, D. M. Identification and localization of an actin-binding motif that is unique to the epsilon isoform of protein kinase C and participates in the regulation of synaptic function. J Cell Biol 132, 77-90 (1996).

105. Olah, Z., Karai, L. & Iadarola, M. Protein kinase Cα is required for vanilloid receptor 1 activation. J Biol Chem 277, 35752-35759 (2002).

106. Jung, J. et al. Phosphorylation of vanilloid receptor 1 by Ca2+/calmodulin-dependent kinase II regulates its vanilloid binding. J Biol Chem 279, 7048-54 (2004).

107. Woodbury, C. J. et al. Nociceptors lacking TRPV1 and TRPV2 have normal heat responses. J Neurosci 24, 6410-5 (2004).

108. Adamski, F. M., Zhu, M. Y., Bahiraei, F. & Shieh, B. H. Interaction of eye protein kinase C and INAD in Drosophila. Localization of binding domains and electrophysiological

characterization of a loss of association in transgenic flies. J Biol Chem 273, 17713-9 (1998).

109. Tsunoda, S. et al. A multivalent PDZ-domain protein assembles signalling complexes in a G-protein-coupled cascade. Nature 388, 243-9 (1997).

110. Tsunoda, S., Sierralta, J. & Zuker, C. S. Specificity in signaling pathways: assembly into multimolecular signaling complexes. Curr Opin Genet Dev 8, 419-22 (1998).

111. Tsunoda, S. & Zuker, C. S. The organization of INAD-signaling complexes by a multivalent PDZ domain protein in Drosophila photoreceptor cells ensures sensitivity and speed of signaling. Cell Calcium 26, 165-71 (1999).

112. Levitan, I. B. Signaling protein complexes associated with neuronal ion channels. Nat Neurosci 9, 305-10 (2006).

113. Morenilla-Palao, C., Planells-Cases, R., Garcia-Sanz, N. & Ferrer-Montiel, A. Regulated exocytosis contributes to protein kinase C potentiation of vanilloid receptor activity. J Biol Chem 279, 25665-72 (2004).